DESIGN AND IMPLEMENTATION OF A LINEAR MOTOR FOR MULTI-CAR ELEVATORS

by

ENDER KAZAN

Submitted to the Graduate School of Engineering and Natural Sciences
in partial fulfillment of
the requirements for the degree of
Master of Science

Sabanci University
Spring 2009

DESIGN AND IMPLEMENTATION OF A LINEAR MOTOR
FOR MULTI-CAR ELEVATORS

APPROVED BY

Assist. Prof. Dr. Ahmet ONAT .....
(Thesis Supervisor)

Prof. Dr. Sandor MARKON .....
(Thesis Co-Supervisor)

Assoc. Prof. Dr. Mahmut AKSIT .....

Assist. Prof. Dr. Gullu KIZILTAS .....

Assist. Prof. Dr. Ayhan BOZKURT .....

DATE OF APPROVAL: .....

to my family

Acknowledgments

First and foremost, I would like to thank my supervisor Ahmet Onat, for his tireless support and encouragement throughout the duration of my studies (i.e. 7 years). I feel fortunate to have had the opportunity to both learn from and work alongside him. I appreciate the effort he has given to ensure my career got off to a good start.

Secondly I would like to thank Sandor Markon, my external advisor, for giving me the opportunities starts from an internship in Fujitec, Japan through the this joint project as my study. His comments, suggestions and advice have been invaluable for completing this work. I have learned a lot not only from his knowledge but also from his life and work style.

Next, I would like to thank my labmates, specifically Cagri Gurbuz and Nese Tufekciler for their support and ideas during stressful times. I am most grateful to my family who have fostered my curiousity, interests and education from the very beginning. Last but not least, I wish to express my gratitude to my wife, Hilal, not only for her constant encouragement but also for her patience and understanding thorughout.

This thesis was further made possible by funding from the Fujitec Co., Ltd., Japan and was a joint work with Cagri Gurbuz, Ahmet Onat (Sabanci University, Turkey), Norio Takahashi, Daisuke Miyagi (Okayama University, Japan), Yasuhiro Komatsu (Ritsumeikan University, Japan) and Sandor Markon (Kobe Institute of Computing, Japan)

Abstract

The multicar elevator system (MCE) is a revolutionary new technology for highrise buildings, promising outstanding economic benefits, but also requiring new technology for propulsion, safety, and control. In this thesis, new components for linear motor–driven multi-car elevators have been analysed and experimented successfully. It is shown that linear motors with optimized design and a new presented safety and control system can be considered as core components of a new generation elevator systems. The obtained results concern the development of a safety system integrated into the propulsion system, the design of a linear motor optimized for the multi-car elevator task, and the motion control system that is expected to be usable for extra high-rise buildings.

Ozet

Table of Contents

Acknowledgments v

Abstract vi

Summary vii

1 Introduction 1

2 Literature Survey 3

3 Selection and Design of the Motor 6
- 3.1 Functionality Requirements . . . 6
- 3.2 Selected Motor Type . . . 8
  - 3.2.1 Comparison of Motor Types . . . 9
  - 3.2.2 Why Air Core PMSLM? . . . 10
- 3.3 Structure of the Motor . . . 10
  - 3.3.1 Design of the Stator . . . 13
  - 3.3.2 Design of the Mover . . . 20
    - 3.3.2.1 Halbach–Type Mover . . . 20
    - 3.3.2.2 Yoke–Type Mover . . . 23
- 3.4 Optimization of Air Core Yoke–Type Mover with Brake Feature 27
  - 3.4.1 Optimization of Yoke Thickness . . . 29
  - 3.4.2 Optimization with respect to Magnet Width . . . 33
  - 3.4.3 Minimization of Force Ripple . . . 34
  - 3.4.4 Minimization of Effect of Brake Currents . . . 39
  - 3.4.5 Optimization with respect to Mover Array . . . 44

4 Fail-Safe Design 50
- 4.1 Linear Motor Coils as Brake Actuators . . . 51
  - 4.1.1 Magnetic Field of the Linear Motor Coils . . . 52
  - 4.1.2 The Effect of Winding Pattern . . . 55

4.2 Mechanical Part of the Brake Device 59
4.3 Drive of the Motor and Fail-Safe Device 62
4.3.1 Modified Motor Drive for Brake Operation 62
4.3.2 Position Control Method 63
4.3.3 Distributed Drive for Cars and Collision Problem . . . 66

5 Performance Simulations of Designed Motors 69
5.1 Magnetic Properties of Materials used in Simulations 70
5.2 Simulation Results of Implemented Motor 1 and Motor 2 . . . 74
5.3 Simulation Results of Motor 3 Optimized with Stronger Magnetic Materials 76

6 Experimental Results 79
6.1 Experiments on Thrust Force and Payload Capacity 82
6.2 Experiments on Motion 83
6.3 Experiments on Motor Characteristics 84
6.4 Experiments on Brake Device 84

7 Conclusion 94

List of Figures

3.1 Illustration of air-core double sided permanent magnet motor . 12
3.2 Illustration of PMLSM with 3 phase coils 13
3.3 Cross section of a rectangular coil 14
3.4 Alignment of 3 phase coils on the same frame 14
3.5 Different forms of coils and their alignment on the same plane (a)Form 1 - two types of coils are used (b)Form 2 - one type of coil bent in opposite directions (c)Form 3 - one type of coil bent in the same direction. 16
3.6 Cross section of the stator 17
3.7 Dimensions of coils 17
3.8 Change of payload and cost vs thickness of coil 18
3.9 Halbach-type mover 21
3.10 Pareto optimal solution 24
3.11 Efficiency of Halbach-type motor 24
3.12 Yoke-type mover 25
3.13 Comparison of initial cost C_i and running cost C_r ($L_2 = 20$ mm) 26
3.14 Model of the mover to be optimized 27
3.15 Magnetic flux and brake current distribution 28
3.16 B-H curve of 1018 steel 30
3.17 Thrust force vs yoke thickness with different magnet widths . 30
3.18 Payload vs yoke thickness with different magnet widths 31
3.19 Optimal yoke thickness search 32

3.20 Change on payload capacity with magnet dimensions 32
3.21 Change on payload capacity with magnet thickness 33
3.22 Optimal magnet thickness search 35
3.23 Optimum yoke thicknesses vs magnet dimensions 36
3.24 Optimal thicknesses vs magnet width 36
3.25 Payload vs magnet width 37
3.26 Force ripple during movement 38
3.27 Force ripple vs magnet width 39
3.28 Effect of brake currents during movement 40
3.29 Effect of brake currents vs magnet width 41
3.30 Change of design criteria vs magnet width 41
3.31 Change of total costs vs magnet width 43
3.32 Array of 4 movers 44
3.33 Comparison of payload and optimal thicknesses when mover is single and in an array 46
3.34 Comparison of payload per magnet weight when mover is single and in an array 46
3.35 Comparison of force ripple and brake effect when mover is alone and in an array with same dimensions 47
3.36 Flux density in an array of 3 movers (a)40mm width magnet (b)50mm width magnet (c)60mm width magnet 48

4.1 The safety system using coil sections as brake actuators (a) Thrust force with motor magnets on sides (b) Brake force with brake magnets on coil top (c) Thrust and brake force together 52
4.2 The currents i_a, i_b, i_c injected into 3-phase coils 53
4.3 Field distribution from Biot-Savart's Law (a) field distribution on 1 pole (b) field distribution on multiple poles 54
4.4 Winding patterns (a) segmented winding pattern (b) balanced winding pattern 56

4.5 Plan view of the segmented winding stator for one electrical phase (Figure 4.4-a) 58
4.6 Plan view of the balanced winding stator for one electrical phase(Figure 4.4-b) 59
4.7 Illustration of mechanical part of the brake device 60
4.8 Implemented Brake Device 61
4.9 Suggested motor driver for brake operation 63
4.10 PWM timing diagram for brake operation 64
4.11 PWM waveforms for brake operation 64
4.12 Current waveforms for brake operation 65
4.13 Block diagram of the position control system 65
4.14 Linear motor control over a communication network. 67

5.1 B-H curve of steels 71
5.2 Demagnetization curves of permanent magnets at 20^0C . . . 72
5.3 Flux density of Motor 2 72
5.4 Simulated flux density change between magnets of Motor 2 . . 73
5.5 Measured flux density change between magnets of Motor 2 . . 73
5.6 Force ripple and effect of brake currents on Motor 1 and Motor 2 74
5.7 Thrust force of Motor 1 and Motor 2 vs position under drive current of constant phase 75
5.8 Integral of B on a single coil in Motor 2 vs mover position . . 76
5.9 Force ripple and effect of brake currents on Motor 3 77
5.10 Integral of B on a single coil in Motor 3 vs mover position . . 77
5.11 Change of B on a single coil in Motor 2 and Motor 3 while mover is traveling in a constant speed 78

6.1 Motor 1, Designed and built 80
6.2 Motor 2, Designed and built 81

6.3 Payload capacity vs position under DC currents (a)one mover with A-type magnets (b)one mover with B-type magnets (c)array of two movers with A-type magnets 86
6.4 Thrust force vs drive currents of Motor 1 and Motor 2 87
6.5 Thrust force of Motor 2 vs position under drive current of constant phase 87
6.6 Motion and current profile vs time (a)array of 10 movers traveling up (b)array of 10 movers traveling down 88
6.7 Motion and current profile with payload vs time (a)traveling up with self weight (b)traveling up with self weight and 40kg payload 89
6.8 Circuit diagrams of measured back-emf voltages (a) circuit 1 (b) circuit 2 89
6.9 Back-emf and voltage constants on circuit 1 90
6.10 Back-emf and voltage constants on circuit 2 91
6.11 Brake force vs position on balanced winding Motor 1 92
6.12 Brake force vs DC-brake currents on balanced winding Motor 1 92
6.13 Brake force vs position on segmented winding motor at 93

List of Tables

3.1 Dimension of stator set for designing mover 19

3.2 Dimensions, Thrust, etc. 22

3.3 Thrust, Weight, etc. (Halbach–type, $L_2 = 20$ mm) 22

3.4 Examined Combination of L_1 and L_3 ($L_2 = 20$ mm) 26

3.5 Thrust, Weight, etc. (yoke–type, $L_2 = 20$ mm) 26

3.6 Limitation of Design Variables 29

3.7 Optimal values of L_1 and L_3 with respect to L_2 35

3.8 Force ripples of $20mm$, $30mm$, $40mm$ width magnets 37

3.9 Brake effects of $20mm$, $30mm$, $40mm$ width magnets 40

3.10 Examined combinations of k_1, k_2, k_3, k_4 43

4.1 DC currents for different operations 58

5.1 Structural differences of Motors 1,2 and 3 70

Chapter 1

Introduction

Multi-car elevator systems (MCE) with independently moving elevator cars in the same hoistway hold the promise of large improvements in the space utilization of urban buildings. There exist a two–car elevator system on the market, implemented by using conventional traction drive elevator technology. However, for obtaining substantial improvements over single–car systems, multi–car elevators should convert three, four or more banks of zoned single–car systems into integrated multi-car systems. To do this, there is need to use three or more cars in hoistways spanning several hundred meters [6], [7], [14], [26]. For huge scale multi–car systems, a new technology is needed, which can be realized by linear motors [16]. Although design of linear motors have been studied as general purpose actuators in industrial applications [13], their use in elevators pose new challenges.

Linear motor elevators have been studied for several decades. One major topic in this research area is the design of linear motors with a high ratio of payload to self-weight. We used permanent magnet linear synchronous motors in our project, as they appear to be the best solution so far [30], [27], [21].

In this research, our aim is to find a safety system which is still an unsolved problem in multi-car elevator systems. At the same time, we need to ensure that cost of a proposed propulsion system with a safety device is still acceptable.

The work done in this thesis is given as follows. First, a summary of related work and background information about multi-car elevators and their types are included in Chapter 2. The characteristics and functional requirements of linear motors to be used in elevators are described in the beginning of Chapter 3. Later in the same chapter, the design decisions compatible with the requirements are explained and discussed by showing simulations on each step. Based on the safety device with its control method described in Chapter 4 and the optimization method given in Chapter 3, two linear motors are designed and implemented to test their functionality and performance on the requirements. By the simulation results given in Chapter 5 and experimental results given in Chapter 6, the proposed concepts in this thesis have all been validated.

Chapter 2

Literature Survey

Multi-Car Elevator (MCE) systems correspond to multiple cars in the same hoistway moving independently. These systems have been implemented in the past but only as simple systems. There have been problems regarding the transportation length and the number of cars that could move in the same hoistway was too few. For example, currently a German elevator manufacturer company is using the rope-driven method in the TWIN multi-car system (i.e. two elevator cars built in the same shaft) [18]. However, multi–car elevators should convert three, four or more banks of zoned single–car systems into integrated multi-car systems.

For noticeable improvements in MCE systems, rope-driven method, used in conventional elevators, should not be used [32], [4]. On the contrary, the rope-less method, which implements the installation of linear motors [17], [24] should be used as this method has the advantage of unlimited transportation lengths and allows the implementation of many independently moving cars in the same hoistway.

Recent studies shows that the idea of MCE systems is getting popular because their efficiency could be increased by improving linear motors and scheduling algorithms for multi-mobile systems. Therefore, in order to improve MCE systems, studies focusing on scheduling algorithms and linear motors (i.e. core component of the propulsion system) should be done.

On scheduling of MCE systems, considerable amount of research related to the driving and control are being performed. For example, Suzuki et al. have proposed an optimization method for MCE driving control rules using Genetic Algorithm (GA) [26], [5]. Markon et al. have proposed a control algorithm which uses a continuously running real-time GA method [22]. Ikeda et al. have proposed an application for traffic-sensitive MCE controller [8]. Suzuki has a study about intra-shaft operating methods for MCE systems [25]. Shiraishi et al. have proposed an autonomous distributed control method [9]. When the simulation results of these studies are analysed, it can be seen that MCE system, when implemented in an efficient way, provide substantial improvements over single-car elevator systems.

There have been some studies on realizing MCE systems as well. For example, Chevailler et al. presents the results of the multi criteria design procedure that determines a technical solution for linear motors [1]. However, in general, there are more studies related to the vertical transportation of MCE systems, but these approaches are still single-car systems. For example, Cruise et al. have proposed a rope-less lifting as a solution for mining applications where efficiency of conventional hoisting systems is not sufficient after a certain depth [3]. Another interesting research by Thornton shows that linear motors that are used for the Japanese high speed Maglev Project can be also used for vertical transportation [2]. In the same way, in some research rope-less lifting is introduced to be used for elevators [11], [29].

There have been more studies on how to improve the linear motors in terms of power consumption, controllability, initial and running costs which are very important in case of rope-less elevator system. First, to reduce the initial cost, linear switched reluctance motors (LSRM) are introduced as a solution for ropeless lifting [11], [12]. Then, to improve the costs and efficiency by utilizing the advances in magnet technology, permanent magnet linear synchronous motors (PMLSM) are introduced [31], [28], [19], [2], [1]. While some of these

works have been done to improve PMLSMs, the others show the advantage of PMLSMs in ropeless lifting. In [31] and [20], methods for reducing cogging, leakage, and end effect of linear motors are proposed. In [19], the authors present several optimization methods for increasing the efficiency of PMLSMs in addition to the usage of a Halbach array which a new magnet alignment method. The multi objective optimization design on PMLSMs is also given in [28] to increase the thrust while decreasing the magnet volume.

The methods introduced in [11] and [12] can not be used for elevators in spite of the reduced initial cost, because LSRMs have very high force ripple characteristics. The problem in [31] is that the design of PMLSM is single sided where large attractive forces between the PM mover and the iron stator exist and the linear bearing system must carry all this force. However, with two-sided design like in [1], the force can be balanced out. There could be also an improvement in [1] as an alternative to iron cored stator to reduce the construction cost.

Although solutions are presented for controllability and cost issues, there is another problem that must be solved for MCE systems. An unsolved problem is how to prevent elevator cars from falling in case of all failure modes, and how to prevent collision of independently moving cars in the same hoistway. Although [3] and [29] introduced that when a power failure interruption occurs, short circuiting of the coils in the motor can be used to create generative counter force that slows down the elevator, there is need for a better solution that can be operational in all failure modes and a solution for the collision problem that has not yet been introduced.

In our research, we are introducing a PMLSM, that is the harmony of previously given methods, optimized to be used in elevator. We also add a safety device into the structure of the PMLSM, which can handle all failure modes. This feature makes our approach unique when compared to the other methods introduced so far.

Chapter 3

Selection and Design of the Motor

Since the propulsion method is the core component of new multi-car elevator (MCE) systems, it needs to be purpose designed to hande not only lifting the elevator car, but also several other requirements. Therefore, care must be taken in selection and design of the linear motor such that the correct type can be selected and designed to meet each requirement.

3.1 Functionality Requirements

It is important to determine the requirements clearly to have a sufficient design for the purpose. In our project, motor will be used not just as an actuator but also as the working machine of the overall system. Therefore, other than the major properties such as torque, power consumption and size additional requirements related to mechanical and control properties, need to be included as design criteria.

A linear motor that will be used for MCE applications should have the following properties;

High thrust force - To get rid of all ropes and cables, there will be no counterweight in the system. This leads to necessity of trust force which is high enough to lift the elevator cage including payload without help of counterweight.

Low force ripple - Although closed-loop control can compensate up to

a certain amount of force ripple, it is important to have low force ripple for accurate control on position to reduce the vibration in the motion even with open-loop control.

Brake Operation - As there is movement and gravitational force, there must be a brake device capable of mechanically stopping and holding the car at any position. For safety, it should also be independent of power and control issues.

Spanning whole hoistway - Removing ropes causes another disadvantage that it is not possible to transfer lifting force through the hoistway. Therefore, the motor has to span the whole hoistway.

Independent Control of Sections - As the key point of MCE, there must be at least one actuator for each elevator car on the hoistway to have independent control over all of them. As it is not feasible to build different actuators or linear motors for each car, the motor can be divided into different sections electrically. In this way, each car can be controlled independently by using the sections which are currently assigned to different cars.

Unlimited Length - Since MCE systems will be used in extremely high buildings, the motor needs to be designed in such a way that it should not limit the height of the building; on the contrary it should be used for any length.

Modularity - It is not possible to construct the motor in length of hundreds of meters at once. Therefore, the motor must be in a modular fashion to be constructed part by part to be assembled into each other within the hoistway. Similarly, when there is need for replacement of a section in the motor, the related module can be replaced instead of whole motor.

Position Sensing - For accurate control there is need for feedback from the system. Since the length of movement is assumed as unlimited and any cable traveling with car is undesirable, using conventional position encoders is not suitable for position sensing. The motor itself should be able to measure

the position of the car.

Power and Signal Transfer - Similar to removing all the ropes from the system, any cable for power or signal transfer to elevator car must also be removed. Since there is still need for signal and power transfer for the car, the motor itself should also be available to be used for power and signal transfer between the building and elevator car.

3.2 Selected Motor Type

The conventional lifting method of an elevator depends on a mechanical connection i.e ropes between the actuator motor and the elevator cage to transfer the lifting force along the whole hoistway. In multi-car elevator systems, availability of the lifting force at any position along the hoistway is also needed for each car. By a suitable mechanical alignment, same method which depends on ropes or pistons could still be used for lifting a small number of elevators on the same hositway. However, this new system with just a few elevator cars may not give substantial improvement over a single-car system. Therefore, to obtain more efficient MCE system with many cars, there is need for an alternative solution which will get rid of the alignment problem between the actuator and the car. One solution can be having a propulsion system which is available through the whole way instead of having it at a single point and transferring to other locations. This limitation leads us to use linear motors as the propulsion method. In this way, the lifting force is available at any location on the hoistway and no additional mechanical connection is needed to transfer the lifting force to other locations.

To meet the requirements given in Section 3.1, Permanent Magnet Synchronous Linear Motor is selected as the motor type, and it is explained more in the following Sections 3.2.1 and 3.2.2.

3.2.1 Comparison of Motor Types

As it is the case for all of electric motors, linear motors can be also divided into two groups as alternating current (AC) supplied or direct current (DC) supplied types. The advantage of brushed DC (BDC) motors is the convenience of driving; but the disadvantage is short lifespan because of unavoidable wear on brushes during operation and comparatively low efficiency. Since lifespan is very important criterion in industrial applications like elevators, it is not suitable to use BDC linear motors. In this sense, the AC motors should be used with their brushless structures.

When the rotor and stator parts of the motors are taken into account individually, the motors can be further grouped as synchronous and asynchronous. Induction motors (IM) as the most typical example of asynchronous motors have different frequency of rotating rotor and rotating stator flux operation. Just like the transformers, current on the rotor windings is created by electromagnetic induction given from stator windings. To be able to induce these currents, the frequency of the drive current must be different than the rotation of the field on the rotor. Although digital controllers enable good torque and speed control even for asynchronous motors, there is need for speed and position feedback of rotor to calculate required inductive current on the stator. Another disadvantage about induction motors is the need for very small air gap to get sufficiently high magnetic field density. Maintaining the small air gap require rigid guidance against the large attractive force between the IM stator and mover. Also there is heat dissipation on the mover which is not desirable when being close to the passengers. Therefore IM is not suitable to be used for elevators. The synchronous motors can be further grouped as the ones with windings on their rotors, and the ones with just permanent magnets. The classical synchronous motors, which were more popular in the past, have the windings instead of magnets on the rotor because of inefficiency of old magnets and low initial cost of windings. But, continuous improvements

on magnet materials and magnetization techniques lead to permanent magnet synchronous motors to be widely used because of their high efficiency and high force capability. Another advantage is that there is no need for brush-type or brushless exciters to supply current to the rotor. This advantage finally enables lifting the elevator car without using any rope or any cable.

3.2.2 Why Air Core PMSLM?

Linear synchronous motors can be either iron core or air core (coreless) design. Air core PMSLM was selected over cored once for several reasons.

First, there is an advantage on construction cost. The stator is by far the dominant component of a linear motor elevator. With air core, there is no need to provide iron core for the long stator all over the hoistway, only the windings are still needed. This reduces costs, weight, makes construction easier.

Second, another disadvantage of an iron core is that attractive force between the PM mover and the iron stator is huge, typically on the order of 10 times the thrust. With single-sided design, the linear bearing system must carry all this force. With two-sided design, the force can be balanced out, but the construction is more complicated and delicate.

Lastly, with iron core, the slots produce harmonics in the thrust. This can be reduced by slanting the slots or the magnets, but both will reduce the thrust because of the angle between them (see Equation 3.5), and further increases the construction costs.

3.3 Structure of the Motor

The selected motor type discussed in Section 3.2 is the permanent magnet synchronous linear motor. It consists of two major parts: the stator, which consists of coils and fixed to the ground and the moving part called 'mover' where permanent magnets are assembled. Since the mover consists of an assembly of magnets and possibly a yoke, the motor can also be called as moving

magnet synchronous linear motor. Both stator and mover can be designed in many shapes and dimensions.

As the core priority of a motor, the structure of the motor should be formed to get high thrust force with low power consumption. In this sense, the general electromagnetic principles must be implemented carefully to obtain high efficient motor which can also meet the requirements given in Section 3.1. The design of the motor will be outlined next.

Force on a charged particle can be found by using Lorentz Rule,

$$\boldsymbol{F} = q\boldsymbol{v} \times \boldsymbol{B} \tag{3.1}$$

where q is charge of the particle, v is the velocity of the particle, and B is the magnetic induction. The force F is proportional to the value of the charge and the vector cross product between v and B.

The rate of flow of charge (q) can be described as conventional current (I) as in Equation 3.2. and the velocity ($\boldsymbol{v}$) can be described as rate of distance ($\boldsymbol{l}$) traveled by the charge as in Equation 3.3,

$$I = dq/dt \tag{3.2}$$

$$V = d\boldsymbol{l}/dt \tag{3.3}$$

Equations 3.1, 3.2 and 3.3 can be combined as follows,

$$\begin{aligned} \boldsymbol{dF} &= dq(\boldsymbol{v} \times \boldsymbol{B}) \\ &= Idt(\boldsymbol{v} \times \boldsymbol{B}) \\ &= I(\boldsymbol{dl} \times \boldsymbol{B}) \end{aligned} \tag{3.4}$$

where $\boldsymbol{dl}$ vector is in the direction of the current.

To find the force perpendicular to current direction (also the l direction) Equation 3.4 can be simplified since the conductor of current can be taken as straight for a linear motor:

$$F = B\ I\ l\ sin\theta \tag{3.5}$$

where θ is the angle between the magnetic flux and the current.

Equation 3.5 shows that to get high force, there is need for high current flow (I), high magnetic flux (B), or long current conductor which is wire (l) and perpendicularity of magnetic flux over current direction (θ). Therefore, in the design of motor structure, it is necessary to optimize these variables.

As described in Section 3.2.2, the stator is designed to be coreless, aka air cored. It is also mentioned that the magnetic flux of coils in the stator is caught by the magnets on the mover since it is an air core motor. As an illustration, Figure 3.1 shows the cross section of an air core double sided permanent magnet motor. The conductor where the conventional current (I) flows is shown as the coil section in the figure. The magnetic flux (B) is induced by permanent magnets. The omitted 3rd dimension in the figure, which is depth (l), is the length of the conductor immersed in the uniform magnetic field.

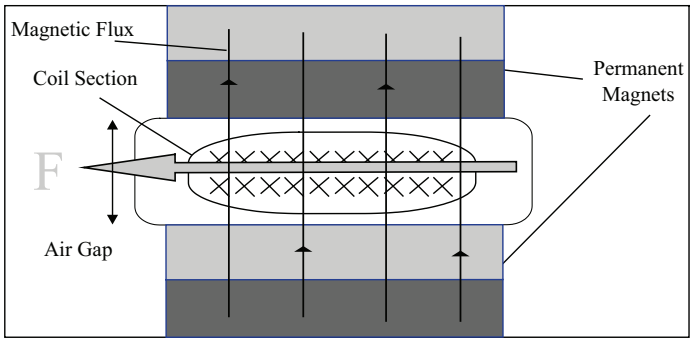

Figure 3.1: Illustration of air-core double sided permanent magnet motor

In this chapter, Section 3.3.1 discusses how to design the stator in order to

maximize the current density within the space available between the magnets of mover, and to solve the problem of mechanical strength of coreless structure since there is no supporting iron core and it is surrounded by air. Next, Section 3.3.2 shows how to design the mover in order to maximize the magnetic flux induced by the permanent magnets, and to maximize the payload with a low magnet volume. In addition to improving parameters that influence the thrust force, it shows how to design each part of the motor to meet the functional requirements given in Section 3.1.

3.3.1 Design of the Stator

Equation 3.5 states that the Force (F) is proportional to current (I), and magnetic field (B). Since most of the magnetic field is generated using permanent magnets involved in a magnetic circuit, flux density within the circuit has a large effect on the field produced across the air gap. In order to increase the cross section of current conductor which is coil, the air gap shown in Figure 3.2 should be increased. On the other hand, to increase the magnetic field strength by using the same volume of magnets, the air gap should be decreased. Therefore, determining the distance of air gap is an optimization problem in the design.

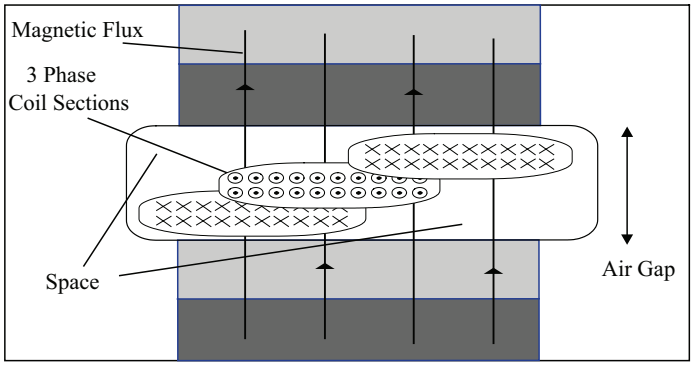

Figure 3.2: Illustration of PMLSM with 3 phase coils

The first step on reducing the air gap is to find a way to align the coils

which are arranged at multiple of 120^0 electrical degrees in such a way that the amount of space can be minimized to increase the flux density between the magnets (Figure 3.2 where no wire inserted in the stator). Filling the air gap space with wires is possible with aligning the coils in the same plane instead of letting them lie on top of each other. Additionally, the cross section of the coils should be suitable to align without leaving space between them. In this sense, such a simple cross section can be a rectangle as shown in Figure 3.3. The coils could have complex cross sections in sinusoidally slope for better back-emf and force ripple harmonics. This problem, however, is attached as a design problem of the mover rather than the stator. This is explained in Section 3.3.2. The cross section of coils, and their alignment on the same plane is shown in Figure 3.4.

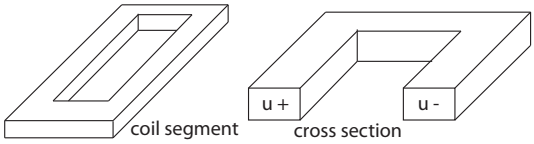

Figure 3.3: Cross section of a rectangular coil

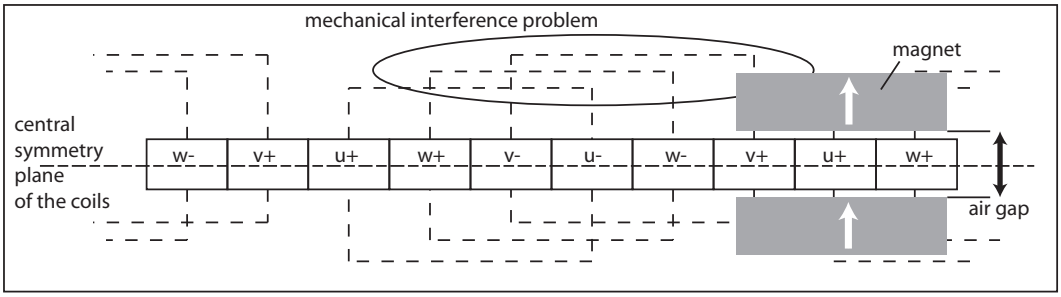

Figure 3.4: Alignment of 3 phase coils on the same frame

Aligning the coils on the same plane without leaving space is possible by sliding coils within others. However, a simple form of rectangular coil, shown in Figure 3.3, is not suitable to be aligned in the same frame of others, because there will be a mechanical interference between the coils on their ends. A solution to this problem can be to modify the form of coil by bending the end

parts where the interference occurs. This bending is in fact the usual method used in the manufacturing motors, even those with the windings placed in slots of an iron core where the bent part is called the 'end winding'.

There can be several forms of coils depending on how they are bent. Three example forms and their alignments that were considered are shown in Figure 3.5. The first alignment example uses two different forms of coils: one of them is bent and the other remains planar. The second and third examples need a single form which is an advantage in reducing design parameters and manufacturing.

Remaining problems additional to interference are as follows: how to preserve the form of winding against external forces, how to assemble coils with each other mechanically, and how to mount them to a common base plate with the linear bearings that support the mover. One of the solutions for holding together and attaching the coils can be to use epoxy molding mostly on end parts of the coils where bending is done. Using the flat surface in this way where thrust force will be obtained, the bent end parts can be used for mechanical assembly so that the air gap need not to be increased because of thickness of coil and thickness of epoxy on flat the surface. Figure 3.6 shows the cross section of the stator perpendicular to the direction of motion which has the coils assembled by using the epoxy mold technique. The mold at one side can be wider to mount on base plate by any connection like screws.

The minimum air gap must be slightly larger than the total of thicknesses of coil and epoxy shield. Therefore, it is advantageous to get rid of the shield that causes additional air gap. In this way, an improvement on mechanical assembly can be achieved by winding stand-alone coils that do not need additional mechanical support as shield under certain external forces. There may be no solution for this problem by using usual copper wires coated with enamel for only electrical insulation since they have no structural strength. Instead, a solution can be using bonded wire that is covered by an additional adhesive

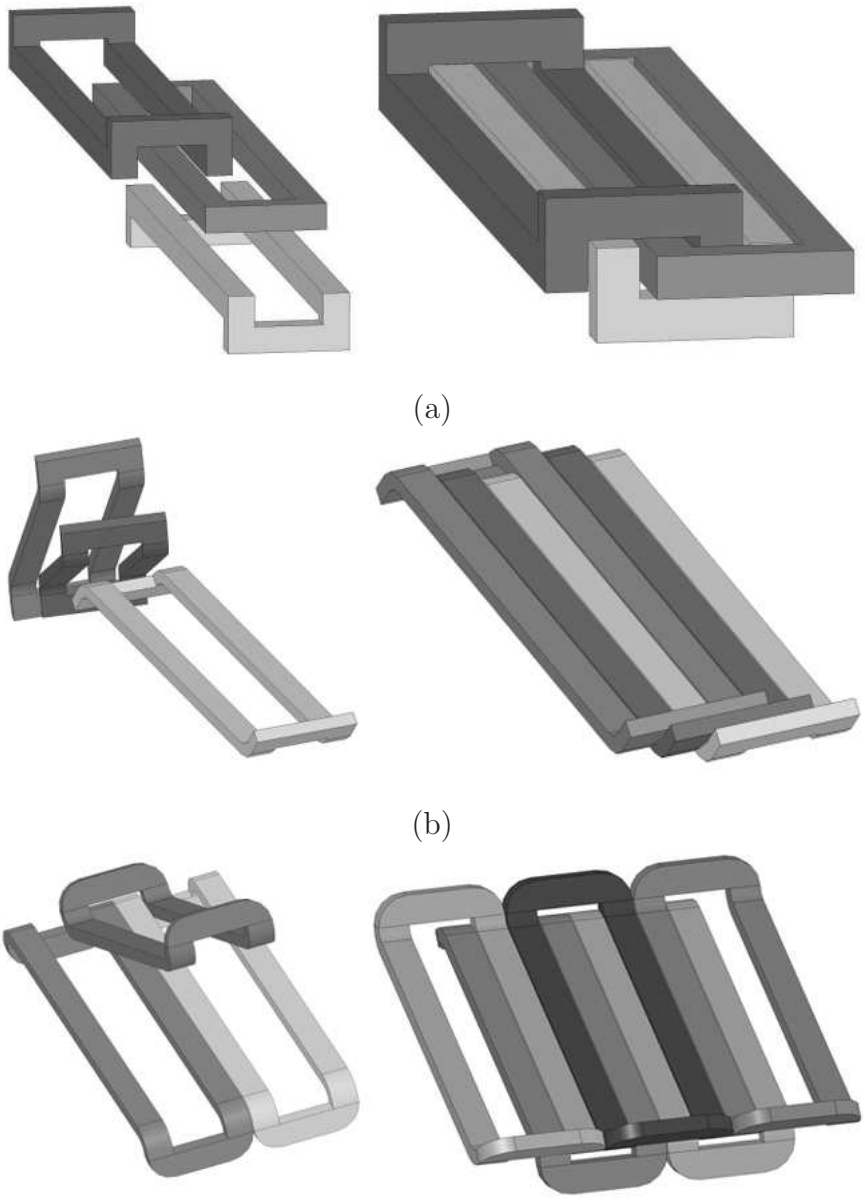

Figure 3.5: Different forms of coils and their alignment on the same plane (a)Form 1 - two types of coils are used (b)Form 2 - one type of coil bent in opposite directions (c)Form 3 - one type of coil bent in the same direction.

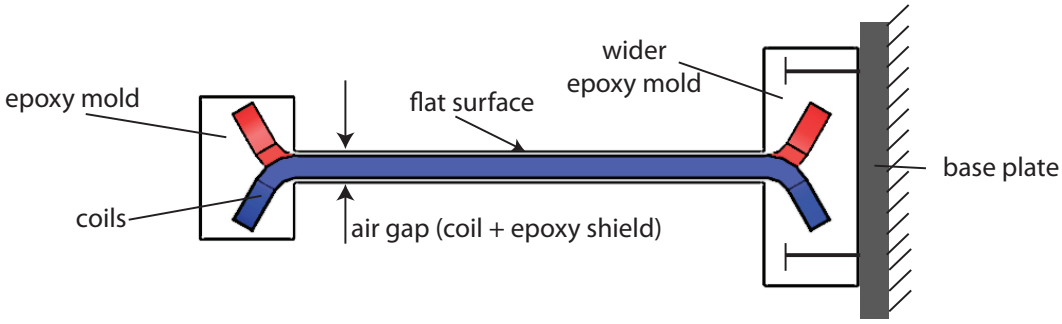

Figure 3.6: Cross section of the stator

material on its surface that can melt at high temperature and harden again when cooled down. In this way, bonded wire has rigidity when it is winded as a coil, heated and strands bonded together. This gives the advantage of producing tightly wound coils with no extra bonding material coating and reducing the air gap where higher thrust forces can be obtained. The improvement in using bonded wire can be seen by comparing the experimental results given in Section 6.1 of two implemented motors where one of them has the coils with standard wire, and other has the coils with bonded wire.

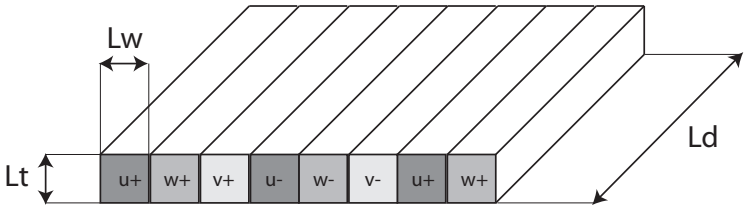

Figure 3.7: Dimensions of coils

Once the structure of the stator is determined as explained above, the optimization of dimensions in the structure can be examined. The parameters that can be used in design optimization are given in Figure 3.7 as thickness of coils (L_t), width of coils (L_w), and length of flat surface (L_d) on the stator. The length L_d does not stand for the length of the coil, but it stands for the distance between the epoxy molds shown in Figure 3.6. As it can be seen in the same figure, one side of the coils is floating because it is not mounted

on a base. Therefore, the length L_d should be chosen short enough to have sufficient mechanical strength against the side forces that can create moment on the coils. Additionally, the parameter l linear to force given in Equation 3.5 states that L_d should be chosen longer for higher forces. Therefore, L_d should be icreased as much as possible provided that the mechanical strength of the stator is sufficient. For 2D FEM analyses the dimension L_d can be taken as the depth of the problem and it is selected as $200mm$ for the simulations and experiments shown in Chapters 5 and 6.

The width of coils (L_w) is equal to 1/6 of the length of one electrical phase which can be chosen as any value by a designer. As an initial value, length of one phase is selected as $120mm$ for the analysis and experiments. Therefore, L_w is fixed as $20mm$. On the other hand, L_t should be chosen high in terms of increasing mechanical strength and number of wires for higher current flow, and also it should be chosen low in terms of decreasing the air gap and better heat dissipation for better electrical overload toleration. Figure 3.8 shows how payload capacity, and payload per amount of wire change with respect to thickness of coil (L_t) under the condition where rest of the variables are fixed.

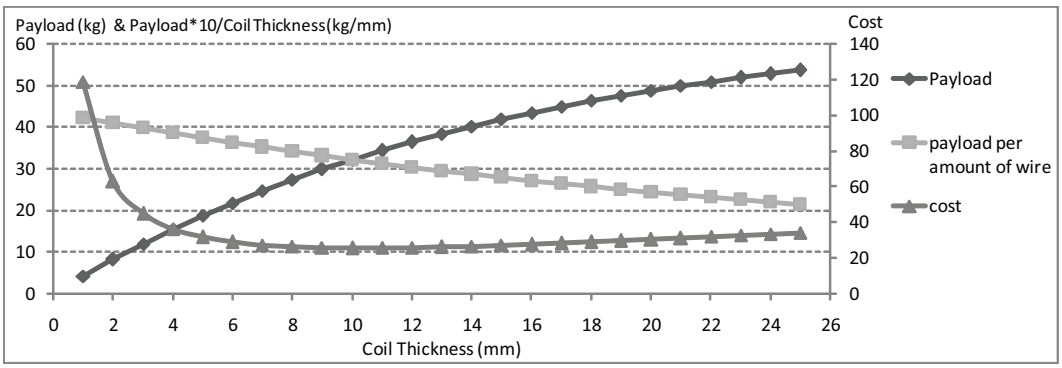

Figure 3.8: Change of payload and cost vs thickness of coil

The payload (P) is continuously increasing when coil thickness (L_t) increases. Therefore, for higher payload, higher L_t should be chosen. On the other hand, payload per amount of wire, which is proportional to L_t is contin-

uously decreasing when L_t increases. Therefore, for an efficient result in terms of initial cost of stator, lower L_t should be chosen. A simple cost function to be minimized for thickness of coils (W_{tc}) can be formed as,

$$W_{tc} = k_1 W_1 + k_2 W_2 \tag{3.6}$$

where,

$$W_1 = 1/P \tag{3.7}$$

$$W_2 = L_t \tag{3.8}$$

A designer can determine the coefficients k_1 and k_2 as the priority of payload and cost of stator respectively. The cost graph given in Figure 3.8 shows the result when $k_1 = 500$ and $k_2 = 1$. It can be seen that optimal coil width (L_t) can be in a wide range from $6mm$ to $16mm$ where it has the minimum cost value at $L_t = 10mm$.

The performance with respect to L_d is straightforward in terms of payload since it is a linear relationship. However, its relationship with mechanical strength must be proven using experiments. This was not performed, since the structural strength of the coils is not uniform within one coil, and may show a variation between different coils in the small prototype production that has been built for the experiments done. However, in the closely controlled mass production environment, it will be more rewarding to perform structural strength tests.

In conclusion, the dimensions of the stator are shown in Table 3.1 to be used as reference dimensions of stator for optimization of mover in Section 3.3.2.

Table 3.1: Dimension of stator set for designing mover

L_t	$10mm$
L_w	$20mm$
L_d	$200mm$

3.3.2 Design of the Mover

As shown in Table 3.1, the dimensions of stator are determined before designing the mover. The mover is studied for two different types. One of them is named as Halbach-type where only magnets are used in alignment of Halbach array [23]. The other one is named as yoke-type mover where iron or steel plate is used to complete the magnetic flux circuit. Both types have multiple free variables needed to be optimized against multiple design criteria. The Halbach-type mover is optimized in the following Section 3.3.2.1 by using evolution strategy (ES) method [23] and Pareto optimal solution is obtained. The yoke-type mover is also analysed in Section 3.3.2.2 by creating multiple models to be compared with the Halbach-type. The optimization by using ES method in Section 3.3.2.1 and the comparison of yoke-type movers and Halbach-type movers in Section 3.3.2.2 is a work of Prof. Norio Takahashi from Okayama University, Japan who is a member of this research group [27], [19], [26]. This work is included and discussed for the sake of completeness.

Additionally, an optimal yoke-type mover including brake feature is also studied in Section 3.3.2.2 by introducing an optimization method with an algorithm explained in detail to reduce the problem space to be solved.

3.3.2.1 Halbach–Type Mover

The model to be optimized can be designed using several dimensions held as variables. As it is seen in Figure 3.9, there are two free variables (L_1,L_2) which are the dimensions of magnets. As a starting point, the distance between a magnet and stator coils can be set as 4 mm, where air gap between magnets becomes 14 mm in total. Since the half of alternating current phase is also set to 60 mm in movement distance, the width of horizontally magnetized magnets is calculated as $60 - L_2$ in mm. The final dimension parameter which is depth

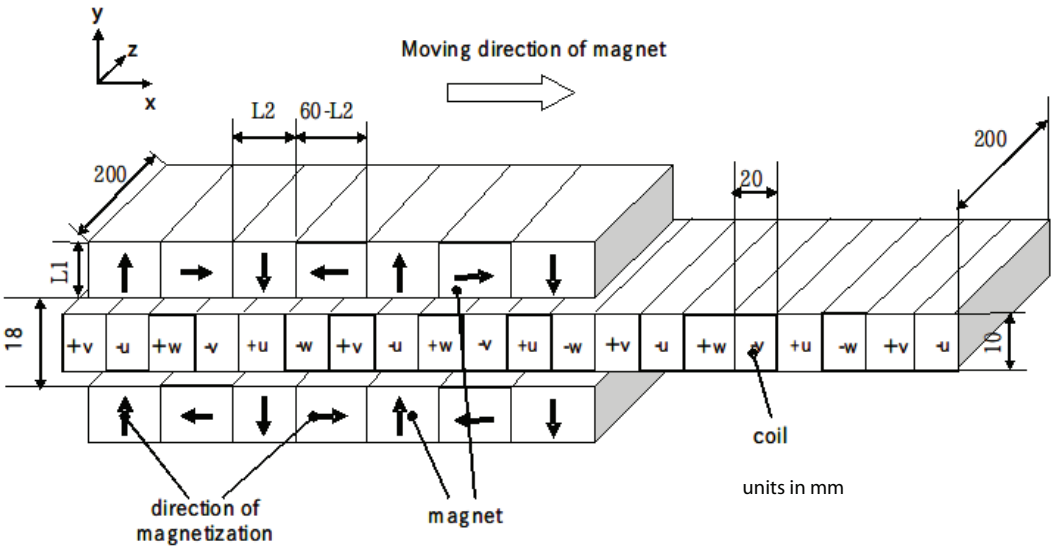

Figure 3.9: Halbach-type mover

of the motor is also fixed as 200 mm.

For the optimization, high thrust force, low magnet volume, and low force ripple can be taken first. To be used in evolution strategy (ES) method [23], the free variables can be limited as $0 \leq L_1 \leq 50$ and $0 \leq L_2 \leq 60$ in mm.

As the ES method, a child vector is generated from one parent vector by comparing the objective functions of each vector. Once the most dominant objective function is found, the respondent vector is assigned as a parent vector of the next generation.

The objective function can be chosen as;

$$W = k_1 W_1 + k_2 W_2 + k_3 W_3 \tag{3.9}$$

where,

$$W_1 = 1/F_{xave} \tag{3.10}$$

$$W_2 = W_g \tag{3.11}$$

$$W_3 = r_d = \left(F_{xmax} - F_{xmin}\right)/F_{xave} \times 100 \tag{3.12}$$

To get about equal weight from each function, the coefficients k_1, k_2, k_3

are also can be chosen as

$$k_1 W_1 = k_2 W_2 = k_3 W_3 \tag{3.13}$$

By minimizing the function given in Equation 3.9, the model can be configured with high thrust force (F_{xave}), low magnet weight (W_g), and low force ripple (r_d). The Table 3.2 shows the comparison of initial shape and optimal shape of the results with ES method. It can be seen that better F_{xave}, and r_d combination can be obtained by increasing the W_g comparing to initial shape.

Table 3.2: Dimensions, Thrust, etc.

	Initial shape	Optimal shape
L_1 (mm)	10	30
L_2 (mm)	30	20.9
F_{xave} (kgf)	40	71.9
W_g (kg)	6.3	18.1
r_d (%)	4.83	0.2
η	0.343	1.867

Table 3.3: Thrust, Weight, etc. (Halbach–type, $L_2 = 20$ mm)

L1	F(kgf)	Q	W	P	η_1	N	Ci	Cr
10	36.34	6	6	30.34	5.06	6.6	39.56	6.6
20	58.4	12	12	46.4	3.87	4.3	51.73	4.3
30	71.63	18	18	53.63	2.98	3.7	67.12	3.7

The term η in Tables 3.2, and 3.3 refer to efficiency of the motor calculated as,

$$\eta_1 = \left(F_{xave} - (W_g + 20)\right) / W_g \tag{3.14}$$

where 20kg payload is desired per mover. Therefore, if F_{xave} is high enough to lift both weight of the magnets and the desired payload, η becomes larger then 0.

When total required payload is set to 200kg as a design criterion, running cost (C_r) is taken as the number of needed movers (N), and initial cost (C_i) which is proportional to magnet weight are calculated as,

$$C_r = N = 200/\left(F_{xave} - W_g\right) \tag{3.15}$$

$$C_i = 200/\eta \tag{3.16}$$

There are also some result of Halbach-type mover in different dimensions in Table (3.3) and it can be seen that running cost gets better while the initial cost is increasing. At this point, the optimum parameters are found by using the equations W_1 $(1/F_{xave})$ and W_2 (W_g). It is possible to do true multi-objective optimization, by requiring two or more of the objective functions to simultaneously decrease until reaching non-dominated solution points. Figure 3.10 shows the graph of such a Pareto optimal solution for the objective functions of weight and inverse thrust at around Point A from the viewpoint of small W_1 (large thrust) and small W_2 (light motor). The efficiency can be also seen at Figure 3.11.

3.3.2.2 Yoke–Type Mover

One of the other alternatives for mover can be using yoke-type structure seen in Figure 3.12 which has the advantage of simpler manufacturing and reduced initial cost by decreasing magnet weight.

While Halbach-type mover is formed by using only permanent magnets, the yoke-type mover is formed by permanent magnets together with iron or steel plate which is the yoke. The yoke in the structure is for completing the path of magnetic flux on the mover.

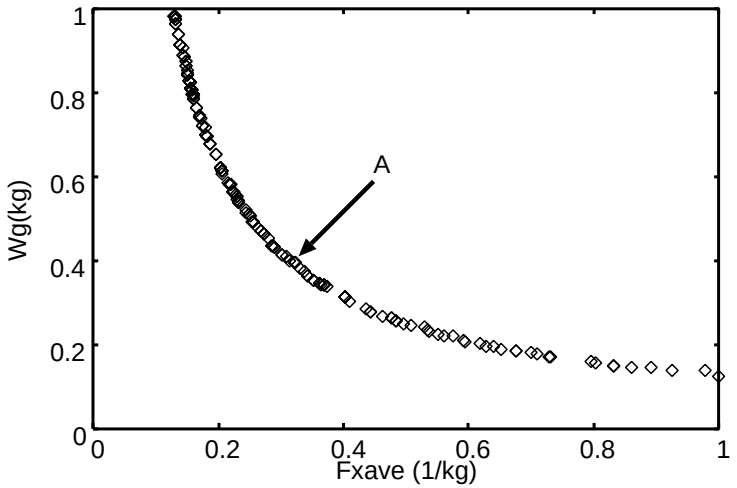

Figure 3.10: Pareto optimal solution

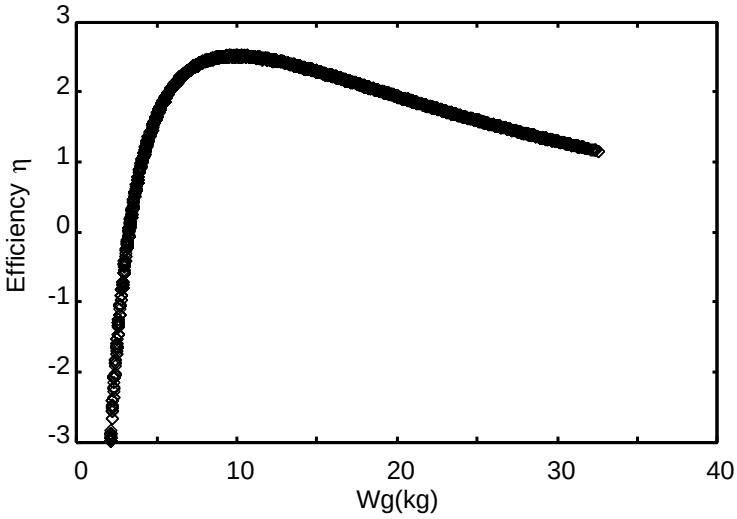

Figure 3.11: Efficiency of Halbach-type motor

It is possible to design a yoke-type mover with complicated three dimensional shape to reduce force ripple and sinusoidal back-emf harmonics. A better back-emf harmonic is determined as future work, and not included as design criterion for this study. Therefore, the simplified structure seen in Figure 3.12 is determined to be optimized.

Additional to free variables of magnet sizes (L_1, L_2), a new dimension

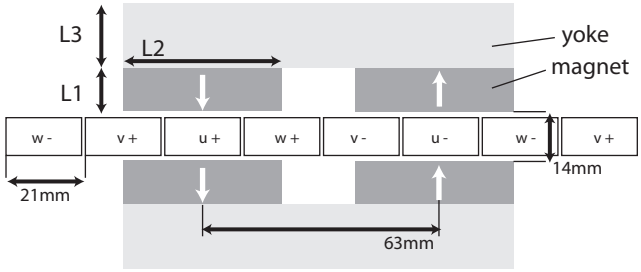

Figure 3.12: Yoke-type mover

which is the thickness of yoke (L_3) is also a free variable for the optimization problem. The optimal solution given in Table 3.2 shows that width of the vertically magnetized magnets can be chosen as close to width of a single coil section. Therefore, L_2 can be fixed to 20mm for simplicity.

The efficiency (η_2) of the motor can be chosen as,

$$\eta_2 = (F - Q) / W_g \tag{3.17}$$

where F refers to thrust per mover, and Q refers to total weight of the mover including the yoke, and W_g is still the weight of magnets.

When the required payload is taken as 200 kg including the weight of the cage and passengers, required number of units of movers (N) which is equal to running cost (C_r), and the initial cost (C_i) can be found as,

$$C_r = N = 200/ (F - Q) \tag{3.18}$$

$$C_i = 200/\eta_2 \tag{3.19}$$

Table 3.5 shows the thrust force, weight, efficiency, costs, etc. at $L_2 = 20$ mm for the several combinations of L_1 and L_3 given in Table 3.4.

Figure 3.13 shows the comparison of several examined models of both Halbach and yoke-type movers. While Halbach-type mover is better in running cost (C_r), yoke-type mover can be build with better initial cost (C_i). Therefore, when C_i is in higher priority, one of the models in Table 3.5 with significant η_2

Table 3.4: Examined Combination of L_1 and L_3 ($L_2 = 20$ mm)

Model	1	2	3	4	5	6	7	8	9
L_1	10.0	10.0	10.0	20.0	20.0	20.0	30.0	30.0	30.0
L_3	5.0	10.0	15.0	5.0	10.0	15.0	5.0	10.0	15.0

Table 3.5: Thrust, Weight, etc. (yoke–type, $L_2 = 20$ mm)

Model	F(kgf)	Q	W	P	η_2	N	C_i	C_r
1	26.38	5.4	2.4	20.98	8.74	9.5	22.88	9.5
2	29	8.4	2.4	20.6	8.58	9.7	23.3	9.7
3	29.33	11.4	2.4	17.93	7.47	11.2	26.78	11.2
4	32.66	7.8	4.8	24.86	5.18	8	38.61	8
5	35.58	10.8	4.8	24.78	5.16	8.1	38.74	8.1
6	36.24	13.8	4.8	22.44	4.68	8.9	42.77	8.9
7	35.7	10.2	7.2	25.5	3.54	7.8	56.46	7.8
8	37.87	13.2	7.2	24.67	3.43	8.1	58.38	8.1
9	38.55	16.2	7.2	22.35	3.1	8.9	64.43	8.9

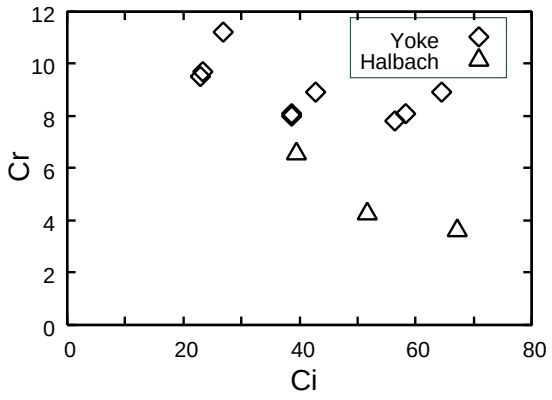

Figure 3.13: Comparison of initial cost C_i and running cost C_r ($L_2 = 20$ mm)

can be selected. In this sense, Model 1 is the most appropriate one for initially low cost movers. On the other hand, when large thrust and small running cost is in higher priority, the optimal design given in Table 3.2 can be selected.

3.4 Optimization of Air Core Yoke–Type Mover with Brake Feature

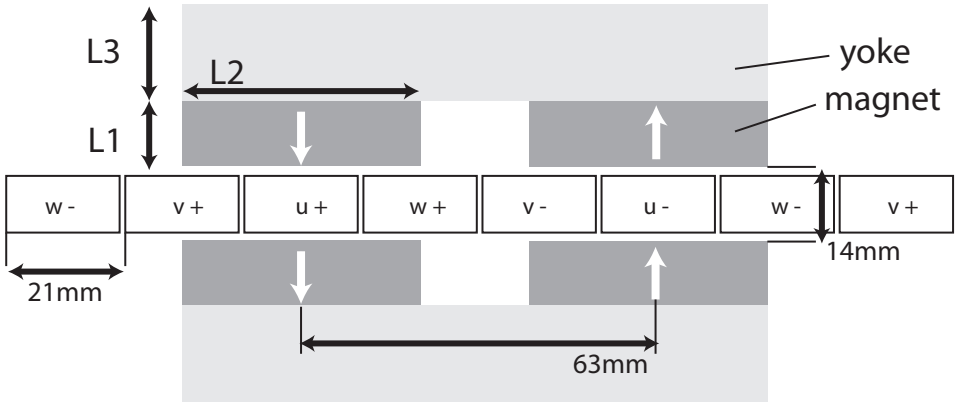

Figure 3.14: Model of the mover to be optimized

Although most of the design criteria are similar for most of the electric motors, the linear motor with requirements explained in section 3.1 needs additional important criterion for the proposed brake feature explained in Chapter 4. It is also declared in section 4.1 that the currents used for actuating brake mechanism should have negligible effect on thrust force of the motor. Therefore, the motor needs to be designed so that the effect of brake currents is minimized additional to high thrust, low weight, and low cost properties.

As discussed in Section 4.1.1, the effect of brake currents can be minimized by having special distributed field on the coils. Figure 3.15 shows the half of the mover with the line of symmetry. When the brake currents are applied, the coil sections of A and C are fed by additional negative current ($-DC$) but coil section of B is fed by positive current ($+DC$). Therefore, if total amount of magnetic flux on coils A and C, and amount of magnetic flux on coil B can be distributed equally, then the total thrust due to the brake current can remain zero.

Since the flux distribution changes non-linearly with respect to the air gap between magnets and the magnetic strength, finite element method analysis

can be applied by checking the difference on the thrust force with and without brake currents. During the analysis of this section, NdFeB-N45 magnet and 1018 type steel is used as described in Section 5.1. Similar to the determination of force ripple, multiple analysis over different positions on the motor is necessary to find the effect of brake currents. This necessity slows down the search for solution by increasing the number of analysis needed even for a single point in the problem space. In order to find solutions in a faster way, number of analysis can be reduced by an algorithm which reduces the space by finding the solutions with highest payload first, and then examines the force ripple and effect of brake currents over this reduced space.

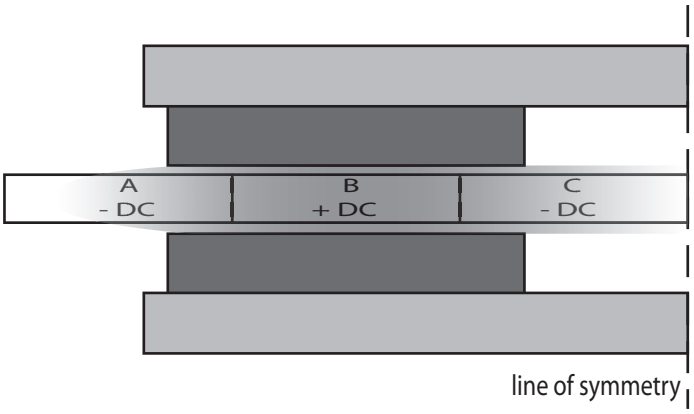

Figure 3.15: Magnetic flux and brake current distribution

As the first step, the problem space can be reduced by looking at only payload without concentrating on the force ripple and effect of brake currents. The stator is fixed in Section 3.3.1, and there are three free variables left for the air-core yoke-type mover to be optimized. The dimensions L_1, L_2, L_3 seen in Figure 3.14 should be limited first. After some initial simulations, it is seen that magnet width (L_2) should be at least the width of one coil, and at most when the distance between magnets becomes much less than the total air gap (14mm). Also, the limits for thickness of magnet and yoke are also determined. As the result of initial simulations, the limits of variables L_1, L_2, L_3 are given

in Table 3.6.

Table 3.6: Limitation of Design Variables

Design variable	Limitation(mm)
L_1	$10 \leq L_1 \leq 40$
L_2	$20 \leq L_2 \leq 60$
L_3	$10 \leq L_1 \leq 40$

An additional improvement on reducing number of analysis can be done by omitting one of the dimensions of the problem space. Instead of including all steps by analysing each of them, an optimum point can be determined faster if the non-linear behavior of that dimension can be estimated correctly. From this point of view, behavior of one of these dimensions (e.g. thickness of the yoke) can be estimated by looking at its effect on the system individually. Mostly, iron or steel with good magnetic properties are used as the core material of the yoke. Although it is not a magnetized material like magnets, it works as a low resistive magnetic conductor instead. The main problem of these soft-magnetic materials is that they show saturation near a certain flux density (mostly about 2 Tesla). This can be seen in the B-H curve of 1018 type steel which is used as the material of the yoke in our simulations. Above the saturation value, the magnetic resistance increases rapidly, and causes the flux to remain constant. The saturation problem occurs when the thickness of the yoke is decreased in order to reduce the weight of the mover. The core starts to be saturated below a certain thickness.

3.4.1 Optimization of Yoke Thickness

As given in Equation 3.5, change in magnetic flux is directly changes the thrust force. Therefore, increasing or decreasing the thickness of yoke can be thought as increasing or decreasing the thrust force respectively. Figure 3.17 shows a simulation result of the model given in Figure 3.14. To understand the

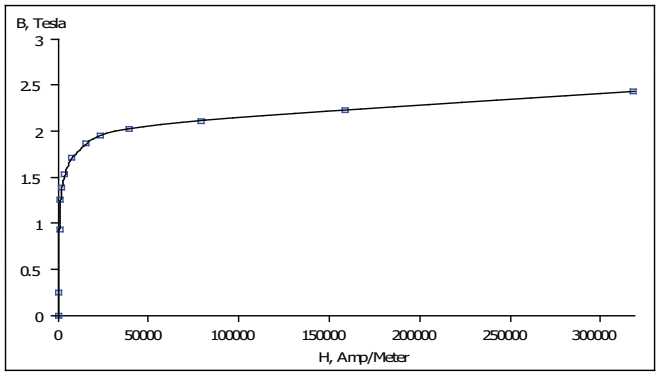

Figure 3.16: B-H curve of 1018 steel

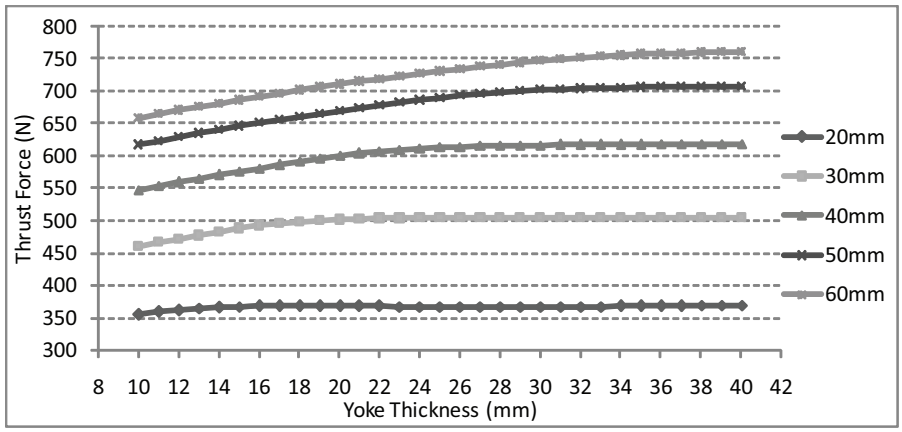

Figure 3.17: Thrust force vs yoke thickness with different magnet widths

behavior of the result, all dimensions except the thickness of yoke are fixed. It can be seen that thrust force is increasing while the thickness is increasing because there is less saturation of flux with thicker yoke. Also, it can be seen that the force remains same after a certain thickness of the yoke, because the flux density is already out of the saturation region. Therefore, to get higher flux density by using wider magnets (like 60mm width in Figure 3.17), there is need for thicker yoke to to prevent the occurrence of saturation in the core. On the other hand, thinner yoke can be used with narrower magnets because the amount of total flux through the core cross section decreases.

If the weight of the mover was not a concern, the optimal thickness of the

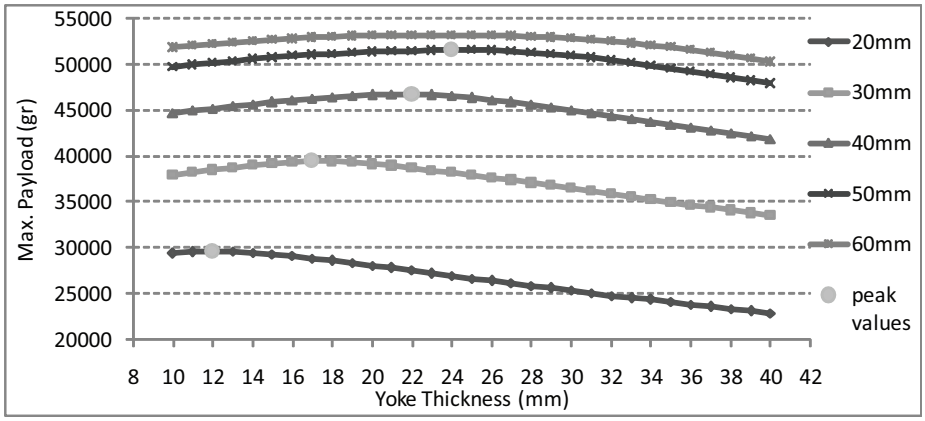

Figure 3.18: Payload vs yoke thickness with different magnet widths

yoke could have been determined by looking at the amount of flux saturation in the yoke. However, as much as thrust force (F_{thrust}), the weight of the mover (Q) is important for a motor with higher payload ($P = F_{thrust} - Q$). In this sense, there must be an optimal thickness for the yoke where the change on weight equals to the change on thrust force. As it can be seen in Figure 3.18, there is an optimal yoke thickness where the payload becomes maximum for each of the magnets with different widths. The result shown in Figure 3.18 shows us that although the effect of yoke thickness is non-linear with respect to payload, the optimal thickness can be set at the point where payload starts to decrease relative to the previous point. This behavior can reduce the optimization time by eliminating the rest of the analysis once the decrease on payload is determined. The flow chart of the algorithm is shown in Figure 3.19.

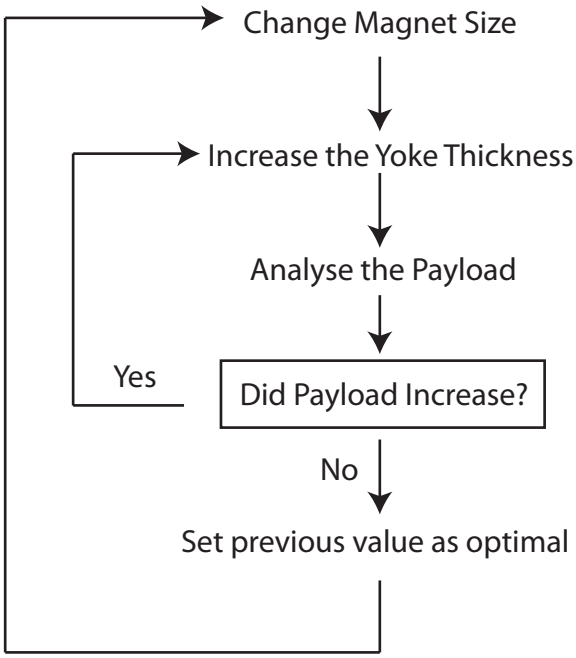

Figure 3.19: Optimal yoke thickness search

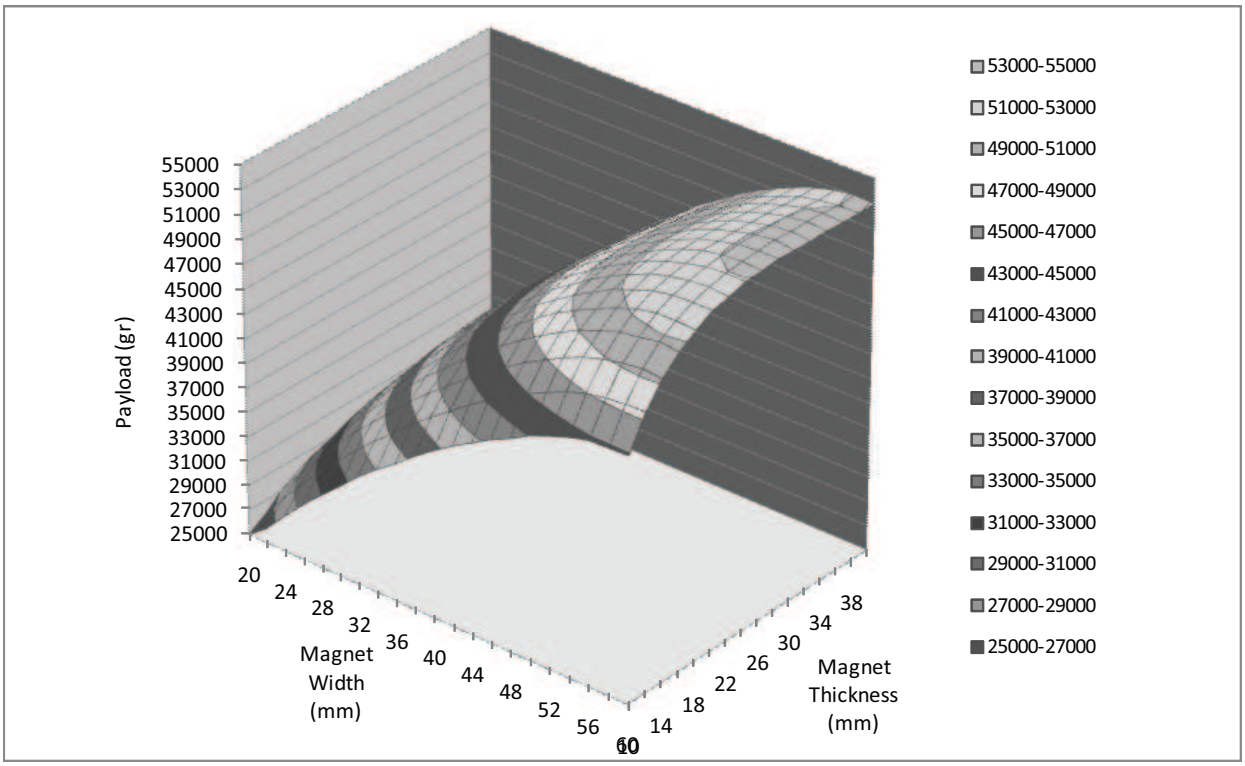

Figure 3.20: Change on payload capacity with magnet dimensions

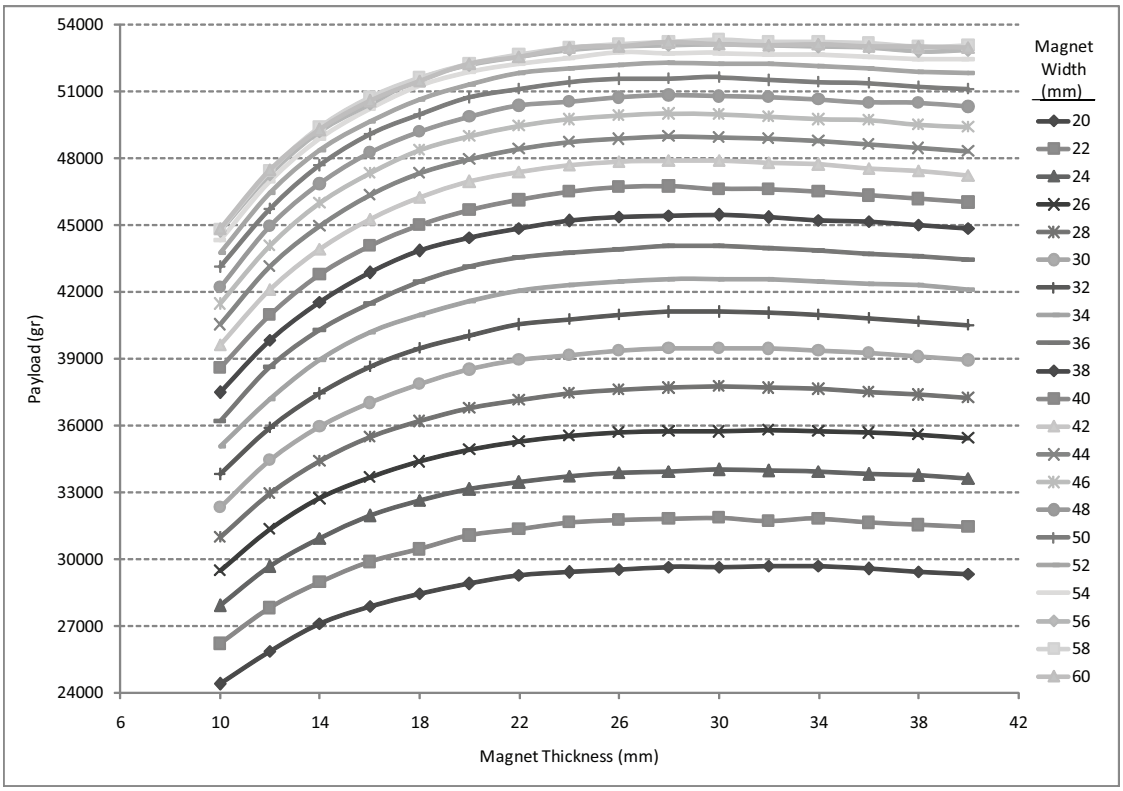

Figure 3.21: Change on payload capacity with magnet thickness

3.4.2 Optimization with respect to Magnet Width

When the algorithm that finds the optimal yoke thickness with respect to maximum payload is used, payload capacity of each magnet size with all combinations of L_1 and L_2 can be obtained. This allows us to understand how payload is changing within the limits of magnet dimensions. The result of simulation on the payload capacity with respect to L_1 and L_2 is plotted in Figure 3.20. It can be seen that the graph is in smooth convex shape and we can find the global maximum value without using complicated optimization algorithms. The smooth convex surface shows that with a fixed dimension of magnet there is a maximum payload result with only one value of the remaining dimension. For example, when the magnet width is fixed during

the analysis, there must be a unique solution for magnet thickness which gives maximum payload with the fixed magnet width. Therefore, the algorithm that searches for the convergence point to find the optimal yoke thickness can be implemented to find the optimal magnet thickness as well, because increasing magnet thickness with the optimal yoke thicknesses has the same effect on payload as increasing yoke thickness case has. The same observation can be also deducted from Figure 3.21 where the payload capacity with respect to magnet thickness is plotted in 2D for varying values for magnet widths. It can be seen that there is a convergence point where the increase on thrust force is not more than the increase on the weight of the mover. In other words, the payload stops increasing after a certain thickness of magnet and this is the optimal point. Therefore, there is no need to continue to analyse the rest of the thickness values. In this way, the same algorithm given in Figure 3.19 can be also used for determining the optimal magnet thickness. The flow chart of the expanded algorithm is given in Figure 3.22.

When the optimal yoke thickness with respect to different magnet sizes is plotted as in Figure 3.23, similar to behavior of payload, yoke thickness has a solution surface in smooth convex. Therefore, the algorithm shown in Figure 3.19 can be improved more to reduce the number of analysis.

3.4.3 Minimization of Force Ripple

Once the optimal thickness of each magnet and yoke that gives the maximum payload are found as shown in Table 3.7, and in Figure 3.24, the remaining examination which is force ripple and effect of brake currents on thrust force can be done by using these optimal values. In this way, the only variable left is the width of magnets (L_2) where magnet thickness (L_1) and yoke thickness (L_3) are already fixed for highest payload result. This is also shown in Figure 3.25.

During a movement of one electrical phase, the force obtained by the mover

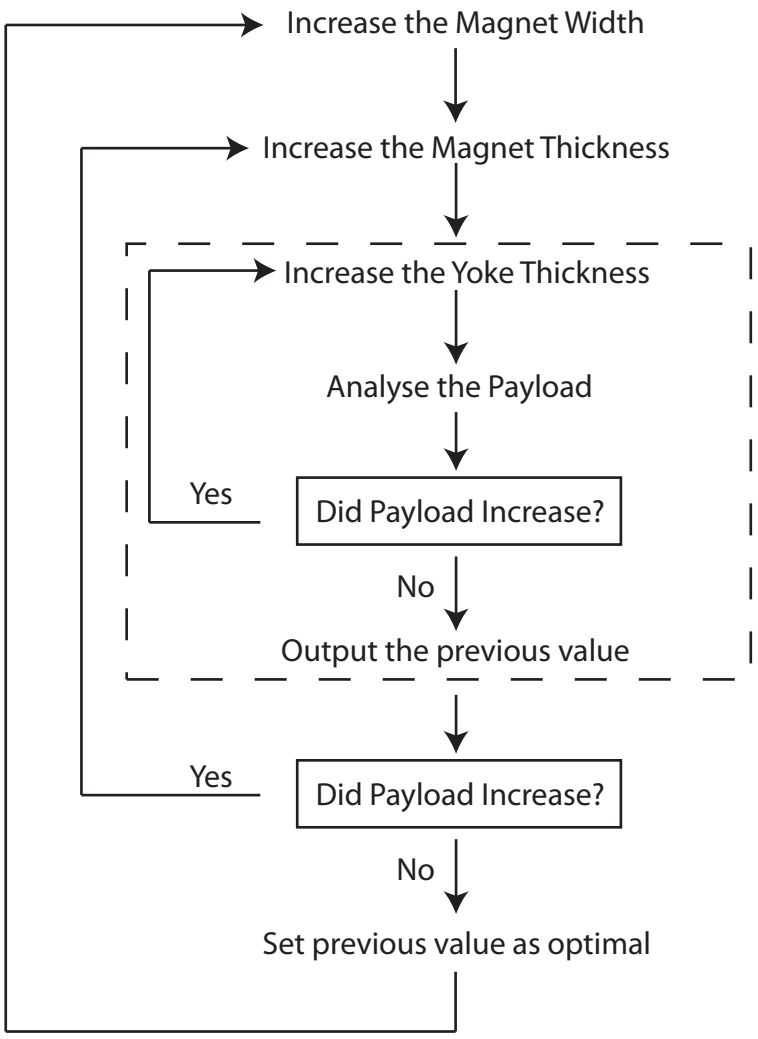

Figure 3.22: Optimal magnet thickness search

Table 3.7: Optimal values of L_1 and L_3 with respect to L_2

L_2(mm)	20	22	24	26	28	30	32	34	36	38	40	42	44	46	48	50	52	54	56	58	60
L_1(mm)	34	30	30	32	30	28	30	28	28	30	28	30	28	28	28	30	28	26	30	30	28
L_3(mm)	12	14	14	16	16	18	18	20	20	20	22	22	24	24	24	24	24	26	24	22	22

is not constant and varies with respect to the position of the mover. The reason is that the change on the amount of electric current of a coil is not equal to the change of the magnetic flux passing through the cross section of the coil. Therefore, there is an unavoidable ripple on the thrust force. Since force ripple is most sensitive to the magnet width, there is need for examining optimal

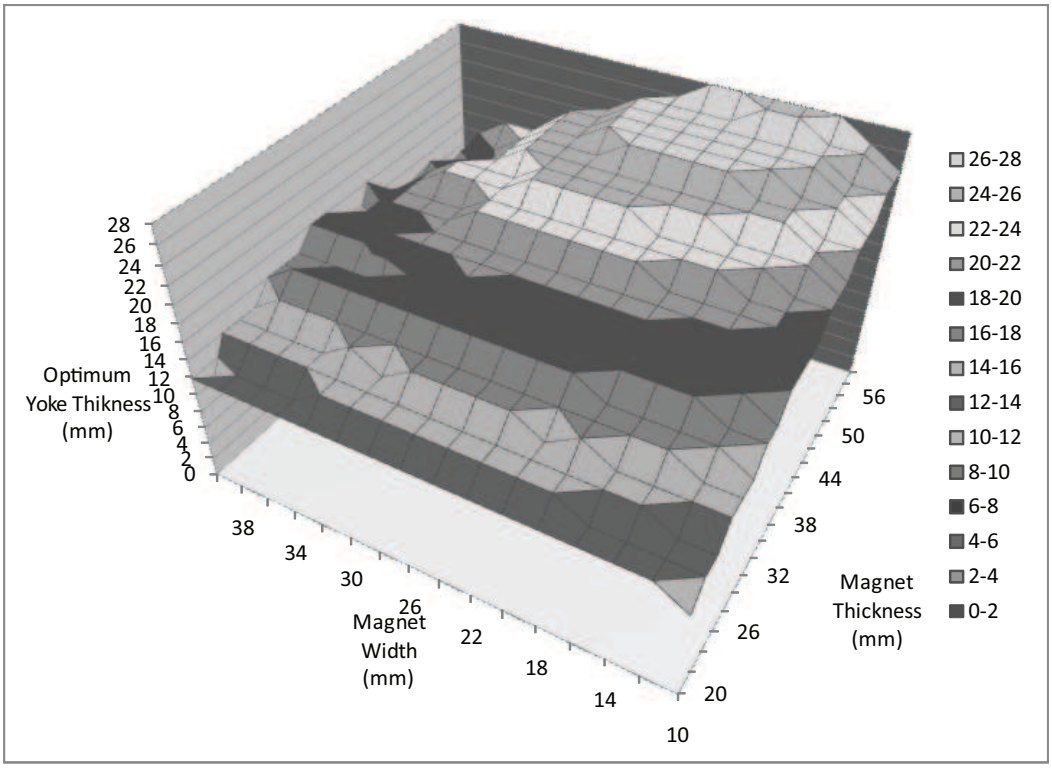

Figure 3.23: Optimum yoke thicknesses vs magnet dimensions

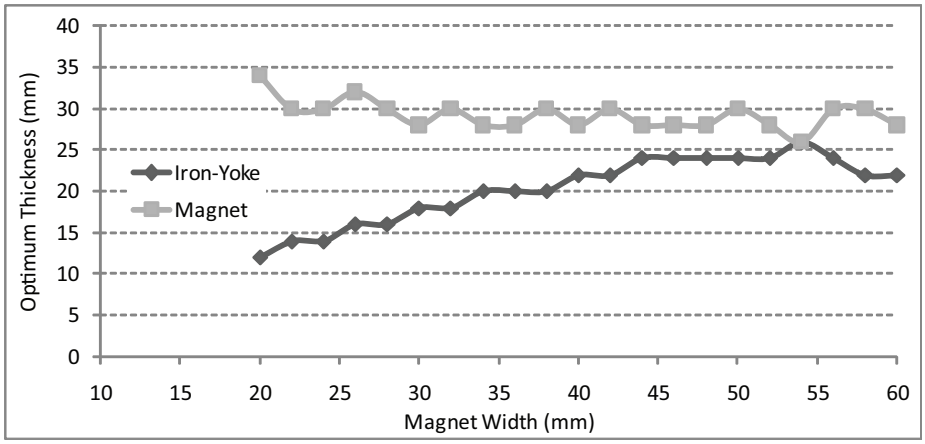

Figure 3.24: Optimal thicknesses vs magnet width

magnet widths to get reduced force ripple. The force ripple is calculated as follows:

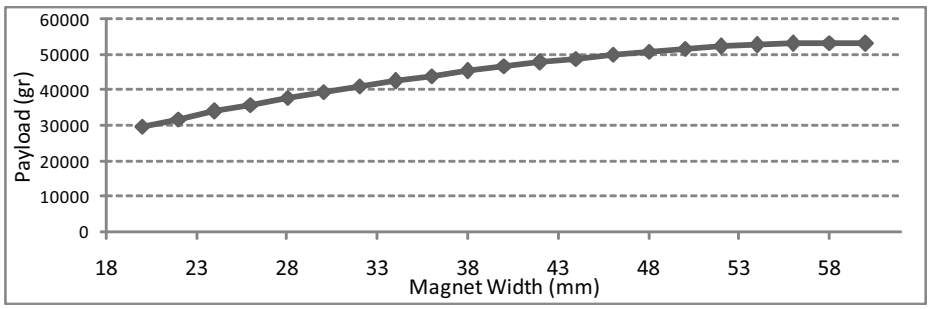

Figure 3.25: Payload vs magnet width

$$r_d = \left(\left(F_{xmax} - F_{xmin} \right) / F_{xave} \right) \times 100 \tag{3.20}$$

where F_{xmax} and F_{xmin} are the maximum and minimum forces that are obtained during the movement of one electrical phase. F_{xave} is the average of the obtained forces at all stations where force calculation is made.

The thrust force with respect to position of a single mover linear motor with three different magnet widths ($20mm$, $30mm$, $40mm$) are plotted in Figure 3.26. As expected, the force is not constant at all phase locations and a force ripple occurs during the movement. Also, it can be seen from Table 3.8 that the ripple does not remain same when magnet width is varied. While the force ripple is about %4.3 with 20mm width magnets, it can be reduced to %1.1 with 30mm width magnets, but it gets worse again to %3.8 with 40mm width magnets. Therefore, optimization for magnet width is needed for minimized force ripple.

Table 3.8: Force ripples of $20mm$, $30mm$, $40mm$ width magnets

L_2	r_d
20 mm	%4.3
30 mm	%1.1
40 mm	%3.8

The result, given in Figure 3.26, shows that the thrust force changes in

a period of 60 degrees and F_{xmax} and F_{xmin} repeat around every 30 degrees. Therefore, to reduce the number of analysis to calculate the ripple, the forces at 30 and 60 degree phases can be examined directly to find F_{xmax} and F_{xmin} instead of spanning a complete electrical phase. However, the local max and local min values may be slightly shifted. Therefore it is better to do multiple analysis around these target phases. In this way, the F_{xmax} and F_{xmin} can be found using Equation 3.22 where a can be limited as $0 \leq a \leq 5$ (deg).

$$F_{xmax} = maxF\left(i \times k + x\right), \quad -a \leq x \leq a, \quad k \in Z, \; i \in \{60, 90\} \tag{3.21}$$

$$F_{xmin} = minF\left(i \times k + x\right), \quad -a \leq x \leq a, \quad k \in Z, \; i \in \{60, 90\} \tag{3.22}$$

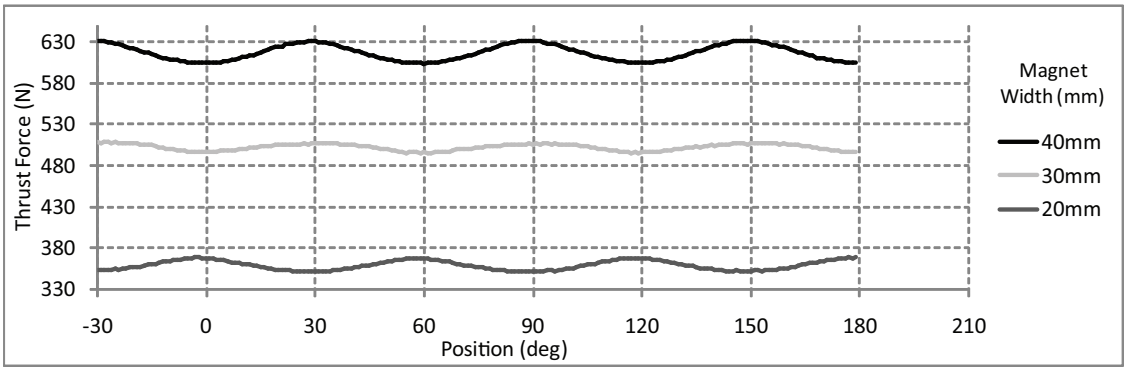

Figure 3.26: Force ripple during movement

The result of change on force ripple with respect to magnet width is given in Figure 3.27. It can be seen that there are two areas where force ripple is minimized. These local minimum values are obtained when the width of magnet is getting closer to 1.5 and 2.5 times the length of 1/6 of one electrical phase, and it can be noted that the ripple is getting worst when width of magnet is around 0, 1, and 2 times the same length. This result shows that width of the magnet should not be close to a multiple of 1/6 of electrical phase length which is $21mm$ for the examined motor.

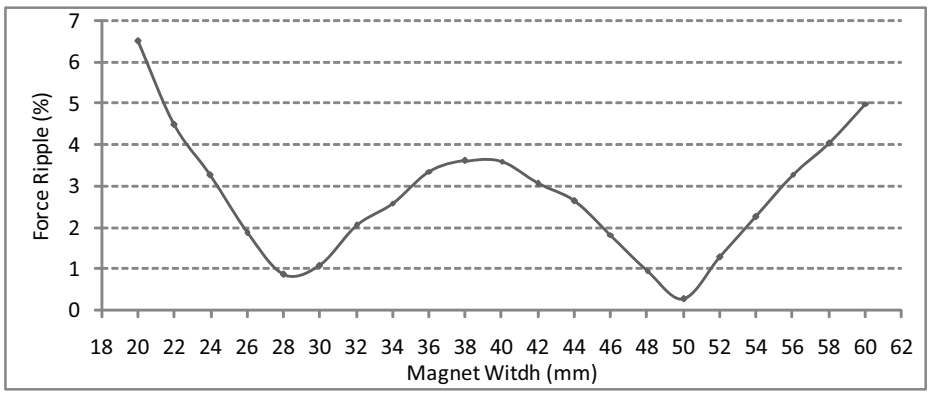

Figure 3.27: Force ripple vs magnet width

3.4.4 Minimization of Effect of Brake Currents

For actuating the safety brake, explained in Chapter 4, there are additional currents called as brake currents fed into coils additional to normal drive currents. If the design of the motor does not include the criterion about reduced distortion of brake current on thrust force, the effect of brake currents may reach high levels where the driver of the motor may not compensate the difference. Figure 3.28 shows the result of brake current effect when these currents are in amplitude of 1/3 of drive currents. As seen in Table 3.9, while brake currents distort the thrust force about %17.2 with 20mm width magnets and %9.4 with 30mm width magnets, the distortion decreases to %1.5 with 40mm width magnets. Since it varies with the magnet width, the optimal width has to be found in order to minimize the brake effect as well. As another observation, the thrust force is mostly distorted in period of 60 degrees because of the brake currents. Therefore, similar to force ripple determination, a similar method of looking only predetermined phase locations can be also applied to find the effect of brake currents in order to reduce the number of analysis. In this way, the effect of brake currents in percent (e_b) can be found using Equation 3.23,

$$e_{bmax} = max\left(\left(F'\left(90 \times k + x\right) - F\left(90 \times k + x\right)\right)/F\left(90 \times k + x\right)\right) \times 100 \tag{3.23}$$

where F is thrust force without brake currents, F' is thrust force with included brake currents. The variable x can be chosen in the limits of $(-a \leq x \leq a)$ with $0 \leq a \leq 5$ (deg) and $k \in Z$.

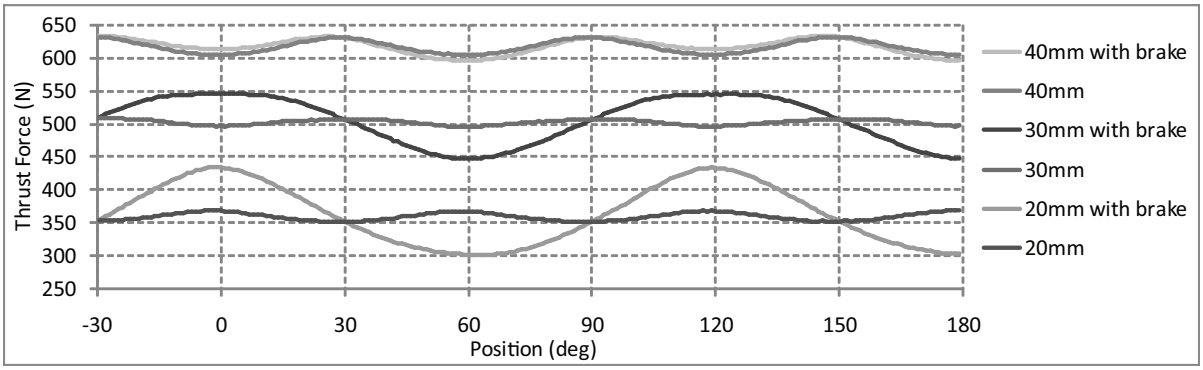

Figure 3.28: Effect of brake currents during movement

Table 3.9: Brake effects of $20mm$, $30mm$, $40mm$ width magnets

L_2	e_b
20 mm	%17.2
30 mm	%9.4
40 mm	%1.5

The calculated change on brake effect with respect to magnet width is given in Figure 3.29. It can be seen that there is a global minimum when magnet width is equal to $42mm$ which is 2 times the length of 1/6 of one electrical phase. If the only design criterion would be the effect of brake currents, it would be straightforward to determine the optimal magnet width which the length of 2/6 of one electrical phase. However, this length has a poor performance in terms of the force ripple criterion. Therefore, there is need for

an objective function to determine the final optimal design depending on the application priorities.

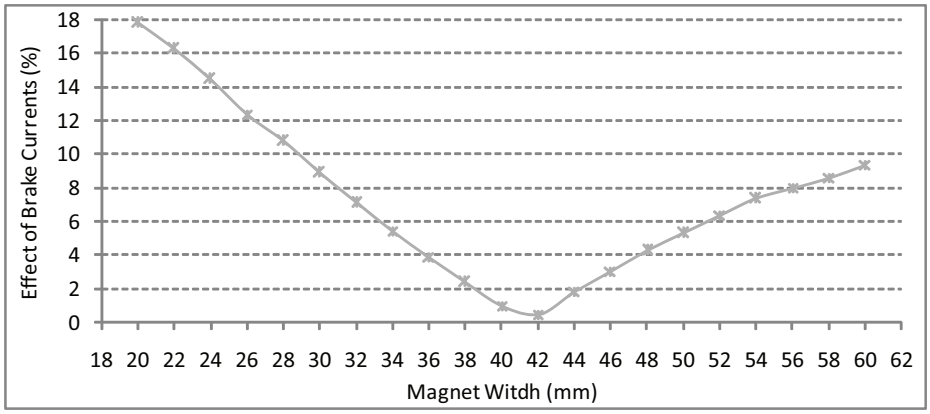

Figure 3.29: Effect of brake currents vs magnet width

By the search algorithm given in Figure 3.22, and Equations 3.20, 3.22, 3.23, the force ripple, brake current effects, and maximum payload capacity for a given magnet width can be examined in a reduced number of analysis. The result of the simulation is given in Figure 3.30.

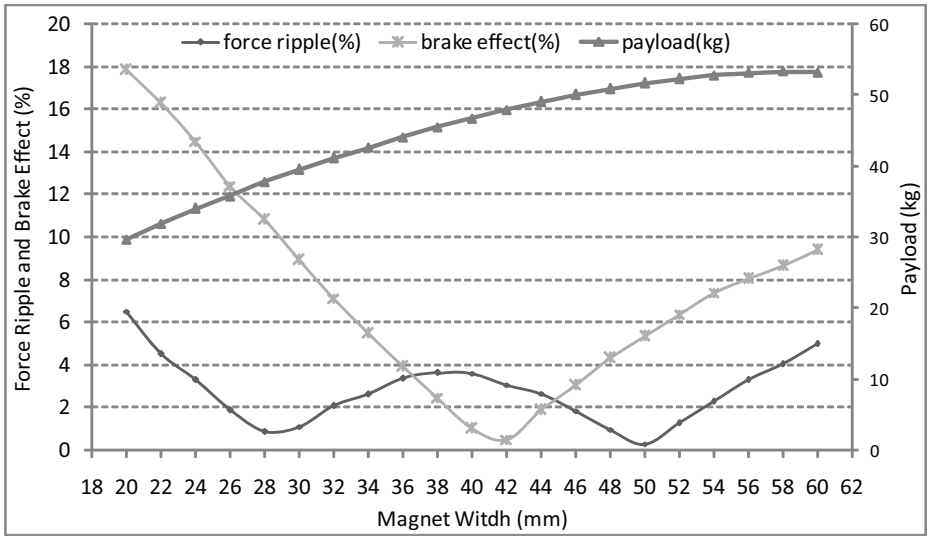

Figure 3.30: Change of design criteria vs magnet width

The cost function can be defined as,

$$W_{mw} = k_1 W_1 + k_2 W_2 + k_3 W_3 + k_4 W_4 \tag{3.24}$$

where,

$$W_1 = e_b \tag{3.25}$$

$$W_2 = r_d \tag{3.26}$$

$$W_3 = 1/P \tag{3.27}$$

$$W_4 = Q \tag{3.28}$$

The cost functions comprise the payload (P), weight of magnets (Q), force ripple (r_d), and effect of brake currents (e_b). It is important to reduce the $(1/P)$ and Q in order to reduce the running and initial costs respectively. On the other hand, it is also important to reduce the r_d and e_b, because controller of the motor may not be able to compensate high ripples and distortions on the thrust force. Therefore, a designer can choose $k_1 ... k_4$ with respect to the weights of cost and controllability of the motor.

Three example combinations of coefficients are given in Table 3.10. In Model 1, priority of payload is set highest over the others by choosing high value of k_3 relative to k_1, k_2 and k_4. In this way, the optimal magnet width that has minimum running costs can be obtained. On the other hand, in Model 2, priority of reduced force ripple and effect of brake currents is increased over initial and running costs. Also, the priority of effect of brake current is doubled over force ripple. As another example, Model 3 is configured as about equally weighted priorities except the initial cost which has slightly higher priority. A designer can create a new model with different priority level depending on the application.

The resultant total cost obtained by using the cost function given in Equation 3.24 and the coefficients given in Table 3.10 are plotted in Figure 3.31. For better visualization, the secondary coefficients (a_1, a_2, a_3) in Table 3.10

Table 3.10: Examined combinations of k_1, k_2, k_3, k_4

Model	1	2	3
k_1	a_1	$10a_2$	a_3
k_2	a_1	$5a_2$	a_3
k_3	$5000a_1$	$5000a_2$	$1500a_3$
k_4	a_1	a_2	$2a_3$

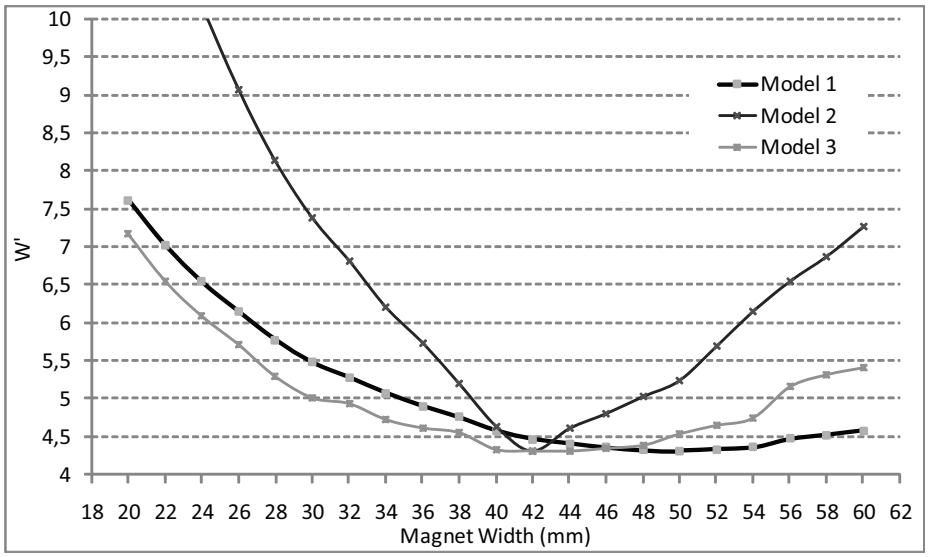

Figure 3.31: Change of total costs vs magnet width

are selected as $0.8a_1 = a_2 = 4a_3$ to scale the graphs into same range. The graph of Model 1, where payload has the highest priority, shows that around $50mm$ is the optimal width for the magnets. When Model 2, where controllability is important, is selected there is a distinct optimal magnet width which is $42mm$. Finally, Model 3 shows that when the costs of design criteria have approximately equal weights, interval between $40mm$ and $48mm$ can be chosen as optimal width of the magnet.

3.4.5 Optimization with respect to Mover Array

The analysis of a single mover, which is in length of one phase, is given in the above part of Section 3.4. To obtain higher payload capacities, n single movers can be mechanically connected to each other to sum up their thrust forces. An example mover array where four single movers are mechanically connected is shown in Figure 3.32. It would be possible to connect the mover yokes together instead of using additional mechanical connection, thus forming a single long yoke. This would slightly reduce the magnetic resistance in the path of the main flux, thus contributing to the thrust. However, the calculations which are not included here show that the increase in the weight due to the additional iron would be even greater, resulting in a net loss in payload.

To get the same thrust from all of the movers, their phase locations are equal to each other. Therefore, the spacing must be set such that they are aligned at integer multiple of a complete electrical phases. To minimize the total length of mover array, the spacing can be set to one times the complete electrical phase. Total payload capacity (P_{total}) of a mover array can be calculated as the number of movers connected (n) times the payload capacity (P_i) of a single mover as seen in Equation 3.29.

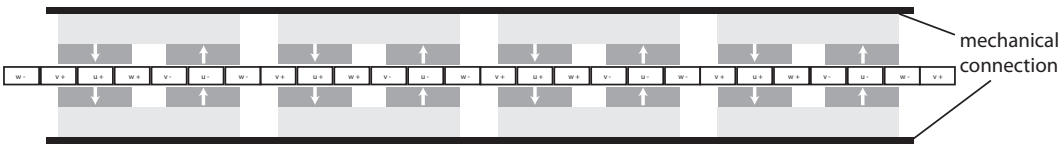

Figure 3.32: Array of 4 movers

$$P_{total} = \sum_{i=1}^{n} P_i \tag{3.29}$$

When the distance between each mover is set as one electrical phase (L_{phase}), the distance between magnets of neighbor movers (L_4) is calculated as,

$$L_4 = L_{phase}/2 - L_2 \tag{3.30}$$

where L_2 is the width of the magnets.

Since the distance between the movers, L_4 depends on the magnet width (L_2), the effect of L_4 on design criteria should be also studied in finding the optimal magnet width. The distance L_4 can be thought as the air gap between the magnets aligned in the direction of motion. Decreasing air gap means less magnetic resistance for the magnetic flux, therefore with less distance between the movers there will be more flux coupling between the magnets of neighbor movers. On the other hand, the air gap between the magnets aligned in the perpendicular direction does not change. Therefore, the leakage flux between the neighbor movers may affect the flux that passes the coils vertically.

To see the effect of distance between the movers (L_4) on maximum payload capacity, the new optimal thickness of both magnet and yoke can be found using the search algorithm given in Figure 3.22. Simulation results of different magnet widths within a mover array is given in Figure 3.33. It can be seen that maximum payload capacity of both single mover and a mover in an array remains the same until certain width of magnet which is about $48mm$ because the attraction between neighbor movers remains low. However, higher payload capacities can be also obtained by wider magnets although there is leakage flux between the movers.

Even though the payload capacity per mover can be increased more within an array, the payload per volume of magnet decreases since the optimal thickness of magnet needs to be increased when the mover is in an array instead of operating alone. The initial cost which is weight of magnet and the payload per the weight is compared in Figure 3.34 for single mover and a mover in an array. It can be seen that the ratio is better when the mover is single except at the width of magnet around $60mm$ where the motor has poor performance on both force ripple and brake effect criteria (Figure 3.30). Since the optimal

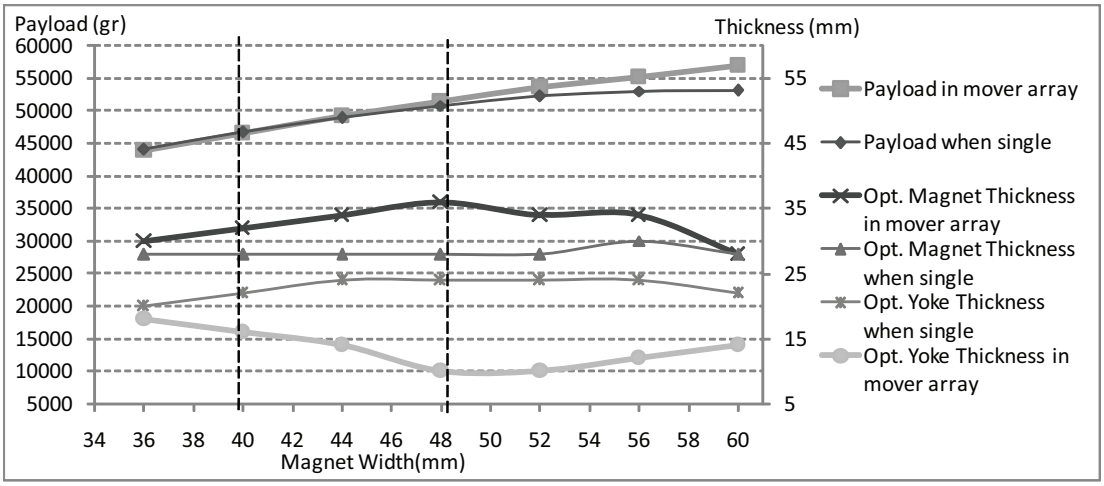

Figure 3.33: Comparison of payload and optimal thicknesses when mover is single and in an array

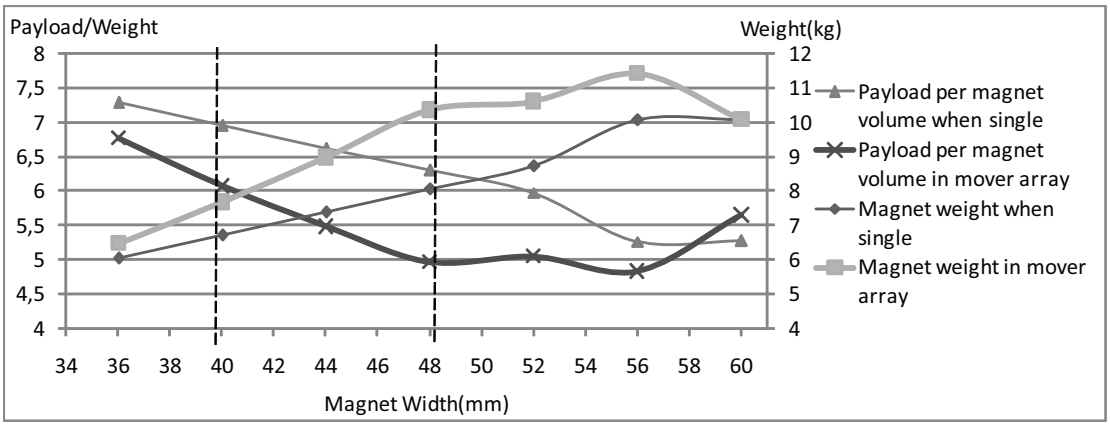

Figure 3.34: Comparison of payload per magnet weight when mover is single and in an array

interval of magnet width found by using objective models given in Table 3.10 is between $40mm$ and $48mm$, it can be seen that the optimized mover array does not give better performance over single mover.

In the interval between $40mm$ and $48mm$ of magnet width, although the optimized mover array does not perform better on payload per mover when compared with the optimized single mover, there is need for examining the

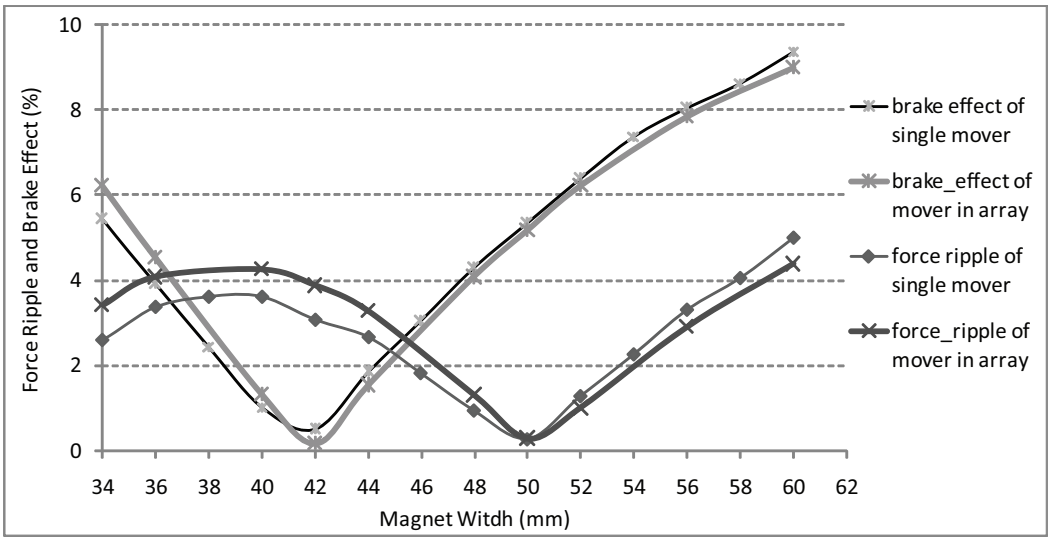

Figure 3.35: Comparison of force ripple and brake effect when mover is alone and in an array with same dimensions

performance of a single mover when used in an array. In this way, it can be understood if the optimization solved for a single mover gives satisfactory result with mover array as well. In this sense, the optimal values found for single mover as given in Table 3.7 are simulated within the mover array, and the result is given in Figure 3.35. When the single mover is used in an array but optimized as it operates alone, the force ripple and brake effect performance of a mover show similar trend with a minor change in amplitude. Therefore, even when there is need for a mover array, the method of optimization of a single mover can be still used to design mover arrays.

A mover array can consist of any number of movers connected to each other. Since magnetic flux of a mover affects the neighbor movers, the effect of movers which are at the end of the array is distributed over others. However, the mover in the middle is the least affected one from end movers, and the amount of distribution depends on the number of movers in the array. The results shown on Figures 3.33, 3.34, 3.35, are the simulation results of the middle mover which is in array of three movers. The analysis could also have

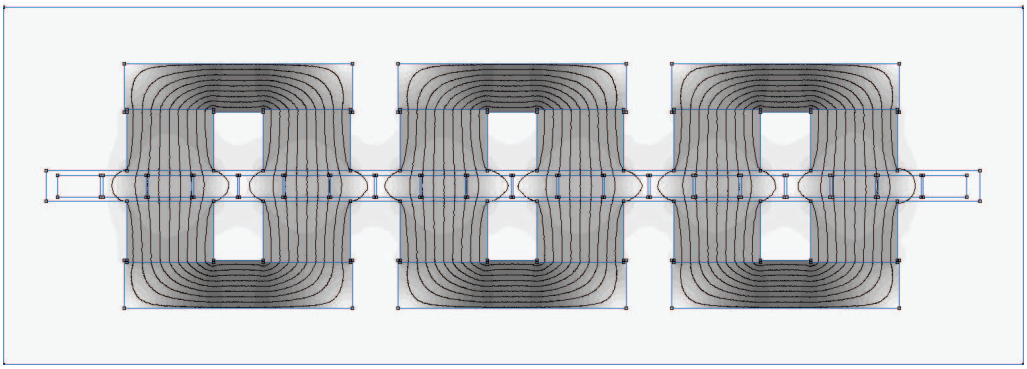

(a)

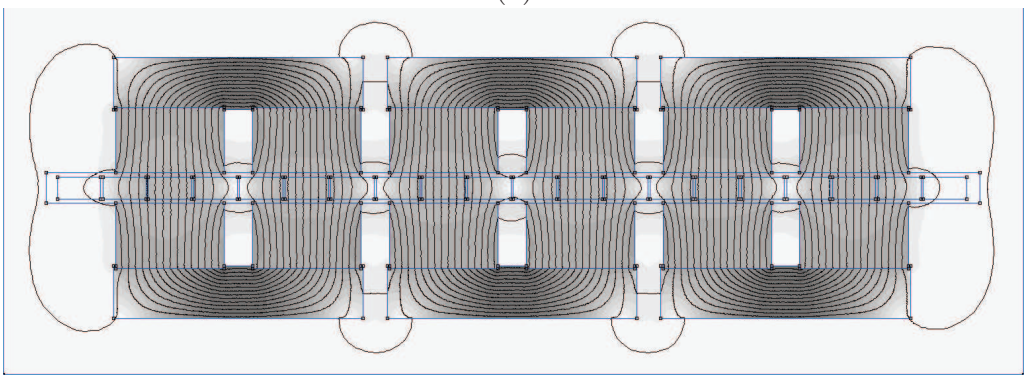

(b)

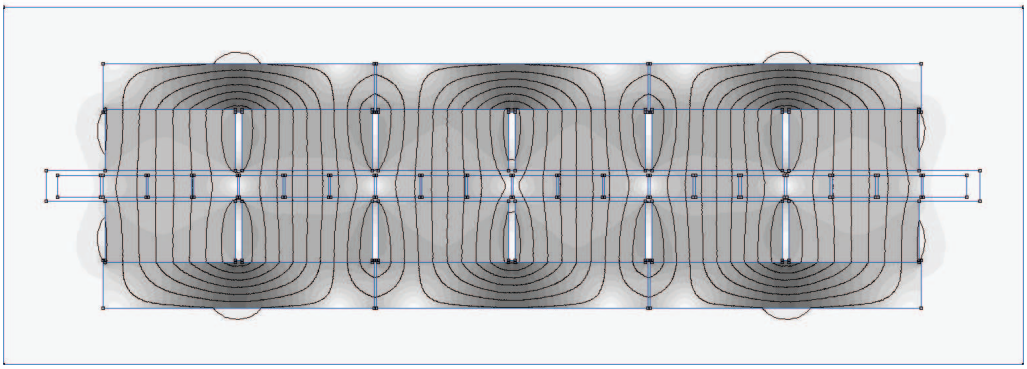

(c)

Figure 3.36: Flux density in an array of 3 movers (a)40mm width magnet (b)50mm width magnet (c)60mm width magnet

been done by using an array of more than three movers. The difference between the results of the movers in the middle of three movers array, and five movers array is examined with 42mm and 54mm width magnets. It has been seen that the difference is %0.013 with 42mm width magnet, %0.287 with 54mm width magnet. A designer can use array of three movers to shorten the analyse time instead of using arrays of more movers.

Chapter 4

Fail-Safe Design

There are two major problems to be solved for linear motor actuated multi-car elevators in order to offer them as a viable alternative for conventional elevator systems. The first one is how to prevent the elevator cars from falling when there is a problem with the propulsion system. The second is how to prevent the collision of the independently moving elevators in the same hoistway.

Usually, elevators have electromechanical brakes installed at a stationary position to stop the traction motor by locking the traction sheave in order to hold the elevator car at a desired position, or to prevent the free fall because of a failure in the power supply. However, for linear motor elevators since there is no rope to be stopped by a brake system, a similar brake device needs to span the whole hoistway to be capable of mechanically stopping and holding the elevators at any position. This solution would not be feasible especially in sense of cost compared to systems with single brake actuator. In contrast, if the electromechanical brake is installed on the elevator car instead of whole hoistway, then there would be need for transmission of signal and power to the moving car for the brake actuator. This transmission is also not feasible because it requires cables that need to travel with the car and it does not fit with the ropeless and cableless design criterion.

One solution can be keeping the electrical part of the electromechanical

brake that needs signal and power on the hoistway side and putting the mechanical part of the brake on the moving car. In this way, the problem of signal and power transmission for brake actuation can be avoided. However, if the electrical part is kept at hoistway side, it would be still not feasible because of the cost of a separate, long actuator device along the hoistway. Instead, there is already a long device spanning the hoistway which is the stator of the linear motor used for propulsion (Section 3.2). Therefore, the long armature can be also available to serve as the actuator for the brake device if it is designed in this way.

The following Section 4.1 shows how the long armature can be used as the actuator for the brake device. Then, in Section 4.2, working principle of the mechanical part of the brake is shown. Finally, how the motor can be driven including fail-safe device and how to avoid collision of independent cars by using the same device is shown in Section 4.3.

4.1 Linear Motor Coils as Brake Actuators

As a general approach, linear motor coils are used only for obtaining thrust force. As described in the beginning of Chapter 4, the long armature which is the stator of the motor can be also a solution to avoid necessity of installing a new long armature as actuator solenoid for brake device. In this way, the linear motor coils which are already installed for propulsion can be used without additional cost for brake device.

As a unique feature, coil top of the linear motor coils can be used as the actuator solenoid of the brake device as discussed in Section 4.1.1. It is shown in Figure 4.1 that while two flat sides of the coil section is used for generating thrust force, one of coil top side of the same coil section can be also used for generating a brake release force that can be used to actuate the brake device. The idea is generating independent force vector components by the same linear motor coil, as in *e.g.* the decoupled control method [10], since

separate magnetic field structures are used for different tasks. Theoretical analyses and experimental results of this approach are given in the following Sections 4.1.1, 4.1.2, and Cahpter 6 respectively.

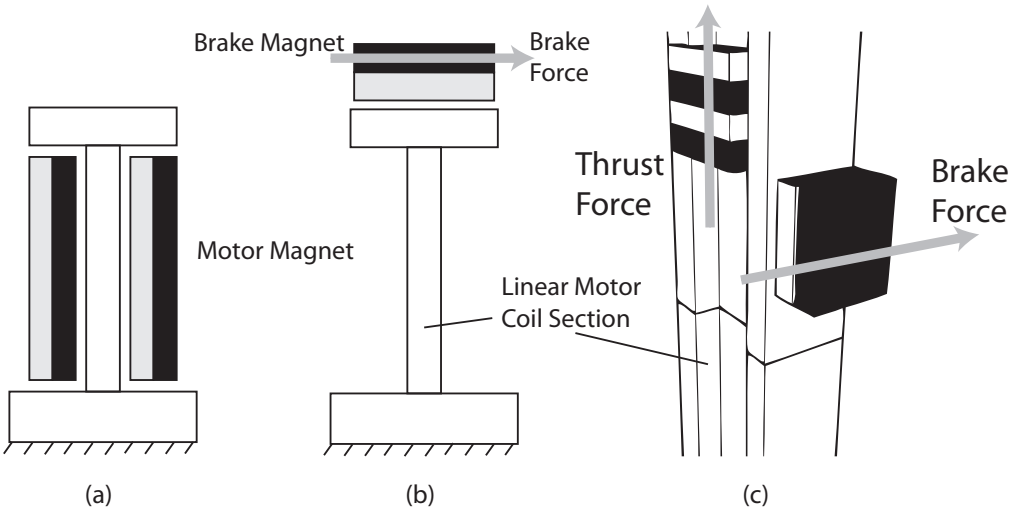

Figure 4.1: The safety system using coil sections as brake actuators (a) Thrust force with motor magnets on sides (b) Brake force with brake magnets on coil top (c) Thrust and brake force together

4.1.1 Magnetic Field of the Linear Motor Coils

In Section 4.1, it is declared that separate magnetic field structures on the stator are used for different tasks which are generating thrust force for propulsion and generating brake force for actuating brake device. In order to analyse the magnetic field around the stator, the magnetic field of a single coil and the total of magnetic field on a coreless 3-phase coil assembly should be considered.

The coils of the motor as shown in Figure 3.4 lie in the central symmetry plane of the assembly and their shapes can be approximated as a rectangular coil. For the case of a rectangular coil with its winding along the path L, the magnetic field generated by the current I_L at a point $\mathbf{r}$ in the absence of magnetic material can be calculated directly from Biot-Savart's law.:

$$\mathbf{B}(\mathbf{r}) = \frac{\mu_0 I_L}{4\pi} \int_L \frac{\mathbf{dL} \times (\mathbf{r} - \mathbf{x})}{|\mathbf{r} - \mathbf{x}|^3} \tag{4.1}$$

In [15] there is an explicit formula integrating Equation 4.1 for coplanar rectangular coils, which is a good approximation of one segment of the 3-phase coreless linear motor coil. By using these formulas, the magnetic field distribution in the vicinity of the coil edge can be obtained.

For the case of identical DC currents injected into each coil where $i_a = i_b = i_c = \text{const.}$ in Figure 4.2, the field is shown in Fig. 4.3. As seen from this illustrative example, the field distribution near the coil top is similar to the field around a single long straight conductor. Therefore, if a permanent magnet is placed in the vicinity of the coil, with one pole facing the coil top surface, there will be predominantly a sideways force acting between the coil and the magnet, which can be used for brake operation.

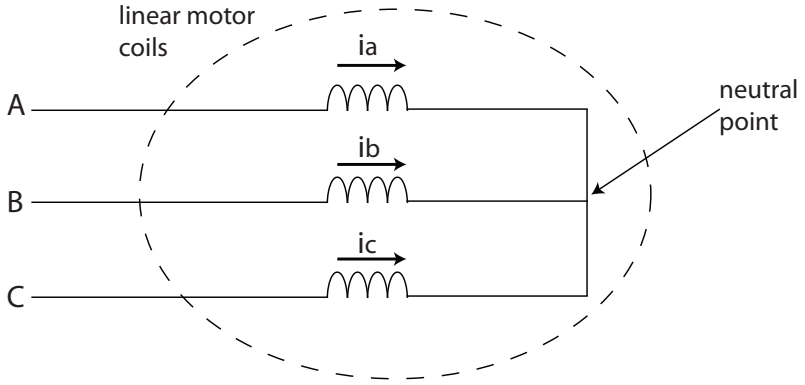

Figure 4.2: The currents i_a, i_b, i_c injected into 3-phase coils

When the coils are fed balanced 3-phase currents, the force on a magnet spanning at least one pole-pair will balance out, with the net force near zero. When DC bias currents are superposed on each phase, their contribution will add up to a net force, that can operate the brake. Thus this superposed DC current is available as an independent control variable, that directly operates the brake.

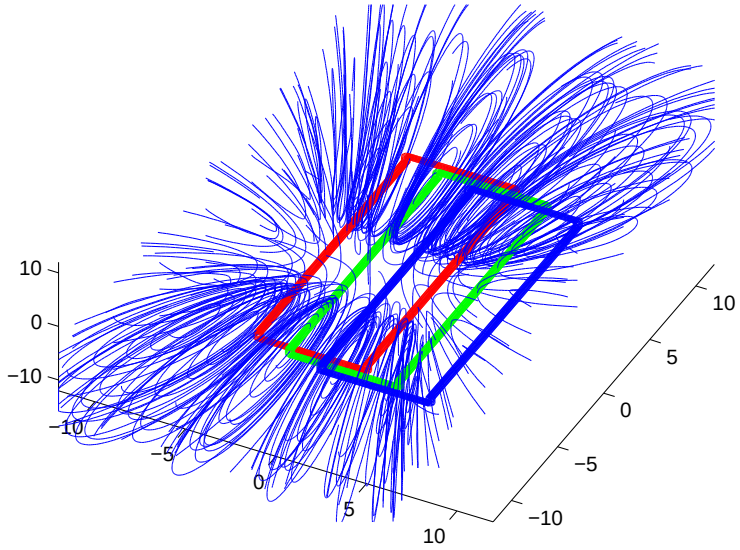

(a)

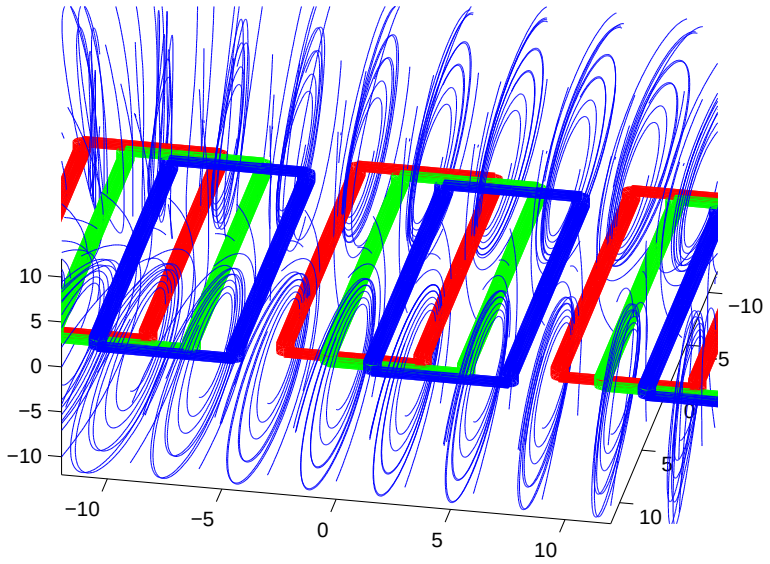

(b)

Figure 4.3: Field distribution from Biot-Savart's Law (a) field distribution on 1 pole (b) field distribution on multiple poles

4.1.2 The Effect of Winding Pattern

A problem may be encountered in implementing the brake actuator in practice because the field distribution of a linear motor stator depends on the actual winding pattern of the coils. The analyses given in Section 4.1.1 is applied for the case of identical coils arranged at 120^o electrical degrees, which can be called as "balanced winding". This winding pattern is shown schematically in Figure 4.4-b where i_a, i_b, i_c are the three phase currents. Note that the actual coil shapes are different, e.g. the coil sides lay in the same plane, and the top edges of the coils have complex 3 dimensional shapes. The details of the physical shapes of the coils is given in Figure 3.5-c.

Different from balanced winding pattern, the common winding method for linear motors has another composition as two phases are wound at 120^o degrees, but the third phase is placed at the 60^o position, and fed a reversed current, as shown in Figure 4.4-a. The advantage of this arrangement, which can be called as "segmented winding", is the convenience in separating the winding into sections, without causing end effects, thus simpler to manufacture.

For the segmented winding, the total coil top field is non–zero during normal running when driven with balanced currents $i_a(t) + i_b(t) + i_c(t) = 0$, since the top field of the 60^o coil will be opposite of the other two phases. It is possible to cancel the stator top field by supplying a special non–balanced current vector satisfying,

$$i'_a(t) + i'_b(t) - i'_c(t) = I_{DC} \tag{4.2}$$

where i'_c is the current in the 60^o coil, and I_{DC} is a constant current. One simple solution to this is to set the new currents such that,

$$\begin{aligned} i'_a(t) &= i_a(t) + 2i_c(t) + I_{DC} \\ i'_b(t) &= i_b(t) + 2i_c(t) + I_{DC} \\ i'_c(t) &= 3i_c(t) + I_{DC} \end{aligned} \tag{4.3}$$

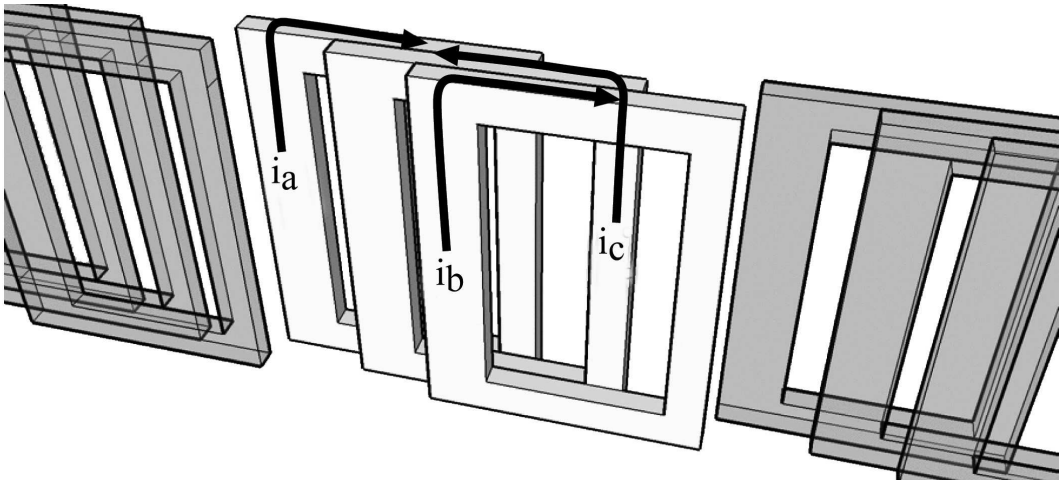

(a)

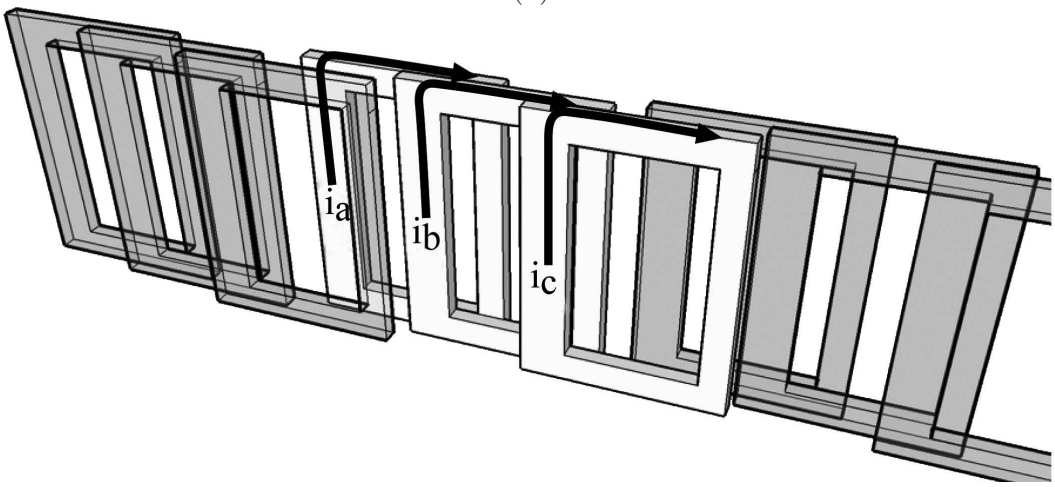

(b)

Figure 4.4: Winding patterns (a) segmented winding pattern (b) balanced winding pattern

Note that the non–balanced currents require that the neutral point of the motor be tapped.

On the other hand, for balanced winding type stators during normal running with balanced currents, the average current generating the coil top field is zero. If the neutral point of the motor winding is tapped to sink a DC current component through all coils, which can be called as brake current I_{brake}, supplied through the motor terminals, the average current vector now becomes nonzero for *any* value of I_{brake}. The current patterns on the straight parts of the coils are the same for each type of stator, but the current has a DC offset.

Using this method, the brake currents can be created independently of drive currents. The total brake current that creates magnetic field on the stator top can be calculated as:

$$I_{brake} = i_a(t) + I_{DC} + i_b(t) + I_{DC} + i_c(t) + I_{DC} \tag{4.4}$$

where $i_a(t) + i_b(t) + i_c(t) = 0$ are normal balanced drive currents. Therefore, I_{brake} is simply equal to $3I_{DC}$.

The balanced winding is better suited for a safety brake operation on linear motor elevators since generating a coil top field requires a special current pattern. The segmented winding on the other hand will generate a zero coil top field in one special case current. In case of emergency where the motor or the motor driver is damaged or power is lost, there is a larger set of possible failure modes in which the balanced winding will not be able to provide the special current pattern and thus the brake will engage to arrest the fall of the elevator car.

The effect of winding pattern on the coil top field can also be observed in Figures 4.5 and 4.6 where the currents flowing through the top of segmented and balanced motors are shown respectively. These figures denote the current at the instant when the amplitude of $|i_c|$ is maximum ($= 2I$) and those of $|i_a|$ and $|i_b|$ are half($= I$). During normal operation, a net virtual current vector is present for the segmented winding, whereas it is zero for balanced winding

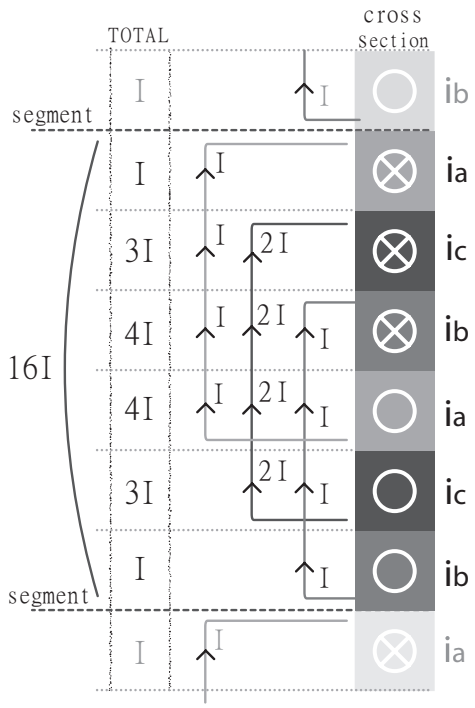

Figure 4.5: Plan view of the segmented winding stator for one electrical phase (Figure 4.4-a)

stators.

Calculated DC currents necessary for different brake operations are given in Table 4.1. For balanced winding, since the system is set up in such a way that brake is engaged for zero brake current and disengaged when brake current exceeds a certain value, another advantage is that there is no need to supply brake current when the elevator car must be stopped.

Table 4.1: DC currents for different operations

Elevator	**Driven (lifting)**	**Brake Active**	**Segmented Winding**	**Balanced Winding**
Moves	Yes	No	$(4i'_a - I_{DC})/3$	I_{brake}
Stops	Yes	No	$(4i'_a - I_{DC})/3$	I_{brake}
		Yes	$4i'_a/3$	0
	No	Yes	0	0

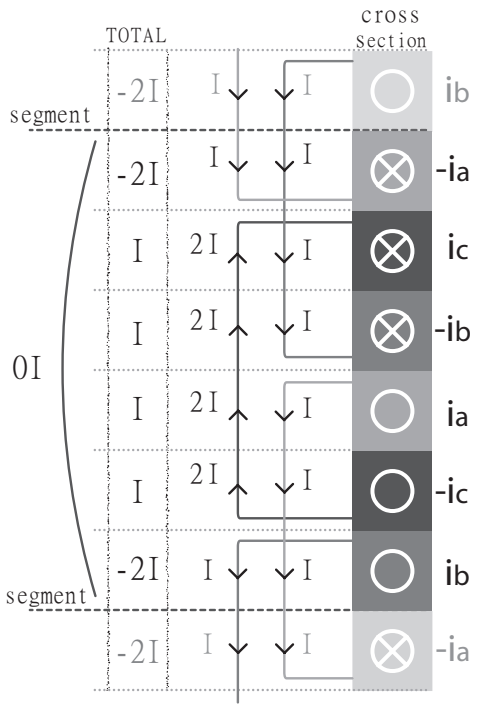

Figure 4.6: Plan view of the balanced winding stator for one electrical phase(Figure 4.4-b)

4.2 Mechanical Part of the Brake Device

It has been shown in Section 4.1 that the coil top can be used as the actuator solenoid of an electromechanical brake. It has been detailed in Section 4.1.2 that by applying suitable currents in addition to standard drive currents an independent force vector component can be obtained apart from lifting force. This additional force which is independently controllable can be used to drive a mechanical brake that is capable of stopping and holding the elevator cage at any position.

There are two ways to use the additional force for brake operation. One of them is activating the brake operation in order to stop the car; on the contrary the other one is releasing the brake operation in order to allow movement of the car. The electromechanical brakes as a safety device in elevator systems uses the force in the second way which is releasing the mechanical brake. In

this way, it can be guaranteed that in case of power failure fall of the elevator can be avoided by the self locked brake device since there will be no force to release it which requires electrical power. Similar safety method can be also applied for linear motor elevators where the brake device will be always locked except when it is released with a continuous counter force. The illustration of such a brake device is given in Figure 4.7. A brake shoe which is connected to a prestressed spring creates friction on a brake plate, and it can be released by the force on opposite direction obtained at the coil top.

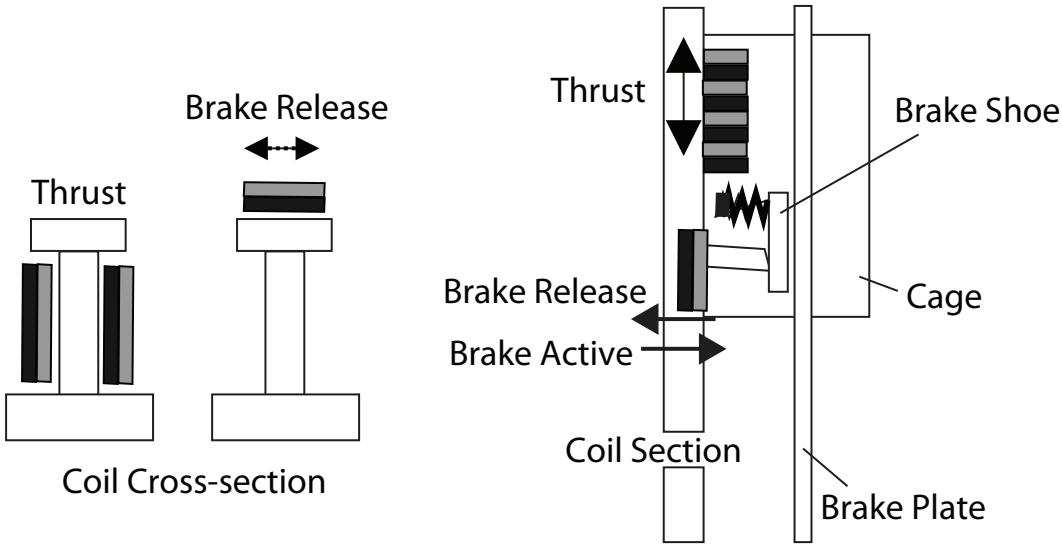

Figure 4.7: Illustration of mechanical part of the brake device

Amount of friction on brake shoes needs to be high enough to hold the weights of cage and passengers safely. In this way, the brake shoes should be highly prestressed in order to create enough friction force. However, releasing a highly prestressed brake device may not be possible with a small force obtained by brake magnets aligned at the edge of the coils. Therefore, there is need for a mechanical gain to increase the actuation force for releasing. Furthermore, since there is no counterweight in the system to balance out the weight of the cage, there is always downwards loads that can be taken as an advantage in designing the brake device.

The brake system that has been tested as the proof of concept is given in Figure 4.8. The special magnetic field produced at coil top moves the magnet plate which is connected to the brake shoes which are designed as calipers. The friction force between the brake shoes and brake plate can be increased dramatically by using these calipers that can turn the weight of the cage as a positive feedback, to friction, instead of the force obtained by the prestressed spring. In other words, the main holding force of the system comes from the weight of the motor sitting on the appropriately angled brake pads, producing the friction. The coil top force only needs to begin engaging the brakes.

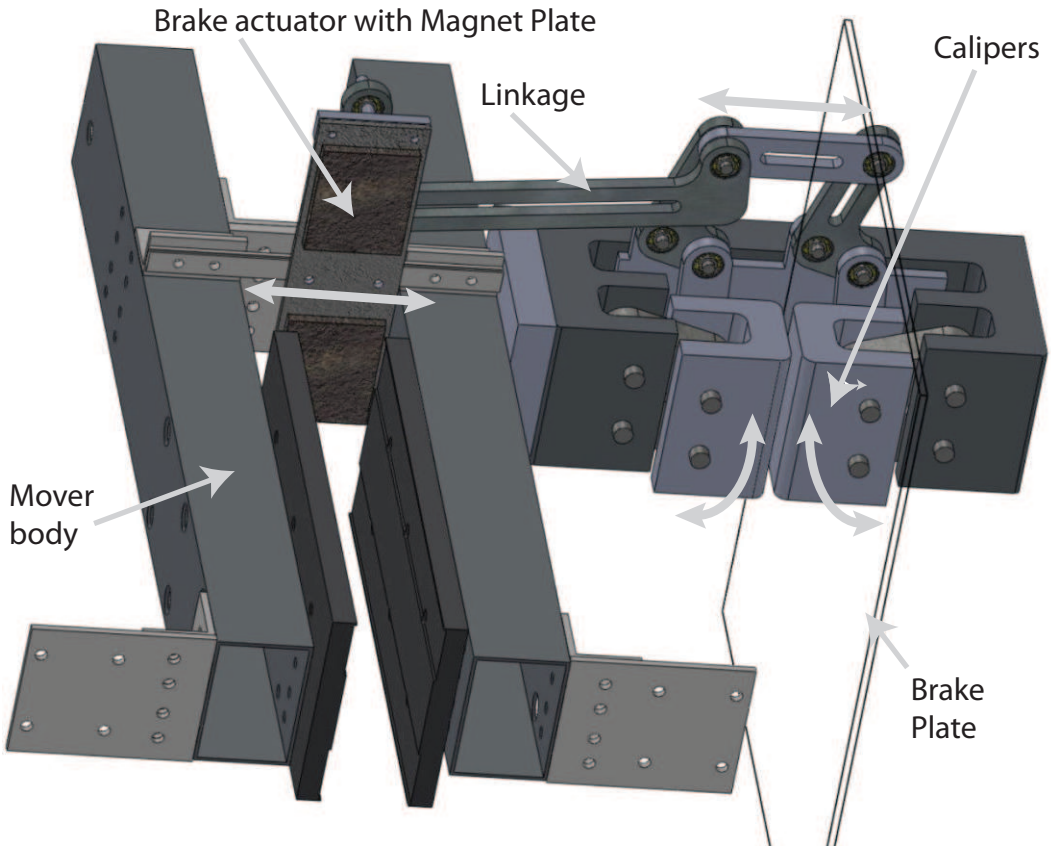

Figure 4.8: Implemented Brake Device

With this mechanical arrangement, when the weight of the elevator car is sitting on the brake, the brake release force supplied by the brake magnet will not be sufficient to release the brake. This is actually one more safety

feature, preventing the inadvertent release of the brake when the car is not supported by the linear motor thrust. Thus the normal sequence of operation will follow the sequence, in both up and down directions; while the car is supported mechanically by brake force, motor thrust is supplied to neutralize car weight first. Then, motor moves car slightly up in order to disengage brake and that time brake release current is supplied to open the brake. As a normal operation, car starts and runs to next stop. When car is fully stopped at the desired destination, brake release current is cut again. Car slowly descends to fully engage the brake, therefore thrust can be removed, and car now supported by mechanical brake again.

In designing such a brake device as given in Figure 4.8, two important criteria are that length of the magnet plate should be an integer multiple of the length of one electrical phase of the motor (see Section 4.1) and the amount of the prestress force should less than brake force can be obtained by the magnet plate but high enough to start the engaging the brake.

4.3 Drive of the Motor and Fail-Safe Device

4.3.1 Modified Motor Drive for Brake Operation

Considering the balanced winding pattern, it becomes clear that using conventional 3-phase motor drives with standard bridges and vector control, it is not possible to supply I_{DC} currents to each coil since the motor neutral point is isolated. One solution is using an additional switch for the common point to ground or DC link shown in Figure 4.9. The basic idea is that different parts of one PWM cycle will be used for lifting and braking.

A typical PWM period T may be divided into the time intervals where V_{0^o} currents are active (T_2), V_{60^o} currents are active (T_3) and no currents flow (T_1). For the proposed brake operation, an extra time interval (T_0) for brake currents can be added as shown in Fig. 4.10. When T is replaced by $T - T_0$, the general formulas for vector control can be still used without modification.

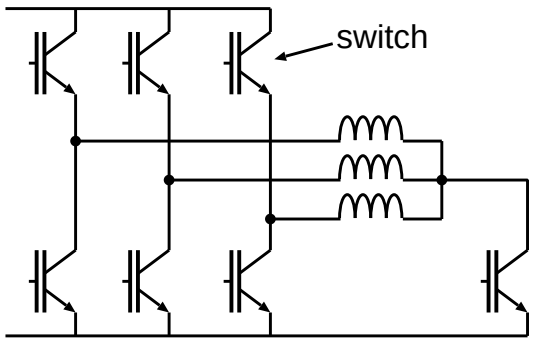

Figure 4.9: Suggested motor driver for brake operation

The brake current timing T_0 can be calculated as:

$$T_0 = I_{brake} \times T / I_{max} \tag{4.5}$$

where I_{max} is determined by the motor dynamics.

Using these equations, the generated PWM ratios and current patterns can be seen in Figs. 4.11 and 4.12 respectively. They are familiar PWM and current waveforms, except being shifted appropriately.

4.3.2 Position Control Method

Control systems for linear motor elevators can be designed by making use of some specific properties of the problem.

First of all, in contrast with the traditional elevator systems, where the unbalanced load of the elevator car and the counterweight could point either upwards or downwards, there are always downwards loads in multi-car system because of absence of the counterweight. The system thus operates only in two quadrants, "motoring upwards" or "generating downwards". Furthermore, the weight of the elevator car together with the mover provides a substantial base load, even with an empty car. This property provides the sufficiency of using a simple position control loop, without considering the switching between quadrants, as during one trip the system always operates in a single quadrant.

It is also important to make the system robust in the event of degraded

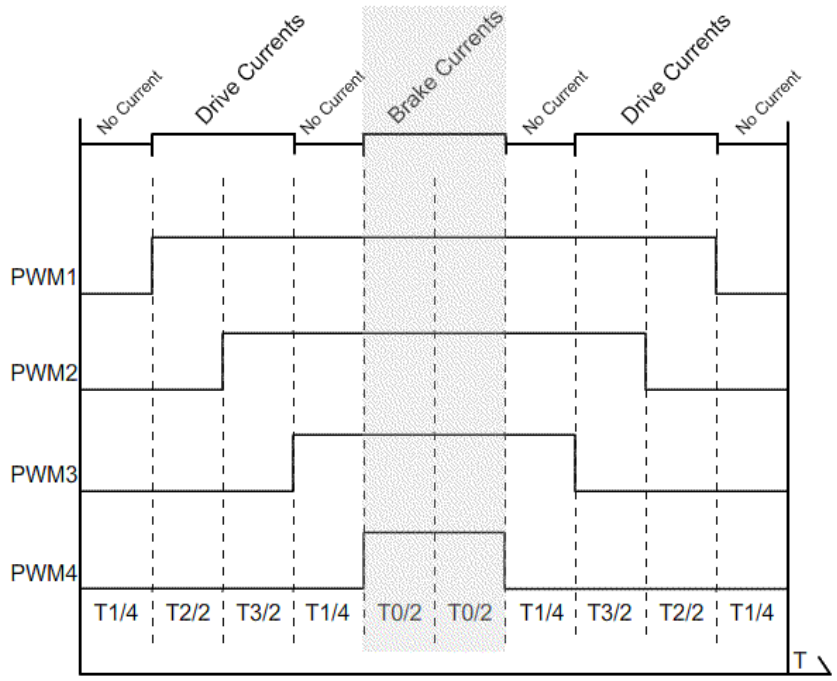

Figure 4.10: PWM timing diagram for brake operation

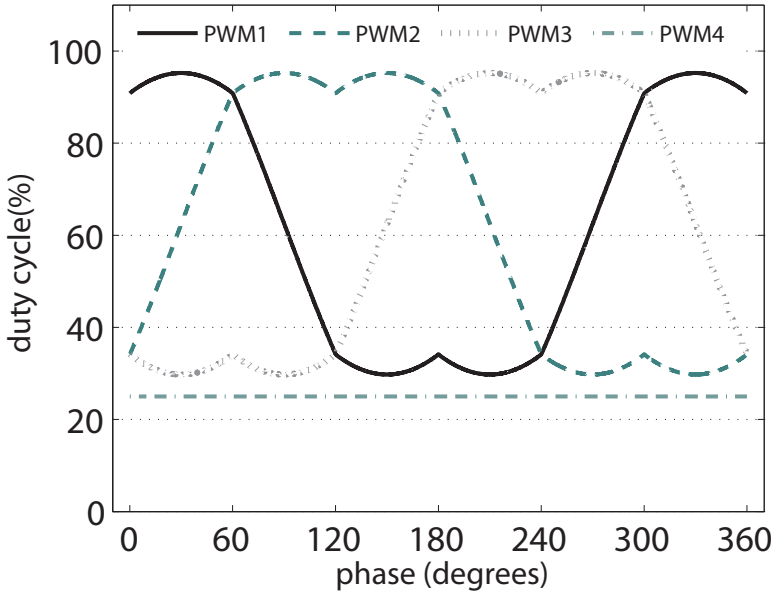

Figure 4.11: PWM waveforms for brake operation

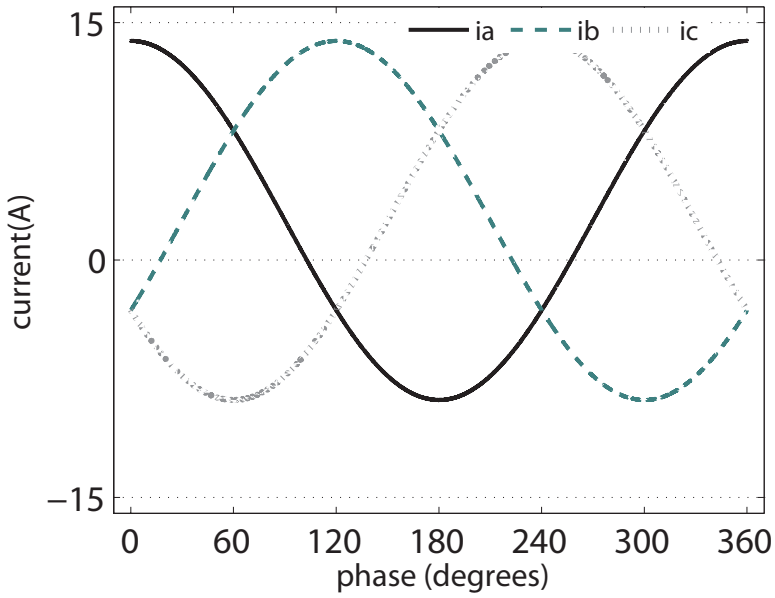

Figure 4.12: Current waveforms for brake operation

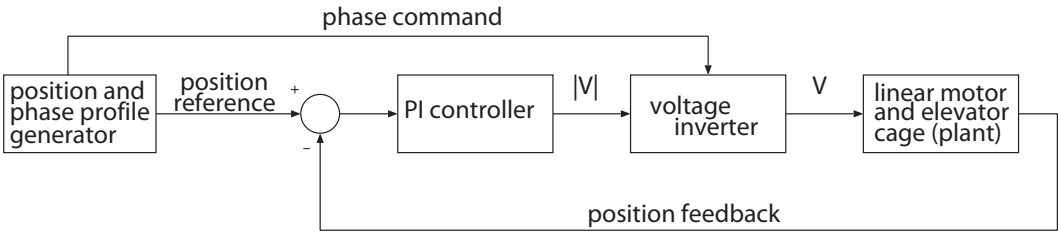

Figure 4.13: Block diagram of the position control system

signal quality for the position signal, which might occur with any of the position sensing methods. Therefore, the phase of the armature current can be dictated, similar the case of open-loop control, and control only the current amplitude. In the case of deterioration of the position signal, the current amplitude command can latch up to the allowed maximum, and the elevator can continue its trip under open-loop operation.

The schematic block diagram used in the experimental setups is shown in Figure 4.13.

As it is seen in the diagram, the usual nested current and speed control loops are disposed, and instead only the position is controlled, through the

inverter voltage command. This kind of a setup has the advantage of implementation on a processor with relatively low computing capacity. Reduced computational load is needed since there is also need for distributed control system, discussed in Section 4.3.3, which also requires some computational source of the processor.

The test results are given in Section 6.2 that this control system, in spite of its simplicity, can still achieve sufficient performance levels.

4.3.3 Distributed Drive for Cars and Collision Problem

The linear motor is designed to be driven in a modular way such that an arbitrary length of motor can be produced and multiple elevator cars manipulated independently. The simplest method for driving such a motor is to implement a centralized control scheme where each module is directly connected to a central controller. However this approach can only be applied to a limited number of movers in the system. Therefore, control of the movers should be shared across local controllers instead of one master controller.

The motor modules must be driven separately, but with certain coordination. If a mover is going to traverse a certain part of the motor, relevant segments along the way must be allocated and deallocated as necessary with a predetermined timing to avoid collisions as well as allowing for high utilization of segments. Such coordination can be either central or decentralized.

Although driving one module of the motor in isolation is not difficult, the synchronization of the electrical phases of several modules can be problematic in terms of timing requirements. By using a real-time computer network, control of the movers can be coordinated by distributed control. During the experiments, it is chosen to use a central coordination mechanism for simplicity, however for scalability it can be switched to a distributed mechanism having the architecture shown in Figure 4.14. Starting from the right column in the figure, the motor which is physically one piece is electrically divided

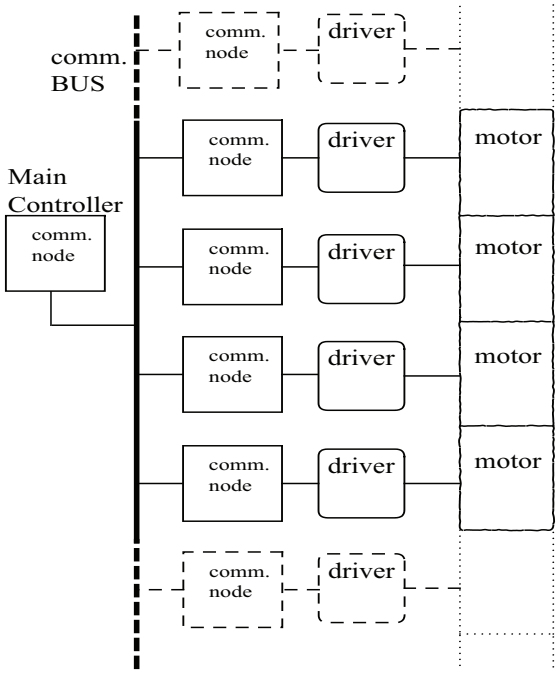

Figure 4.14: Linear motor control over a communication network.

into modules. Each module has its own driver and controller, communicating over a network satisfying the timing requirements. To move an elevator car in a multi elevator system, from one floor to another, first, segments of the motor between these locations are checked to be available by a central coordinator, then they are reserved for this motion, and finally the cage is moved by the coordinated interaction of all of the controllers in the reserved region.

Reservation of modules to only one car by a central coordinator is an important method to ensure that two cars are not accidentally driven into each other. The brake device discussed in Section 4.2 can also be used to construct a such safety system for the collision problem, by using the mechanical brakes on each elevator and controlling the actuator force of each section of motor. In the case of n coil segments, at most n zones along the motor can be set up where the brake actuator force can be controlled independently. By suitable interlocks between the bias currents supplied to adjacent zones, it can be assured that there will always remain a "locked" zone between any two elevator cars. Since

the mechanical brake will stop a car going down if it is not released by the actuator force, and gravity will stop a car going up, no car can approach another car closer than one zone distance. This property guarantees that collisions cannot occur.

Chapter 5

Performance Simulations of Designed Motors

The simulations have been run for three different motors for comparison with each other and with experimental results. The first one, Motor 1, is designed and manufactured with respect to initial optimized values given in Section 3.3.2.2. The second one, Motor 2, is designed and manufactured with improved stator structure in terms of higher current density and less air gap. The mover design is kept the same for both Motor 1 and Motor 2. On the other hand, the third one, Motor 3, is fully optimized with respect to availability of better magnetic materials than the ones used for Motor 1 and Motor 2 but its production is left as a future plan.

The simulation results of Motor 1 and Motor 2 are compared with each other, and with their experimental results. The simulation results of Motor 3 are compared and discussed with the others to show the performance of the optimization method given in Section 3.4.

Table 5.1 shows the structural differences between the three motors. As it can be seen from the table, while Motor 1 has the same mover but different stator with Motor 2, Motor 3 has the same stator but different mover design compared to Motor 2. The reason of the differences is that Motor 1 is designed and implemented first for the initial experiments to test requirements given in Section 3.1. Then, by using bonded wire explained in Section 3.3.1 an improved stator of Motor 2 is designed and implemented to get higher performance on

Table 5.1: Structural differences of Motors 1,2 and 3

		Motor 1	Motor 2	Motor 3
stator	air gap (mm)	17	14	14
	# of windings	250	350	350
mover	magnet size (mm)	25x10x200	25x10x200	42x30x200
	magnet type	N32*	N32*	N45
	yoke size (mm)	90x10x200	90x10x200	107x22x200
	yoke type	1006* Steel	1006* Steel	1018 Steel

*not exact but taken as equivalent

power characteristics. In order to see the change on performances of the first and second stator, the design of the mover is fixed for Motor 1 and Motor 2. As a final step, a new mover of Motor 3 is designed by assuming the availability of stronger magnets and softer magnetic material with less flux saturation.

5.1 Magnetic Properties of Materials used in Simulations

The magnetic properties of the materials used in simulations and in implemented motors are given in Figures 5.1 and 5.2. The B-H curves in Figure 5.1 shows that 1018 type steel has better permeability since it shows same saturation when the field intensity (H) is about 4 times higher compared to 1006 type steel. In manufacturing the mover, a structural steel (ST37-2) which has medium magnetic performance is used as the material of the yoke, but for the simulations, 1006 type steel is chosen from the material list of the open-source FEM program, FEMM, as an equivalent material. However, for designing Motor 3, 1018 steel is chosen because of its better magnetic property. Although 1018 steel is also not better than an ideal pure iron, it was chosen because of its availability of access and to get more realistic results from the simulations instead of using an ideal material.

A better permanent magnet material used for Motor 3 in order to see

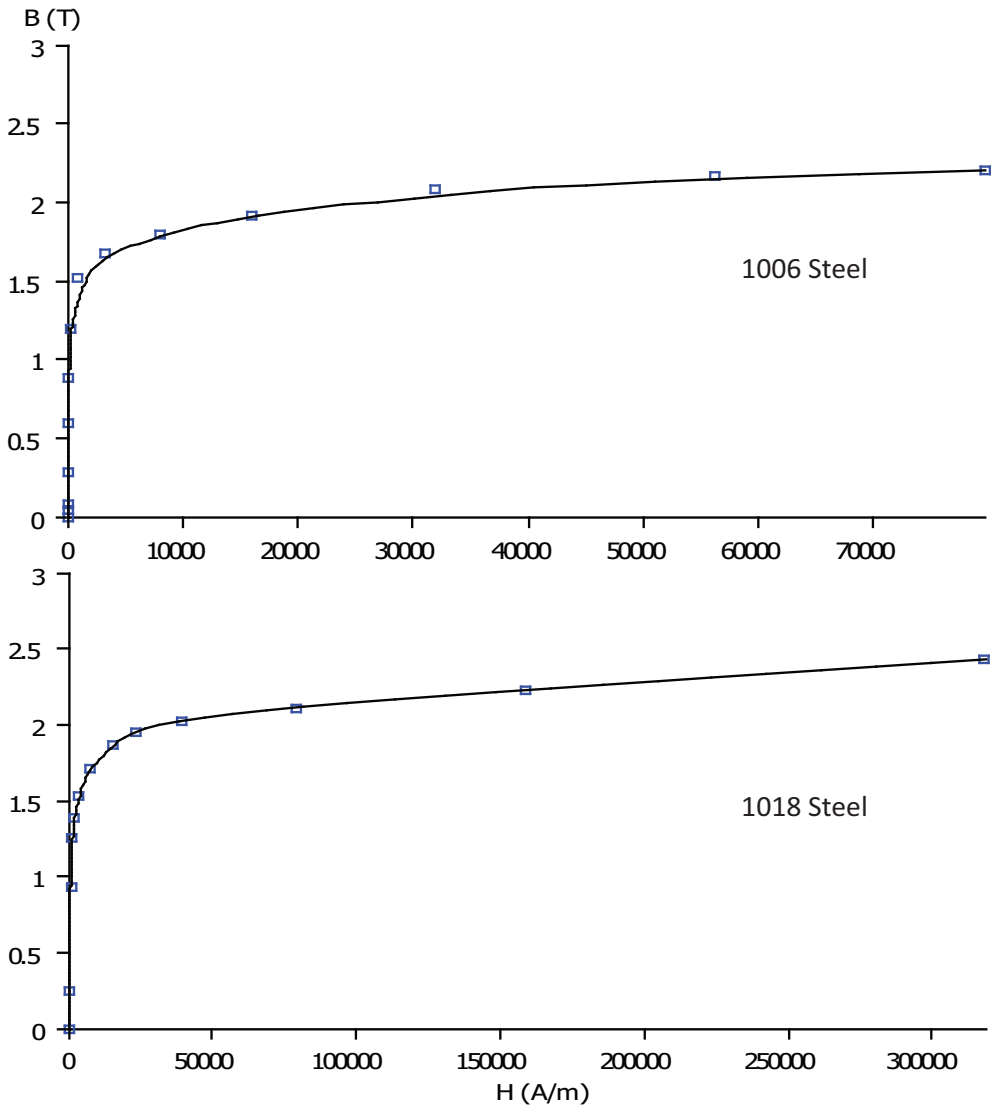

Figure 5.1: B-H curve of steels

the increase of performance with a higher quality magnet. Demagnetization curve of different sintered NdFeB magnets are shown in Figure 5.2 as examples. Although most of the permanent magnets have nonlinear curves, NdFeB magnets generally have linearity in low temperatures. Even if the magnet has nonlinearity, it can be taken as linear if the coercive resistance of the model that is being analysed is in the linear region of the curve. As it can be seen from Figure 5.2 magnets with higher grades (32,..,52) can reach higher flux

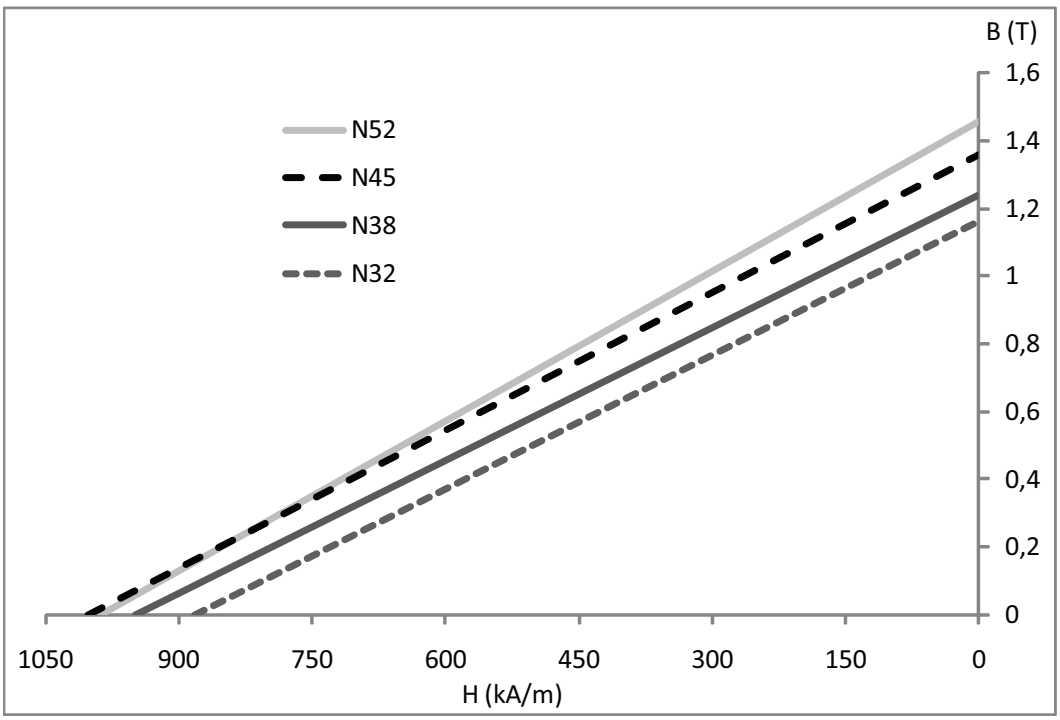

Figure 5.2: Demagnetization curves of permanent magnets at 20^0C

density in case of the same magnetic resistance. Therefore, it would be better to choose the magnet with highest grade in the market, however because of the rising nonlinearity properties and costs, the NdFeB magnet with N45 grade is selected as the material of the mover of Motor 3.

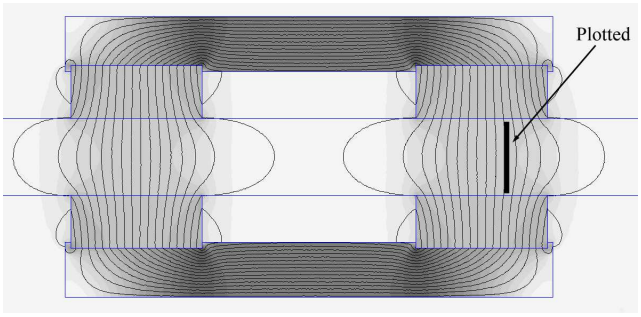

Figure 5.3: Flux density of Motor 2

Additional to comparison of forces obtained in simulations and experiments, the tangential magnetic flux density between the magnets found in simulations and measurement done with a gauss meter is compared to see the

consistency of the simulations. The flux density on the straight line shown in Figure 5.3 is given in Figures 5.4 and 5.5 as simulated and measured data respectively. It is seen that the simulation result is consistent with an error of %3.5.

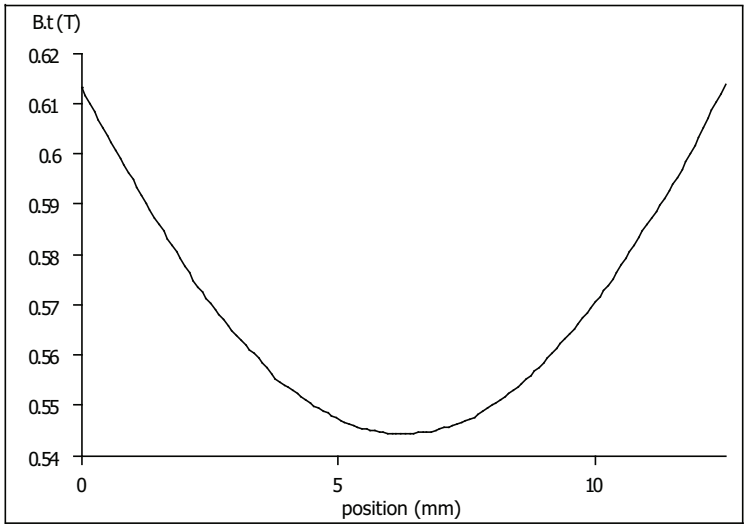

Figure 5.4: Simulated flux density change between magnets of Motor 2

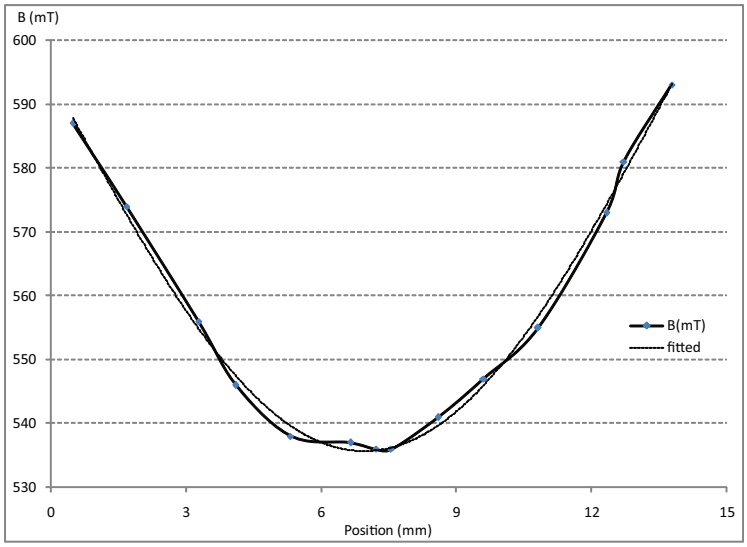

Figure 5.5: Measured flux density change between magnets of Motor 2

5.2 Simulation Results of Implemented Motor 1 and Motor 2

For all of the simulations, the driving bus current, I_{drive} is set as $3A$, and the brake current, I_{brake} is set as $1A$ unless otherwise mentioned.

In order to obtain the force ripple (r_d) and the effect of brake current (e_b) of Motor 1 and Motor 2, the thrust force is analyzed within a complete electrical phase where phase of the current is equal to the position phase of the mover. Furthermore, to analyse the effect of brake currents, the distortion on thrust force is obtained by including the brake currents, which is constant during the motion, while the drive currents depend on the position. The resultant graph is given in Figure 5.6 where higher thrust force of Motor 2 and high e_b for both motors can be seen easily. Since both Motor 1 and Motor 2 have the same mover, it was expected that they get about equal r_d and e_b, however r_d is increased from %15.18 to %17.27, and e_b is increased from %0.97 to %1.6 with Motor 2. This result shows that a mover can have different performance in terms of r_d and e_b additional to thrust force when used with different stators.

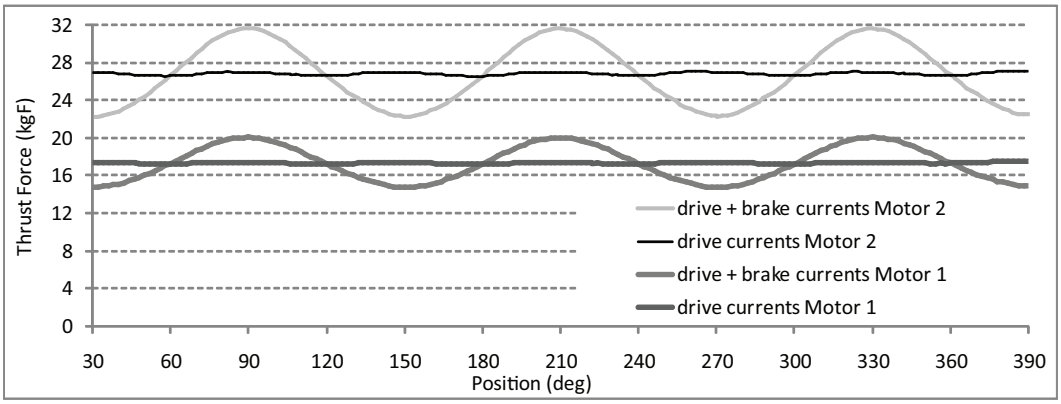

Figure 5.6: Force ripple and effect of brake currents on Motor 1 and Motor 2

The thrust forces that are obtained from Motor 1 and Motor 2 when current phase is kept constant versus the position of the mover is given in Figure 5.7. It can be seen that when the drive current is kept at a constant phase, the thrust force depends on the position of the mover. Therefore, in the absence of

position control, the payload on the motor will change the phase of the mover until the thrust force becomes equal to weight of the mover and payload. This property is also used in the experiments in order to find the maximum thrust force of the Motor 1 which is vertically assembled.

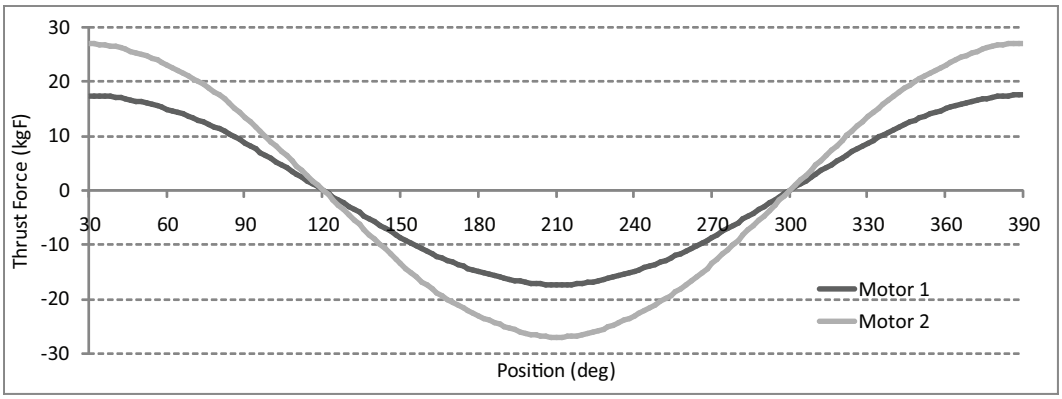

Figure 5.7: Thrust force of Motor 1 and Motor 2 vs position under drive current of constant phase

As a last simulation result for the motors, the back-EMF, induced when the magnetic flux through the coil changes, is analyzed. Although it is not taken as a criterion for the optimization done in Section 3.3, the performance in back-EMF harmonics is also compared for the motors since the harmonics on back-EMF waveform is not preferred for electric motors. In order to find the back EMF waveform while mover travels in a constant speed, total flux across a winding versus position of mover is analyzed. Note that this method also gives the average normal (not tangential) magnetic flux density on the stator when mover stops. The total magnetic flux on a single coil versus the mover position for Motor 2 is given in Figure 5.8. In Section 6.3, the experimental result of the back-EMF of Motor 2 given in Figure 6.10 verifies the simulation result given in Figure 5.8 as the waveform is the same. Note that while the experiments show the result of a single mover, the simulations show the results of both single mover and mover array. It can be seen that the flux density is symmetrical for the mover array case, but not for the single mover. The

reason is that during the time interval while a single mover is passing the coil, initially, one pole of magnets, then two, and then again one pole of magnets are facing the coil. On the other hand, in the case of mover array, the coil is always facing with two poles of magnets and this provides the symmetry.

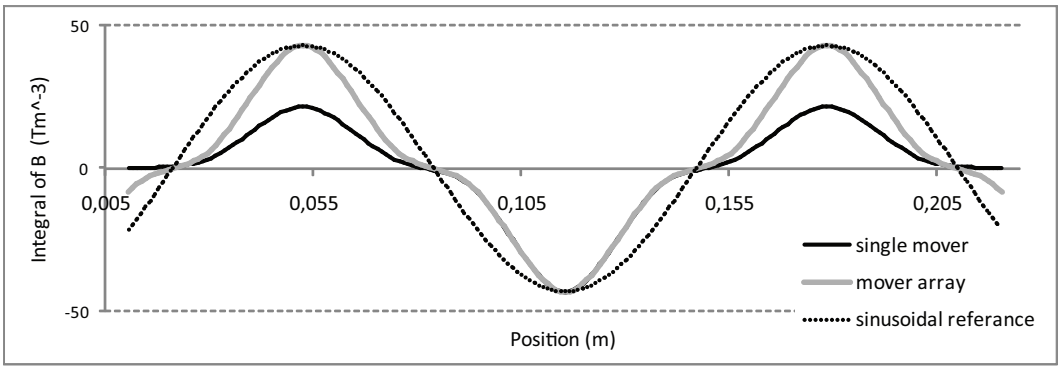

Figure 5.8: Integral of B on a single coil in Motor 2 vs mover position

5.3 Simulation Results of Motor 3 Optimized with Stronger Magnetic Materials

Motor 3, with optimized magnet dimensions $(42mm, 30mm, 200mm)$, is also analyzed in terms of force ripple (r_d), effect of brake currents (e_b), payload capacity, and back-EMF in simulations. As given in Section 3.4, Motor 3 is expected to have very low e_b with slightly higher r_d and higher payload compared to Motor 1 and Motor 2.

Figure 5.9 shows the thrust force of Motor 3 with respect to position of the mover. It can be seen that Motor 3 has very low e_b which is %0.18, and higher r_d with %3.9. It can be seen that the avarage thrust force (F_{avg}) is about $64kgF$. When the weight of mover consist of magnets and yoke is subtracted from the F_{avg}, the payload capacity of Motor 3 is found as about $48kg$.

The analyses on back-EMF is also performed for Motor 3 and the resultant waveform is given in Figure 5.10. It can be seen that the flux density on a single mover while a mover array is passing in a constant speed is sinusoidal.

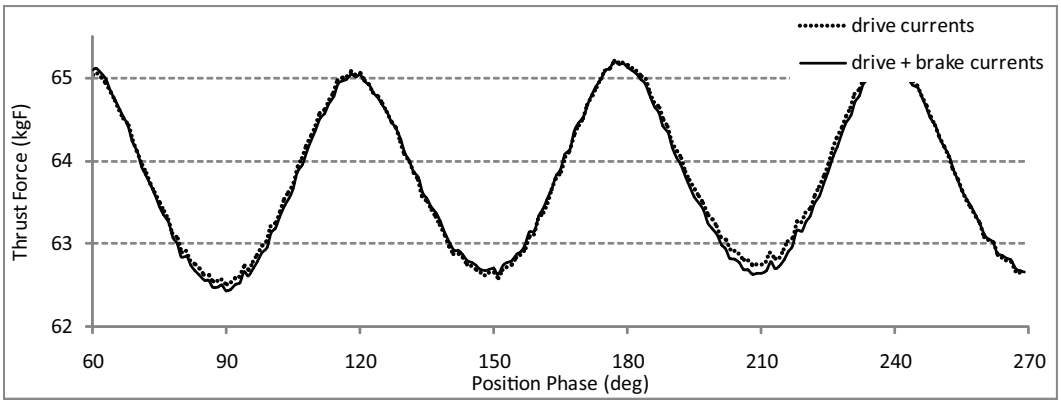

Figure 5.9: Force ripple and effect of brake currents on Motor 3

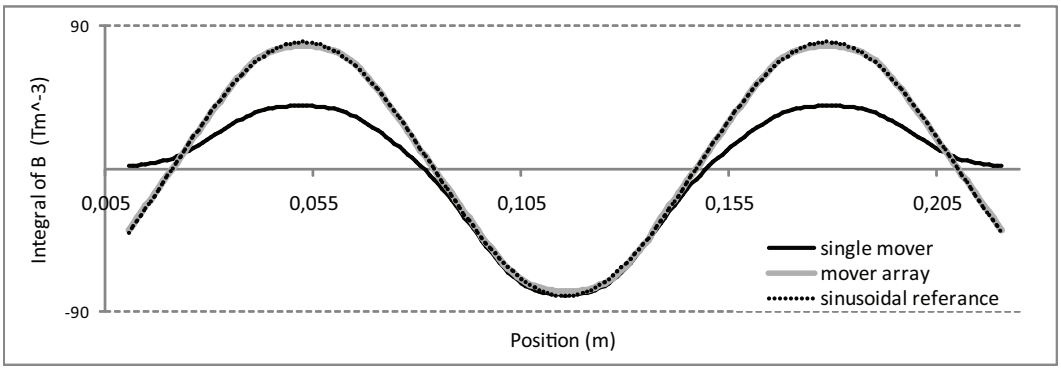

Figure 5.10: Integral of B on a single coil in Motor 3 vs mover position

In order to see how back-EMF waveforms of Motor 2 and Motor 3 is sinusoidal, the derivative of the waveforms is plotted in Figure 5.11 in order to determine if the result is sinusoidal as well. It has been observed that Motor 2 does not have a good result, but Motor 3 has a result which closer to a sinusoidal. More improvements can be still done on Motor 3 in order to get better back-EMF characteristic.

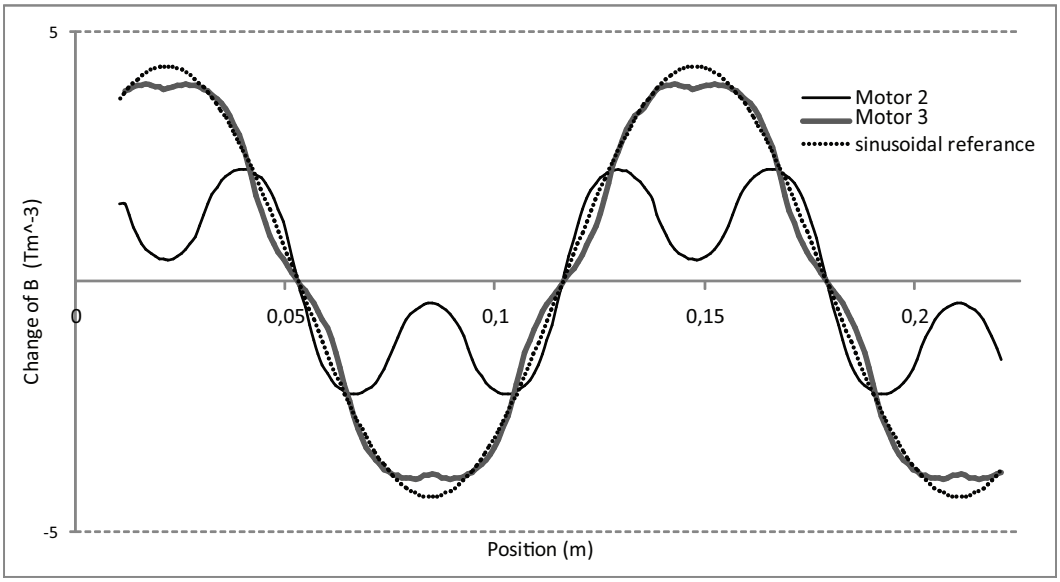

Figure 5.11: Change of B on a single coil in Motor 2 and Motor 3 while mover is traveling in a constant speed

Chapter 6

Experimental Results

Three main elements of the multi-car elevator were validated through experiments : the linear motor, safety device and drive electronics. Three different linear motors have been used for the experiments where all of them are air core permanent magnets synchronous linear motors (PMSLM, Section 3.2.2). The primary difference of one of them, which is stationed at Ritsumeikan University, Japan, is that it was built with segmented winding pattern while the others, which are stationed at Sabanci University, Turkey were built with balanced winding pattern which has fundamental effect on safety device (Section 4.1.2). Since all of the components of the one in Sabanci University (Motor 1 and Motor 2), are designed and manufactured according to analysis and methods given in Chapters 3 and 4, they meet all of the design criteria given in Section 3.1. Therefore, Motor 1 and Motor2 are used for the most of the experiments instead of the other one with segmented winding pattern.

The first implementation of linear motor, Motor 1, with balanced winding is shown in Figure 6.1. It has been divided into four parts elecronically where each part has its own driver electronics in order to have multiple independently controllable sections where multiple movers that can be operated. The safety device is also tested on this motor.

The linear motor implemented second, Motor 2, shown in Figure 6.2 has the same electrical structure as the first one, however it is improved in terms

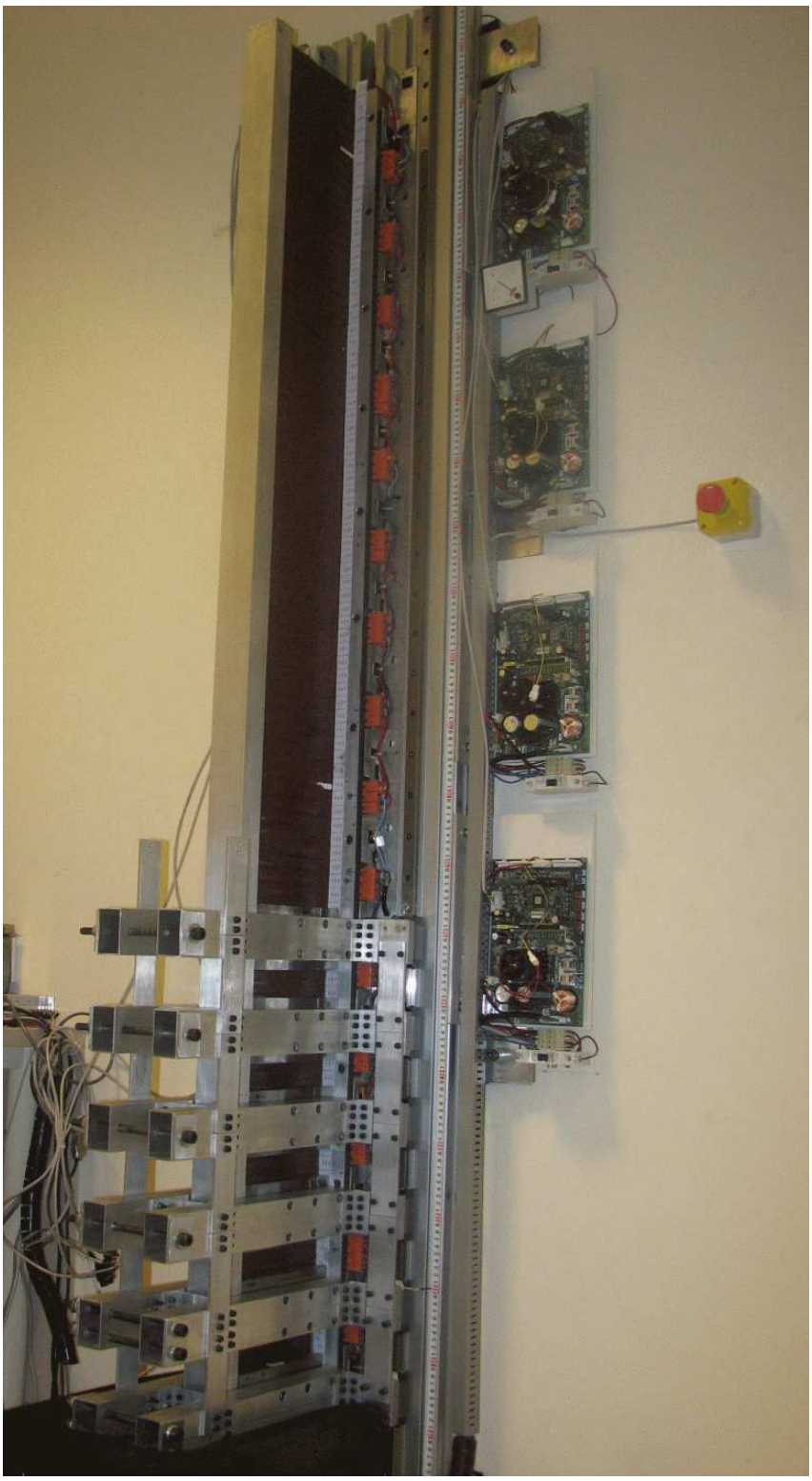

Figure 6.1: Motor 1, Designed and built

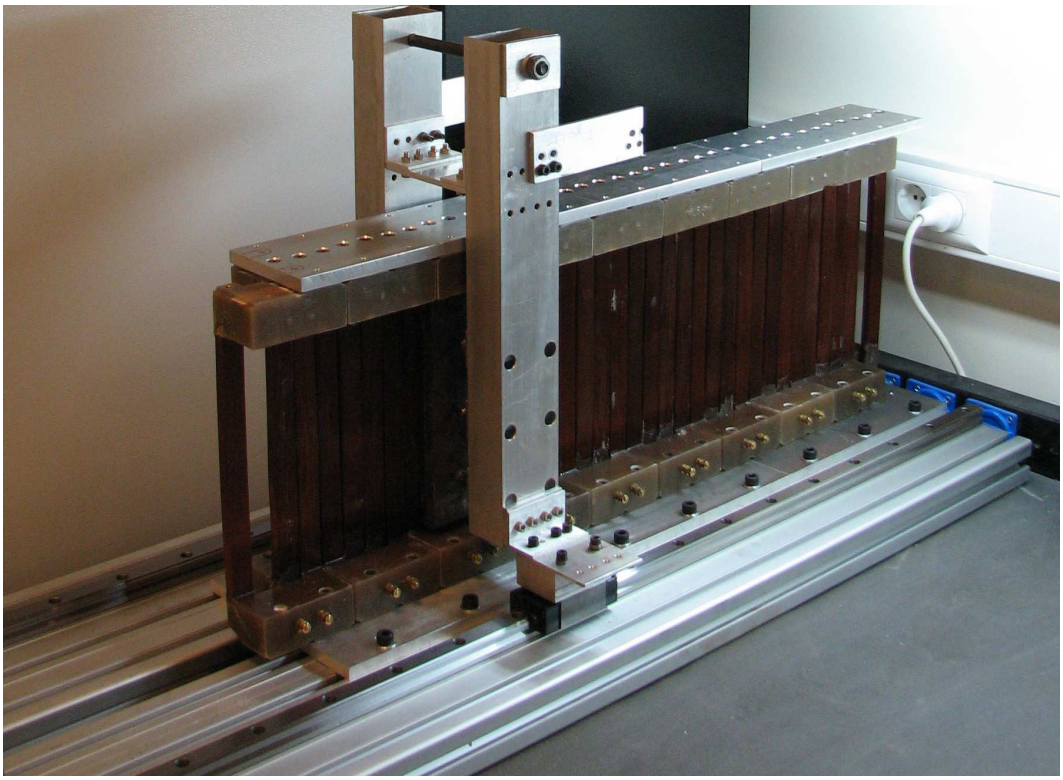

Figure 6.2: Motor 2, Designed and built

of mechanical strength, number of windings, modularity, heat dissipation, and the required air gap.

By comparing the experimental results of these motors, clarification of the declarations given in Chapters 3 and 4 has been provided by showing the improvements of balanced winding pattern over segmented one, magnets with higher energy product (BH_{max}) over lower ones, array of movers over single mover, having higher current density over lower one, and having less air gap over more air gap.

6.1 Experiments on Thrust Force and Payload Capacity

As also shown in simulation results (Section 5.2), when drive current is kept at a constant phase, the thrust force depends on the position of the mover. Therefore, in the absence of position control, a payload on the motor will change the position of the mover until the thrust force becomes equal to the weight of the mover and payload. After measuring position at different payload magnitudes, a sinusoid can be fit on this data. Using this sinusoid, maximum payload capacity (i.e. the value at 90 deg.) can be found. This property is used in the experiments in order to find the maximum payload capacity of different movers on Motor 1 which is vertically assembled.

Figure 6.3 shows the payloads with respect to the positions of the three movers with two types of NdFeB magnets under DC currents. The mover made up of A-type magnets is capable of lifting a maximum of 8 kg. The only difference between the movers in Figure 6.3-a and Figure 6.3-b is the type of magnets. The latter, made up of stronger B-type magnets can lift up to 11 kg of payload. The dependence of the motor load capacity with respect to magnet type can be clearly seen. It can be inferred from this result that the operating costs of the system, mainly the electrical power requirement, can be reduced by using a mover with stronger magnets.

The payload capacity can also be increased by mechanically coupling several movers together, each separated by the distance of one electrical phase, to add up their thrusts. This can be seen in Figure 6.3-c where two coupled movers made up of A-type magnets are measured to lift up to 16.5 kg, which is as expected, approximately double the capacity of a single A-type mover. In the elevator application, enough movers can be connected in this manner to obtain the required thrust, taking care to ensure the correct spacing between movers. Using ten mover units, a payload of 97 kg was obtained during the experiments, enough to support the weight of one person.

The thrust force of Motor 2 versus mover position when current phase is

kept constant is shown in Figure 6.5. Also, the comparison of thrust forces of two motors is given in Figure 6.4. The only differences between the Motor 1 and Motor 2 are number of windings in a coil and the air gap required between the magnets of mover as given in Table 5.1. It has been seen that the thrust force per current of Motor 2 is about $8kgF/A$ while it is $5.6kgF/A$ for Motor 1. Therefore, it can be inferred that higher payload capacities can be obtained by increasing the current density and decreasing the air gap. The thrust force of Motor 3 that has same stator but different mover with stronger magnets without considering initial cost is also given in Section 5.3 that the thrust is about $21.3kgF/A$.

6.2 Experiments on Motion

Some experiments were performed with the Motor 1 in motion in order to measure the current waveforms in cases of traveling up or down, and with low or high payloads. Figures 6.6 and 6.7 shows the position of the mover and a current waveform of one of the phases versus time.

Figure 6.6 shows the difference on the current waveform when the mover traveling up (a) and down (b) when current and position control given in Section 4.3.2 is applied. It can be seen that although the amplitudes of the current on different directions differs, the waveforms are similar. Thus, it shows that the system operates only in two quadrants "motoring upwards" or "generating downwards" as discussed in Section 4.3.2.

Another observation can be seen in Figure 6.7 that the rate of change on position is low when the motor is loaded with 40kg payload even with higher drive current when it is compared with zero payload case. Therefore, in case of higher payloads to be lifted, there is need to drive the motor with higher amplitude of current which may not be possible because of limits on power supply or the possible overheating of the coils. However, instead of increasing the drive currents, the motor can consist of enough movers mechanically

coupled together with respect to allowed maximum payload.

6.3 Experiments on Motor Characteristics

The back-EMF voltage waveform of the Motor 2 is measured and given in Figures 6.9 and 6.10 for feature analyses on speed limits with a certain power supply, and short-circuit limit speed in case all other safety devices fail. The simulation results on back-EMF of Motor 2 and Motor 3 is given and discussed in Sections 5.2 and 5.3. It can be seen that the the experimental data of Motor 2 verifies the simulations. By using the method given in Section 5.2, back-EMF waveform of a designed motor can be obtained to find the generative force due to back-EMF. Note that in the case of the mover is dropped because of a failure, it will fall at a controlled rate due to the opposing forces produced during generation. Under such conditions, the coils of the stator can be short-circuited, ensuring a current path. As the mover falls, the changing flux in the coils induce an back-EMF which results in current flow. This current opposes the original change in flux, hence producing a negative thrust. This property can be used to calculate falling speed of an elevator cage carrying the full rated load. However, the calculations of limits in traveling speed or falling of mover in case all other safety devices fail is not included in this study.

6.4 Experiments on Brake Device

The uniformity of the force generated at the top of the stator for the brake operation has been measured for Motor 1. A magnet plate with the length of one electrical phase and with the width equal to the stator width was built using A-type magnets. It was attached to the mover via a linear bearing enabling motion perpendicular to the plane of the stator, and connected in such a way that the generated force was applied to a strain gage. The terminals of the motor were reconnected so that the same magnitude DC current could be applied to each winding separately, creating the desired coil top magnetic field.

The resulting sideways force on the magnet plate was measured. The results can be seen in Figure 6.11. As the mover changes position, the generated force is nearly constant, and therefore suitable for the brake operation.

The change in the brake force with respect to I_{brake} while the mover is stopped at one location is shown in Figure 6.12. Since the force changes almost linearly, it can be said that the brake actuation is independent of the normal drive currents, and can be controlled by the DC current component applied to the motor using a suitable motor driver, such as the one described in Section 4.3.1.

As it is described in Section 4.1.2, for the case of segmented winding pattern, the force generated by the stator top field of the motor can be obtained by supplying the modified current $i_a + i_b - i_c = I_{DC}$. The brake force has also been measured for the segmented winding with respect to the motor position. It can be seen in Figure 6.13 that when the precise currents are supplied, the stator top magnetic field can be kept relatively constant.

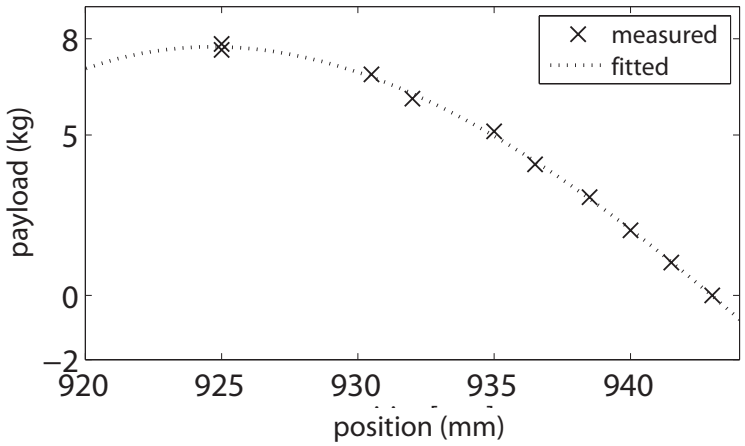

(a)

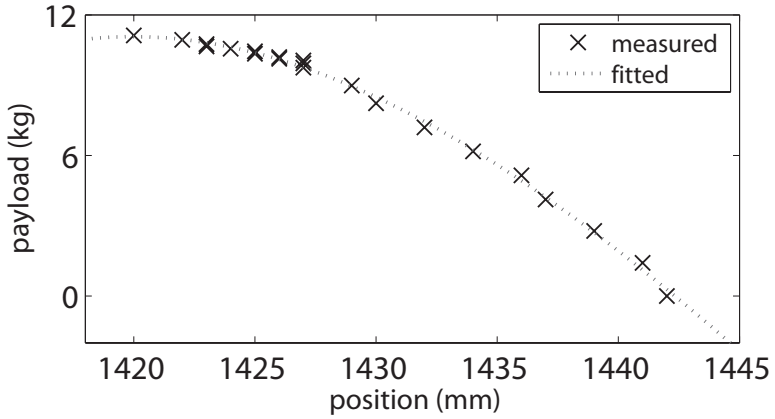

(b)

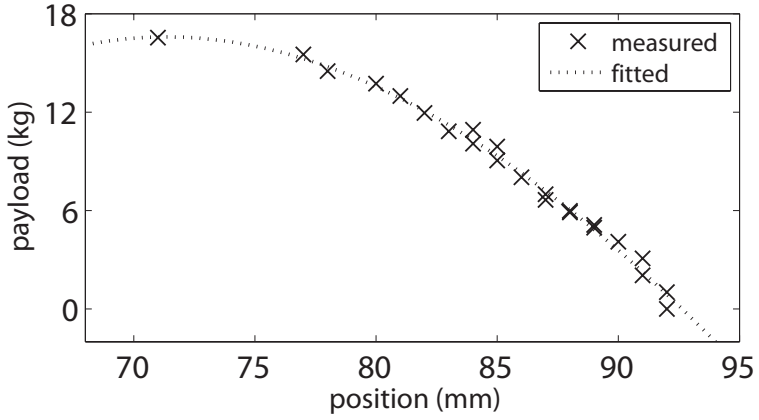

(c)

Figure 6.3: Payload capacity vs position under DC currents (a)one mover with A-type magnets (b)one mover with B-type magnets (c)array of two movers with A-type magnets

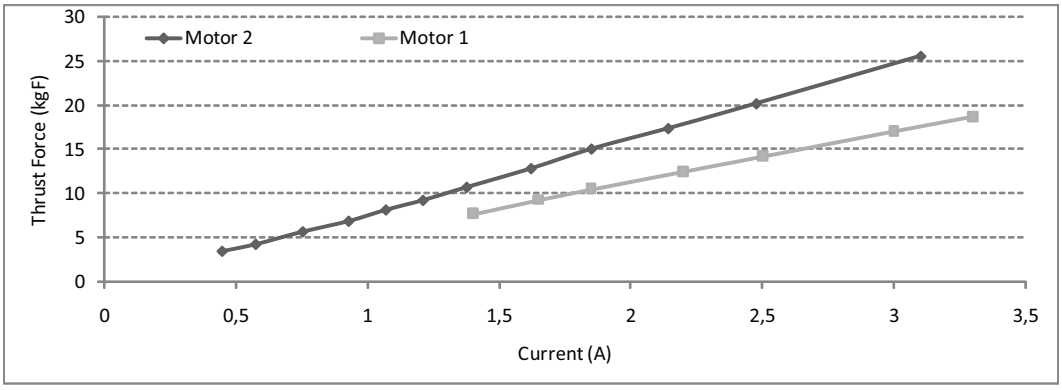

Figure 6.4: Thrust force vs drive currents of Motor 1 and Motor 2

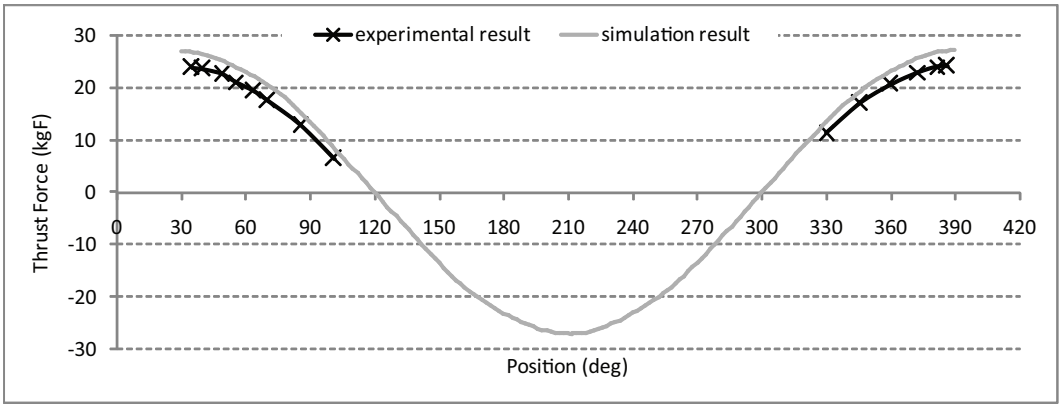

Figure 6.5: Thrust force of Motor 2 vs position under drive current of constant phase

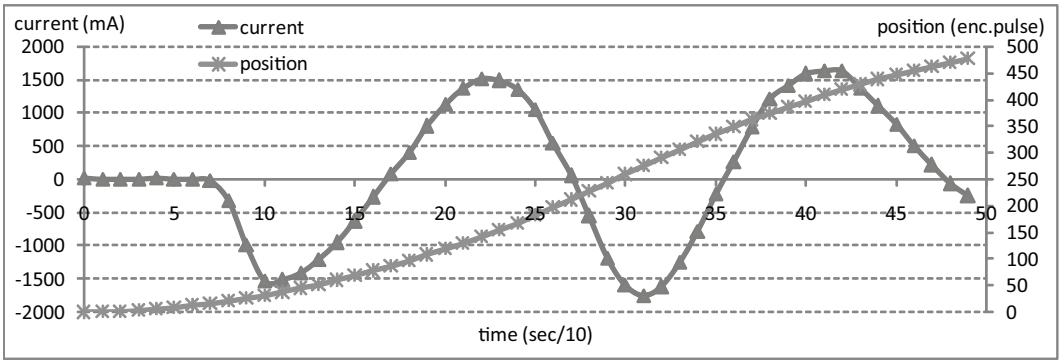

(a)

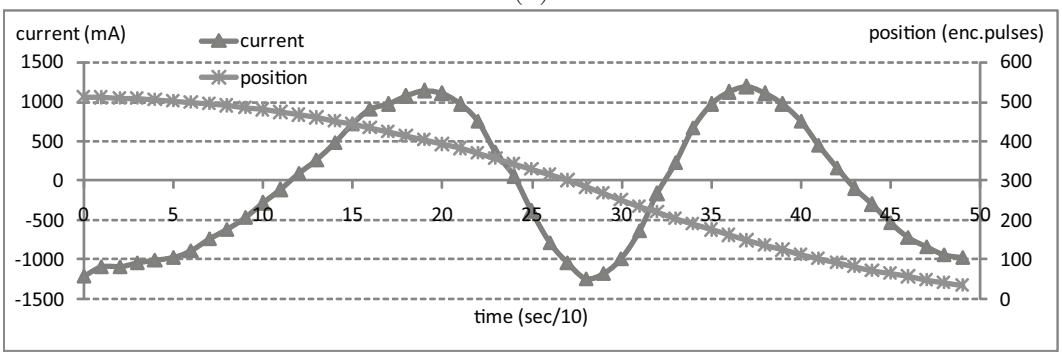

(b)

Figure 6.6: Motion and current profile vs time (a)array of 10 movers traveling up (b)array of 10 movers traveling down

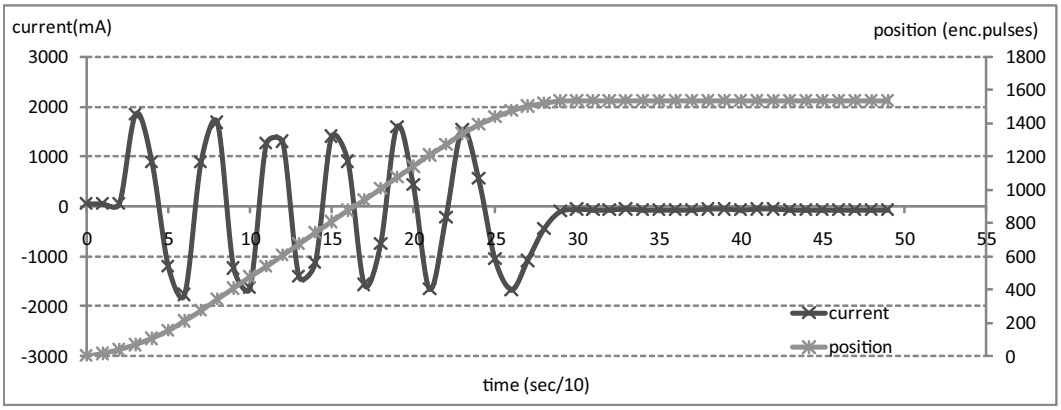

(a)

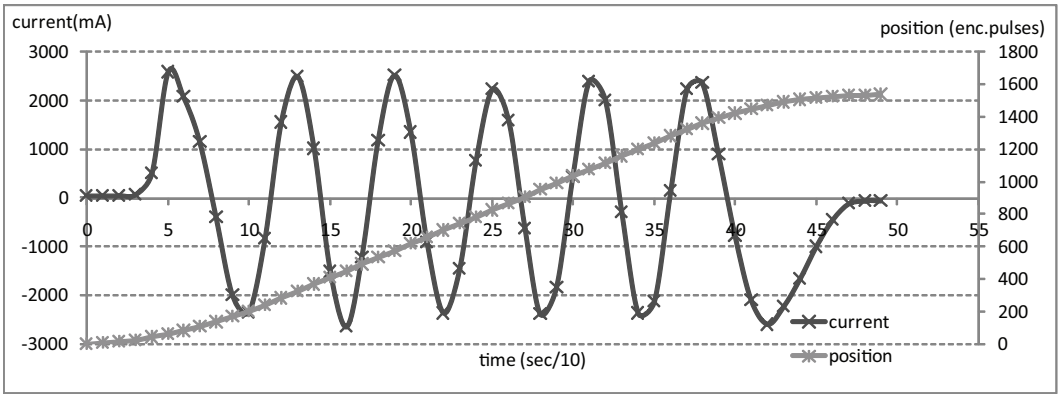

(b)

Figure 6.7: Motion and current profile with payload vs time (a)traveling up with self weight (b)traveling up with self weight and 40kg payload

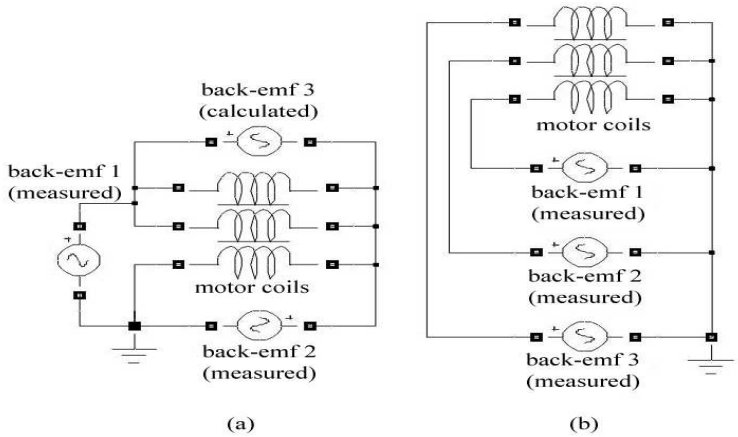

Figure 6.8: Circuit diagrams of measured back-emf voltages (a) circuit 1 (b) circuit 2

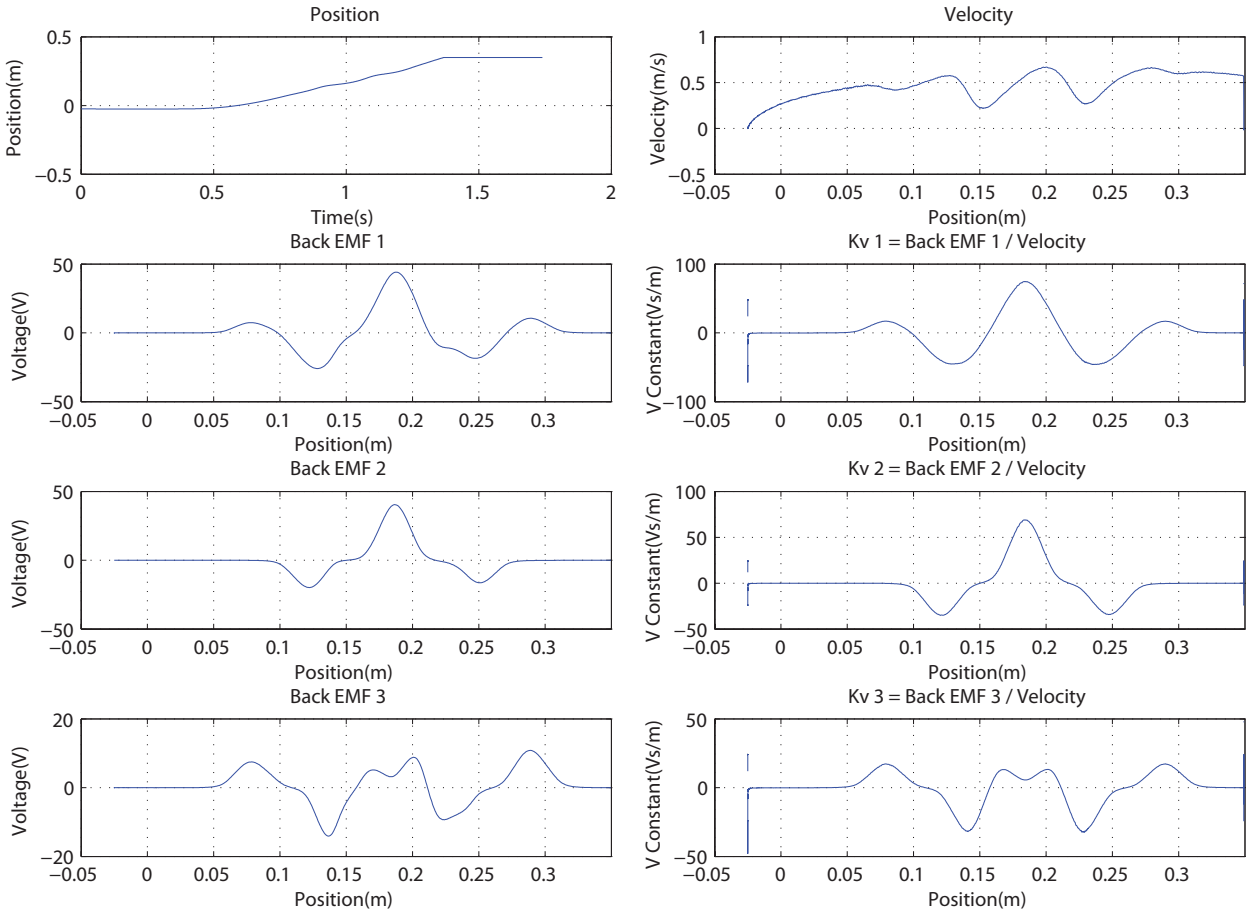

Figure 6.9: Back-emf and voltage constants on circuit 1

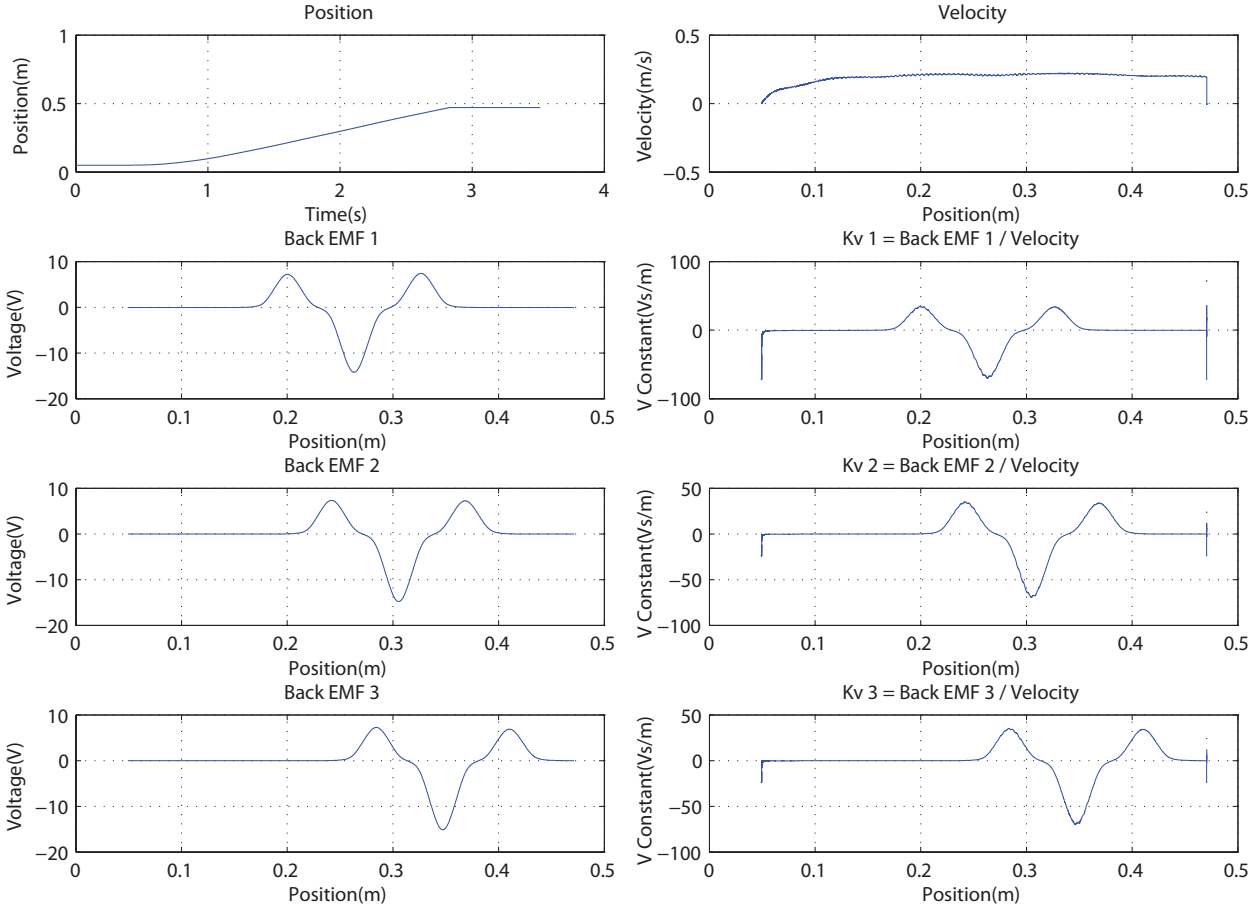

Figure 6.10: Back-emf and voltage constants on circuit 2

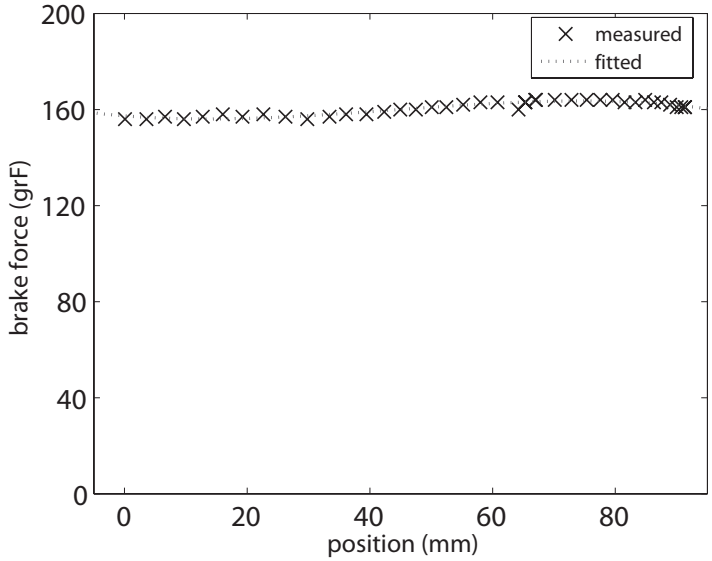

Figure 6.11: Brake force vs position on balanced winding Motor 1

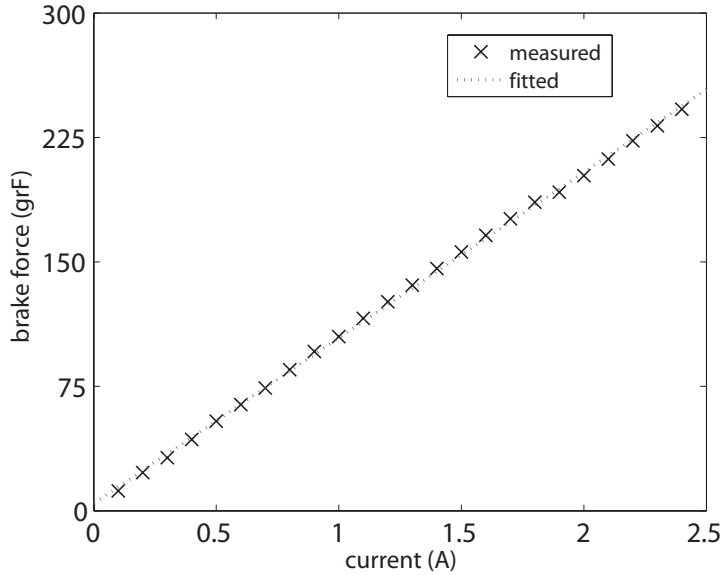

Figure 6.12: Brake force vs DC-brake currents on balanced winding Motor 1

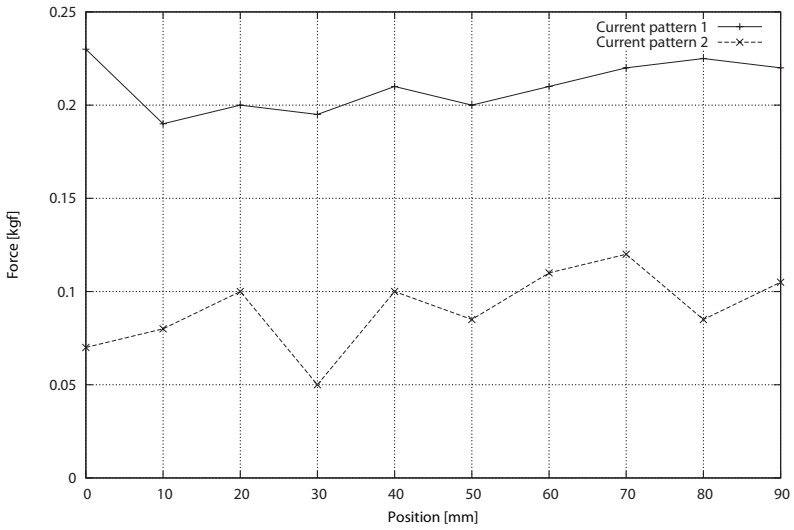

Figure 6.13: Brake force vs position on segmented winding motor at

Chapter 7

Conclusion

In this thesis, design methodology for a linear motor for multi-car elevators that meets performance criteria such as payload, force ripple, initial and running cost, and effect of safety device was given.

A novel safety device that is based on a magnetic field decoupled from the thrust generating magnetic field of the linear motor was also introduced together with its drive and control method.

The complete concept was extensively tested through simulations and design iterations to discover the most suitable mover and stator dimensions.

Finally, fully functional two linear motor prototypes were designed and built and all of the proposed concepts have been experimentally validated.

Bibliography

[1] Jufer M. Perriard Y. Duenser T. Kocher H. Chevailler, S. Linear motors for multi mobile systems. *IAS 2005*, 3:2099–2106, 2005.

[2] Jufer M. Perriard Y. Duenser T. Kocher H. Chevailler, S. Linear synchronous motor design. *IEEE Trans. on Electric Machines and Drives*, pages 1555–1560, 2005.

[3] R.J. Cruise and C.H Landy. Linear synchronous motor propelled hoists for mining applications. *IAS 1996*, 4:2514–2519, 1996.

[4] Tobita T. Fujino, A. and K. Nakagawa. Basic study on mass transportation systems in buildings by means of multiple-cage elevator. *Proc. JSME Elevator, Escalator and Amusement Rides Conf.*, 117(7):815–822, April 1997.

[5] Y. Sano T. Sudo S. Markon H. Suzuki, S. Takahashi and H. Kita. Simulation-based optimization of multi-car elevator controllers using a genetic algorithm. *Trans. SICE*, 40(4).

[6] T. Ishii. Elevators for skyscrapers. *Spectrum, IEEE*, 31(9):42–46, Sep 1994.

[7] W.D. Jones. How to build a mile-high skyscraper. *Spectrum, IEEE*, 44(6):52–53, June 2007.

[8] S. Markon K. Ikeda, H. Suzuki and H. Kita. Designing traffic sensitive controllers for multi-car elevators through evolutionary multi-objective optimization. *Proc. 4-th Intl. Conf. on Evolutionary Multi-Criterion Optimization, LNCS 4403*.

[9] T. Hamagami K. Shiraishi and H. Hirata. Multi car elevator control by using learning automaton. *PIEEJ Trans. IA*, 125(1).

[10] H.Takami K.Yoshida, S.Liming and A.Sonoda. Repulsive-mode levitation and propulsion experiments of an underwater travelling lsm vehicle me02. *Proc. LDIA*.

[11] H.S. Lim and R. Krishnan. Ropeless elevator with linear switched reluctance motor drive actuation systems. *IEEE Trans. on Industrial Electronics*, 54(4).

[12] Krishnan R. Lobo N.S. Lim, .H.S. Design and control of a linear propulsion system for an elevator using linear switched reluctance motor drives. *IEEE Trans. on Industrial Electrics*, 55(2):534–542, 2008.

[13] Chen Z. Yao B. Lu, L. and Q. Wang. Desired compensation adaptive robust control of a linear-motor-driven precision industrial gantry with improved cogging force compensation. *IEEE/ASME Trans. Mechatronics*, 13(6):617–624, Dec. 2008.

[14] Kita H. Markon, S. and H. Kise. *Control of Traffic Systems in Buildings: Applications of Modern Supervisory and Optimal Control (Advances in Industrial Control)*. Springer-Verlag New York, Inc., Secaucus, NJ, USA, 2006.

[15] M. Misakian. Equations for the magnetic field produced by one or more rectangular loops of wire in the same plane. *J. Res. Natl. Inst. Stand. Tech.*, 105(4):557–564, July 2000.

[16] Koseki T. Miyatake, M. and S. Sone. Design and traffic control of multiple cars for an elevator system driven by linear synchronous motors. In *Proc.Symposium on Linear Drives for Industry Applications*, number AP-22, pages 94–97, 1998.

[17] Koseki T. Miyatake, M. and S. Sone. A proposal of a ropeless lift system and evaluation of its feasibility,. *IEEJ Trans. IA*, 119(11):1353–1360, 1999.

[18] Koseki T. Miyatake, M. and S. Sone. Thyssenkrupp's twin lift system. *IEEJ Trans. IA*, 51(7):51–53, 2003.

[19] Y. Okamoto and N. Takahashi. Minimization of driving force ripple of linear motor for rope-less elevator using topology optimization technique. *Journal of Materials Processing Technology*, 181:131–135, 2007.

[20] M. Platen and G. Henneberger. Examination of leakage and end effects in a linear synchronous motor for vertical transportation by means of finite element computation. *IEEE Trans. on Magnetics*, 37(5).

[21] Zhen H.X. Hong-xing W. Quan, K.B. and L. Li-yi. Thrust and thermal characteristics of electromagnetic launcher based on permanent magnet linear synchronous motors. *Magnetics, IEEE Transactions on*, 45(1):358–362, 1 2009.

[22] H. Kita S. Markon, K. Ikeda and H. Suzuki. Direct control of multi-car elevators with real-time ga. *Proc. 11th International Conference on Intelligent Engineering Systems.*

[23] H.P. Schwefel. *Evolution and Optimum Seeking.* John Wiley & Sons, 1995.

[24] T. Sudo and S. Markon. The perfrmance of multi-car linear motor ele-

vators. *Elevator Technology 11 Proc. ELEVCON 2001*, pages 141–149, 2001.

[25] H. Suzuki. A study on intra-shaft operating method for multi-car elevators. *IEICE Technical Report, CST2007-7*.

[26] Kita H. Suzuki H. Sudo T. Takahashi, S. and S. Markon. Simulation-based optimization of a controller for multi-car elevators using a genetic algorithm for noisy fitness function. *The 2003 Congress on Evolutionary Computation, CEC '03*, 3:1582–1587 Vol.3, Dec. 2003.

[27] N. Takahashi, T. Yamada, D. Miyagi, and S. Markon. Basic study of optimal design of linear motor for rope-less elevator. In *7th International Conference on Computation in Electromagnetics*, pages 202–203, April 2008.

[28] S. Vaez-Zadeh and A.H. Isfahani. Multiobjective design optimization of air-core linear permanent-magnet synchronous motors for improved thrust and low magnet consumption. *Magnetics, IEEE Transactions on*, 42:446–452, 3 2006.

[29] Osawa Watanabe T. Yamaguchi, .H. and H. Yamada. Brake control characteristics of a linear synchronous motor for ropeless elevator. *IEEE Trans. on Magnetics*, 37(5):3732–3736, 2001.

[30] K. Yoshida and X. Zhang. Sensorless guidance control with constant air-gap in ropeless linear elevator. In *The 4th International Power Electronics and Motion Control Conference*, volume 2, pages 772–776, Aug. 2004.

[31] Lee J.J. Yoon H.S. Youn, S.W. and C.S. Koh. A new cogging-free permanent-magnet linear motor. *IEEE Trans. on Magnetics*, 44(7):1785–1790, 2008.

[32] Maeda T. Funai K. Nozawa S. Yumura, T. and K. Koyama. Roped multi-elevator concept and the system performance. *Proc. JSME Elevator, Escalator and Amusement Rides Conf.*, pages 1–4, 1997.